

ASSESSMENT OF THE PERMEABILITY OF VRYHEID FORMATION SEDIMENTS

by

Bernardus Jacobus Venter

Submitted in partial fulfilment of the
requirements for the degree of
Master of Science,
in the
Department of Geology and Applied Geology,
University of Natal
1994

Durban
March 1994

PREFACE

The experimental work described in this thesis was carried out in the Department of Geology and Applied Geology, University of Natal, Durban, from January 1992 to December 1993, under the supervision and guidance of Mr. Colin A. Jermy.

These studies represent original work by the author and have not been submitted in any form to another University. Where use was made of the work of others it has been duly acknowledged in the text.

ACKNOWLEDGEMENTS

The author wishes to thank Rand Coal (Pty) Ltd and Majuba Colliery for making available the borehole core used as test material, as well as for the opportunity to visit the mine and investigate the situation underground.

Thanks must be extended to my supervisor, Mr. C.A. Jermy for his role in the organising and execution of the project. My thanks also for his understanding, outstanding support and ultimately his belief in the project.

Further thanks must also be extended to the Department of Geology and Applied Geology of the University of Natal, Durban, prof. F.G. Bell in particular, for affording me the opportunity to do the research, for supplying the equipment and carrying the overhead costs of the project.

To my parents for their financial support throughout and their moral support in the rough patches, it is appreciated beyond what words can express.

Lastly the author wishes to thank Mrs. A. Pieterse for the drafting of the locality map and Mrs. C. Garz for excellent advice concerning many of the other illustrations.

ABSTRACT

Permeability is that physical property of a porous medium that controls the flow of fluids through that medium. The flow of methane and water may be induced by the excavation of a mine opening in methane-bearing strata. Methane flow into a mine opening constitutes one of the biggest hazards in the coal mining industry. It is poisonous to humans and can ignite at concentrations as low as 5 % per volume and create explosions in the presence of coal dust from mining. If the flow of methane and/or water into the mine opening becomes blocked by an impervious layer, excessive pressures may develop, particularly in the roof strata of the mined seam, which can lead to roof falls.

In order to characterize the flow of methane and water into and around the openings in a mine, that was plagued by roof falls suspected of being the result of excessive fluid pressure build-up, a large scale laboratory investigation of the permeability of the roof sediments of the working coal seam in the area was undertaken. The permeability was measured under atmospheric conditions by means of a modified Ohle permeameter, and under triaxial conditions with the aid of a modified Hoek cell. The permeability of the sediments towards methane and water was measured. Nitrogen was used as a control because it is much less reactive than methane towards the sediments used in this project.

It was found that the permeability decreases with increasing gas pressure, in the case of gas being the permeating fluid, and increased with increasing water pressure, in the case of water being the permeating fluid. In some instances anomalous plots of permeability versus reciprocal mean gas pressure were obtained. These were attributed to the effects of methane adsorption or the Klinkenberg effect, and a possible method to determine which of the two processes is dominant is discussed.

To characterize the flow in the roof strata of the coal seam being mined, the permeability was correlated to facies type. The different facies types were numbered from 1 to 14 with increasing grain size for ease of correlation. Due to the variable nature of the sediments, even in a facies type, no single permeability could be obtained for a facies type. Instead permeability ranges were obtained for each facies type. The definition of the lower and upper limits for each range were found to be dependant on the number of tests done on samples for that facies type. Nonetheless a relationship of increasing permeability with increasing grain size was found in the coarser grained facies (facies type 8 and higher). For the finer grained facies types the permeability was found to decrease with increase in grain size.

A graph could be constructed for use in predicting possible hazardous zones by identifying the facies type and then reading the permeability range that can be expected off the graph. Due to the variable nature of the sediments, the graph is, at this time, only applicable to the areas where the samples were obtained. A permeability prediction graph for all localities would be an ideal but is beyond the scope of this project. Such a graph, and the methods discussed have a wide range of applications in the coal mining and methane gas exploitation industries.

TABLE OF CONTENTS

CHAPTER 1: INTRODUCTION	1
CHAPTER 2: GEOLOGY	4
2.1. INTRODUCTION	4
2.2. KAROO SEQUENCE	5
2.2.1. Eccca Group	7
2.2.2. Vryheid Formation	7
2.3. THE GEOLOGY AT MAJUBA COLLIERY	8
2.4. COAL CHARACTERISTICS	10
2.5. PETROGRAPHY	12
CHAPTER 3: THEORETICAL CONSIDERATIONS	16
3.1. INTRODUCTION	16
3.2. THEORETICAL MODELS FOR FLOW THROUGH POROUS MEDIA	18
3.3. THE THEORY OF LABORATORY PERMEABILITY MEASUREMENTS	21
3.3.1. Steady-state methods	23
3.3.2. Transient or pulse-decay methods	23
3.3.3. Steady-state versus pulse-decay methods	23
3.4. LIMITATIONS TO DARCY'S LAW	24
CHAPTER 4: METHODOLOGY	29
4.1. INTRODUCTION	29
4.2. SAMPLE PREPARATION	29
4.3. OHLE CELL	31
4.3.1. Apparatus	31
4.3.1.1. Gas	33
4.3.1.2. Water	33
4.3.2. Test method	33
4.3.2.1. Gas	33
4.3.2.2. Water	37
4.4. HOEK CELL	37

4.4.1. Apparatus	37
4.4.2. Test method	38
CHAPTER 5: RESULTS AND DISCUSSION	42
5.1. INTRODUCTION	42
5.2. OHLE CELL	42
5.2.1. Gas	42
5.2.2. Water	53
5.3. HOEK CELL	56
5.4. POTENTIAL SOURCES OF EXPERIMENTAL ERROR	61
5.4.1. Ohle cell	61
5.4.1.1. Gas	61
5.4.1.2. Water	65
5.4.2. Hoek cell	65
CHAPTER 6: CONCLUSIONS	67
REFERENCES	70
BIBLIOGRAPHY	75
APPENDIX A: Borehole log of borehole ARF 39	80
APPENDIX B: Borehole log of borehole AH 55 - 59	94
APPENDIX C: Borehole log of borehole AH 58	96
APPENDIX D: Borehole log of borehole AH 60	98
APPENDIX E: Borehole log of borehole AH 53	100
APPENDIX F: Borehole log of borehole AH 61	102
APPENDIX G: Data capture sheet - Ohle cell	104
APPENDIX H: Data capture sheet - Hoek cell	106

LIST OF FIGURES

Figure 1.1 Map showing the locality of Majuba Colliery within the Eastern Transvaal Coalfield	2
Figure 2.1 The Karoo Basin: Distribution, stratigraphy and geographic positions of the associated coal-bearing strata	6
Figure 3.1 Plot of permeability versus $1 / P_m$ illustrating the relationship between k_s and k_o . Facies 10, where methane was the permeating fluid	17
Figure 3.2 Regimes of free-surface flow in terms of critical Reynolds numbers	17
Figure 3.3 Various theoretical models for natural porous media used in the prediction of the permeability	20
Figure 3.4 Schematic illustration of the change in the flow velocity at the same point at three different times under different applied pressure regimes	24
Figure 3.5 Twelve schematic flow curves for non-Darcian flow conditions	25
Figure 4.1 Post- or pillar drill setup used for core sample extraction	30
Figure 4.2 Cross-section of the Ohle cell dismantled	32
Figure 4.3 Diagram showing the different components of the Ohle cell for tests involving gas as the permeating fluid	35
Figure 4.4 Diagram showing the different components for the Ohle cell tests involving water as the permeating fluid	35
Figure 4.5 Plot of k_s versus $1 / P_m$ for methane showing erratic behaviour above 400 kPa inlet gas pressure	35
Figure 4.6 Cross-section of the Hoek cell	39
Figure 4.7 Diagram showing the different components of the Hoek cell tests involving methane as the permeating fluid	41
Figure 5.1 Plot of k versus $1 / P_m$ for nitrogen and methane (Facies 9)	43
Figure 5.2 Plot showing the relationship between facies type and k_o range for both methane and nitrogen	46
Figure 5.3 Plot of flow rate versus $1 / P_m$ for nitrogen and methane. Same sample as for figure 5.1	46
Figure 5.4 Plot of k_s versus $1 / P_m$ for methane, showing a negative slope (Facies 5)	47
Figure 5.5 Plot of k_s versus $1 / P_m$ for nitrogen showing a positive	

slope (Facies 5)	47
Figure 5.6 Plot of flow rate versus P_1 for both methane and nitrogen for the same sample as in figures 5.4 and 5.5 (Facies 5)	48
Figure 5.7 Plot of k_s versus $1 / P_m$ with both nitrogen and methane showing a negative relationship (Facies 10)	48
Figure 5.8 Plot of flow rate versus P_1 for nitrogen and methane. Same sample as figure 5.7 (Facies 10)	49
Figure 5.9 Plot of k_s versus $1 / P_m$ for methane, showing variation of k_s and k_{ie} with grain size (Facies 10)	51
Figure 5.10 Plot of k_s versus $1 / P_m$ for methane, showing variations in k_s and k_{ie} with change in flow direction (Facies 10)	52
Figure 5.11 Plot of k_s versus water pressure (Facies 10)	54
Figure 5.12 Plot showing the relationship between k_s for water (at 1000 kPa inlet pressure) and facies type	55
Figure 5.13 Plot showing the change in flow rate with time under a constant external hydrostatic stress of 4 MPa (Facies 8)	56
Figure 5.14 Plot of k_s versus $1 / P_m$, for methane, showing the variation of k_{ie} with an increase in σ_3 (Facies 10)	57
Figure 5.15 Plot of k_s versus $1 / P_m$ for methane showing the difference in reduction in k_{ie} produced by applying different stress loading cycles (Facies 12)	58
Figure 5.16 Plot of k_s versus $1 / P_m$ for methane, showing difference in k_{ie} before and after axial load cycle (Facies 10)	59
Figure 5.17 Plot of k_s versus $1 / P_m$, for methane, showing the change of k_{ie} before and after a series of axial load cycles (Facies 9)	60
Figure 5.18 Plot of k_s versus $1 / P_m$ for methane, showing anisotropic behaviour, even at hydrostatic pressures of 11 MPa (Facies 9)	61

LIST OF PLATES

Plate 2.1 Bulk sample from roof of Gus coal seam showing trough cross bedding of facies type 10.	11
Plate 2.2 Bulk sample from roof of Gus coal seam showing variability in grain size for the same facies type	11
Plate 2.3 Photomicrograph of facies type 10	13
Plate 2.4 Photomicrograph of facies type 5	13
Plate 2.5 Photomicrograph of facies type 7	15
Plate 2.6 Photomicrograph of facies type 12	15
Plate 4.1 Photograph showing the assembled Ohle cell	34
Plate 4.2 Photograph showing the different parts of the Ohle cell	34
Plate 4.3 Photograph showing the Hoek cell with the rubber sleeve inserted	40
Plate 4.4 Photograph showing the modified platens for the Hoek cell	40

LIST OF TABLES

Table 2.1 Correlation between coal seams in different coalfields	9
Table 2.2 Description of tested facies	10
Table 2.3 Average analysis for the coal seams mined in 1986 in the Eastern Transvaal Coalfield	12
Table 5.1 Liquid equivalent permeability ranges for facies types tested with nitrogen as permeating fluid	44
Table 5.2 Liquid equivalent permeability ranges for facies types tested with methane as permeating fluid	44
Table 5.3 Total carbon analysis for different facies types	50
Table 5.4 Liquid equivalent permeabilities for tests in three directions using methane as permeating fluid	52
Table 5.5 Average permeability at 1 MPa water pressure for the facies types tested	54
Table 5.6 Liquid equivalent permeability ranges obtained under a constant 4 MPa hydrostatic stress	57
Table 5.7 Liquid equivalent permeability ranges in three dimensions for methane as the permeating fluid at hydrostatic pressures of 4, 8, 12 and 16 MPa	62
Table 5.8 Table showing the percentage error introduced by varying the inlet gas pressure for a specific sample	64
Table 5.9 Table showing the variation in k_s due to errors in the factors used to calculate it	65
Table 5.10 The influence on the k_{fo} at different hydrostatic stresses due to variations in the factors used to obtain it	66

CHAPTER 1

INTRODUCTION

Majuba Colliery which is owned by Rand Coal (Pty) Ltd was commissioned as one of the collieries to supply Majuba power station with coal. Shortly after operations commenced the mine started to experience roof instability and roof falls thought to be caused by fluid (methane and water) building up excessive pressures in the roof strata of the mine workings. The flow of methane and water may be induced by the excavation of a mine opening in methane-bearing strata. Methane flow into mined openings constitute one of the biggest hazards in the coal mining industry. It is poisonous to humans and can ignite at concentrations as low as 5% per volume and create explosions in the presence of coal dust from mining. If the flow of methane and/or water into the mine opening becomes blocked by an impervious layer, excessive pressures may develop, particularly in the roof strata of the mined seam, which can lead to roof falls. The Department of geology and applied geology of the University of Natal was approached to carry out an initial investigation into the character of the fluid flow into and around the mine openings. It was decided that permeability tests on the roof strata of the mined coal seam was the easiest way to achieve this. To this end a series of experiments were devised to test the geotechnical properties and the permeability of the roof strata (Jermy and Venter, 1993) and relating the results to specific facies types.

Majuba Colliery is located roughly halfway between Amersfoort and Volksrust in the south-eastern Transvaal (figure 1.1). Unfortunately, due to a variety of factors, the mine is no longer active and was closed in mid 1993. The results and techniques in this study, however, are still thought to be of value to mines experiencing similar problems. The results are further of interest because, to the best of the author's knowledge, no other published data of experiments of the nature described in this document exist on the coal-bearing strata of the eastern Transvaal, or indeed in South Africa.

The permeability of the different facies types comprising the roof strata of the mined seam were tested towards methane and water. Their permeability towards nitrogen was also tested because it is less hazardous to work with than methane and in some instances can form a part of the "fire damp" that flows into coal mine openings (Cyrul, 1989). The permeabilities were determined under atmospheric conditions as well as under triaxial conditions to simulate the underground stress regime.

The results obtained can be used in a variety of ways. In terms of roof falls they can point to areas where possible fluid pressure build-up can be expected, i.e. areas of low permeability overlain by areas of relatively high permeability. The permeability data can be used to divide the facies types into possible sources, conduits and barriers to the fluid flow. The usual practice, if an area of high pressure build-up is identified, is to drill a series of holes into the strata and 'bleed' the pressure off. The

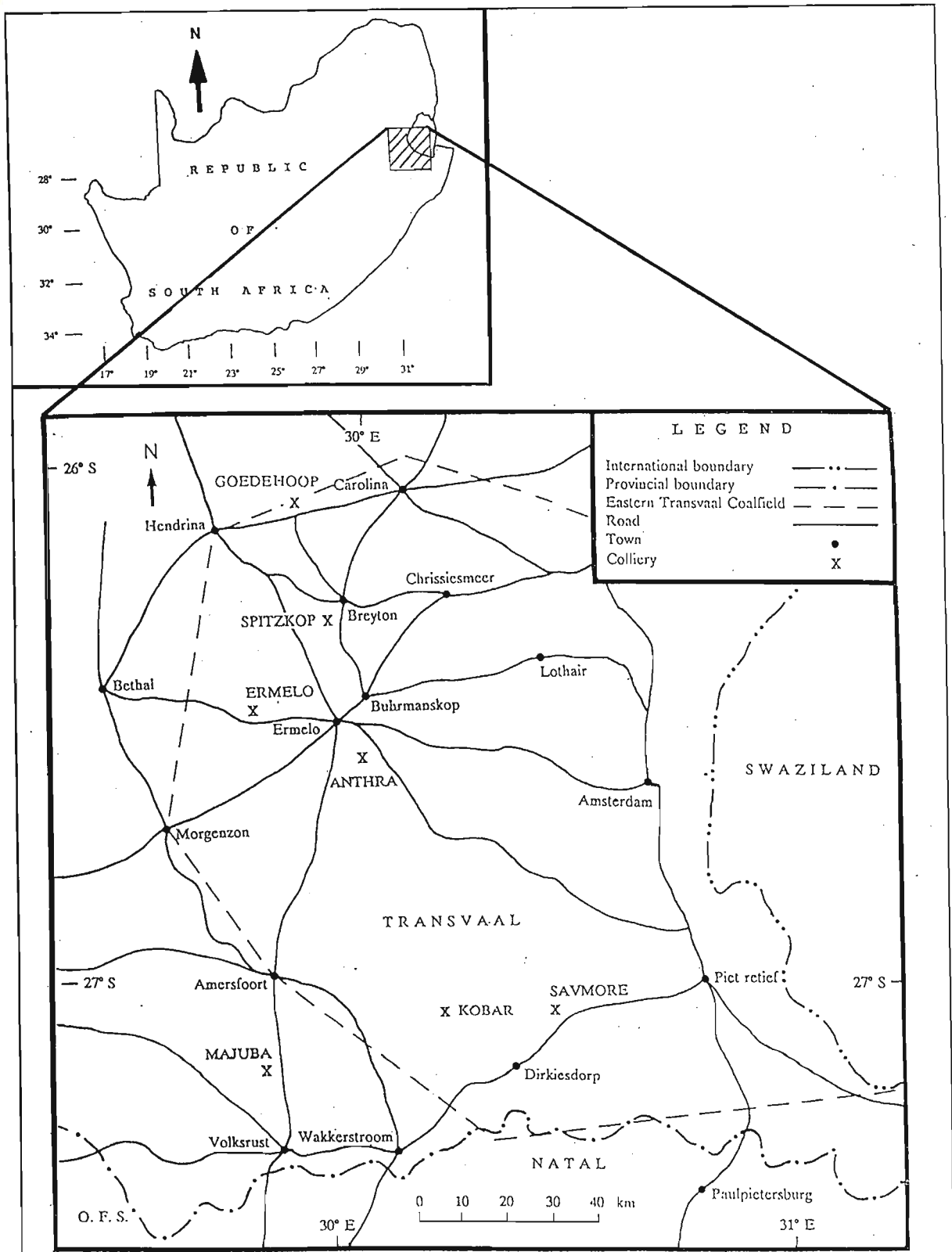


Figure 1.1 Map showing the locality of Majuba Colliery within the Eastern Transvaal Coalfield (after Cadle *et al.*, 1990).

permeability values could be used here to help design the extraction in terms of the length and spacing of the holes because if the permeability could be used to identify the strata blocking the fluid and the strata feeding the area with gas. If a relationship between the permeability and the facies type could be established and a chart or a graph compiled, an idea of conditions in front of the face could be formed without having to take the time to test the permeability of the facies types, it could just be read off the chart or graph. The relationship of permeability with facies types, specifically toward methane, is also important in other areas of the coal mining industry. It could provide useful information on the possible locality of source areas of methane gas which could be commercially extracted, mainly as an energy source. In conjunction with adsorption-desorption data such information could be used to plan the best locations for well development if methane is extracted. Initially the aim of the project was to establish a hazard prediction chart whereby a potential zone of pressure build-up is identified by testing the permeability of core extracted from exploratory drilling in advance of the mining face. Being able to predict methane pressure build-up zones can also help in the prevention of outbursts from the mining face and the information could also aid the design of the drilling programme used to release the pressure before it reaches a critical value. Due to the extremely variable nature of the sediments the emphasis of the project shifted towards the creating of a permeability versus facies type database for the study area rather than a hazard prediction table for the whole Vryheid Formation.

CHAPTER 2

GEOLOGY

2.1. INTRODUCTION

In characterizing the flow or permeation of a fluid through a sediment the two factors that have the biggest influence on the behaviour of the fluid are the character of the fluid and the character of the rock. The internal character of the rock is described by its mineralogy which in turn is the result of the external geological processes that played a role in its formation. Large scale geological factors such as depositional environment, stress history and depth of burial all play a role in determining the flow regime into and around a mine opening.

The permeability of a porous medium, such as a sandstone, is an important physical property of that sandstone that controls the behaviour of a fluid that permeates through that sandstone. The permeability of natural porous media is strongly influenced by variations in the geology of that medium on all scales (Bass, 1987).

Flow or permeation of a fluid around the grains and through the pores of a sediment, called the intergranular permeability (Harpalani and Schruafnagel, 1989), is controlled by factors such as grain size, grain size distribution, packing, angularity and degree of cementation between the grains. Flow on the scale of the grain size might be totally overshadowed by the flow through larger scale structures such as fissures, joints and fractures within the rock (Brace, 1977). Permeability due to these larger scale structures can seldom be investigated in the laboratory due to the size of the samples involved.

Samples used in this study were obtained from the core of six boreholes drilled through the roof strata associated with the Gus coal seam in the area of the Majuba Colliery lease. The lease area is located within the Eastern Transvaal Coalfield (figure 1.1). The Eastern Transvaal Coalfield covers an area of 150 km north-south by 75 km east-west. The coalfield lies between the towns of Carolina in the north and Dirkiesdorp in the south. On the western side it is flanked by the Witbank and Highveld coalfields, and by the Klip River and Utrecht coalfields in the south. The Eastern Transvaal Coalfield is predominantly underlain by the rocks of the Vryheid Formation, Ecca Group, Karoo Sequence (Greenshields, 1986).

According to Greenshields (1986) the stratigraphy is typical of the coal-bearing margins of the Karoo Basin. Pre-Karoo basement is overlain by Dwyka Formation diamictites followed by Ecca Group sediments, with limited occurrences of Beaufort Group sediments in the southern highland areas. The topography is typical Highveld, with low undulating hills capped by dolerite, effectively varying the depth

at which the coal seam occur between different mining areas (Greenshields, 1986).

2.2. KAROO SEQUENCE

The name "Karoo" was first used by Bain in 1856 to describe the strata overlying the extensive tillite horizon, now named the Dwyka Formation (SACS, 1980). Sediments of the Karoo Sequence were deposited in, and into, a large body of water, possibly marine (Cadle *et al.*, 1990). The basin into which these sediments were being deposited was quite large and today the sediments cover an area of roughly 550 000 km² on the southern African mainland (figure 2.1).

In the south the basin is bounded by the mountain chain of the Cape Fold Belt. In the north the sediments lap onto the Kaapvaal Craton. A cross-section drawn from north to south show the basin to be asymmetric, with the thickest succession of sediments towards the south (figure 2.1). Cadle *et al.* (1990) states that the proximity of the basin to a mountain range and its asymmetrical shape classifies it as a foreland basin. The reason for the asymmetry is that the southern margin was tectonically still active during the depositional stages whereas the Kaapvaal Craton in the north was already stable in that time. Accordingly most of the sediment was transported in from the south, with only a minor component from the north (Cadle *et al.*, 1990).

Deposition of the Karoo Sequence sediments started with the melting of the glaciers that covered most of the African subcontinent in the Carboniferous, around 340 million years ago. The melting of the glaciers resulted in the deposition of an extensive tillite horizon, called the Dwyka Formation. Following the retreat of the glaciers the basin was transgressed by the Ecca sea, with active sediment fill from the south and north (Cadle *et al.*, 1990). As the climate slowly warmed the sediment style became more terrestrial. The major depositional style in the Beaufort Group is fluvio-deltaic. Sediment deposition actively continued until it was interrupted by the outpouring of the Drakensberg lavas in the mid Jurassic, roughly 170 million years ago (Cadle *et al.*, 1990).

Economic exploitable coal seams of Permian and Triassic ages occur within the strata that make up the sequence (figure 2.1). The climate, tectonic framework and depositional style in the Permian were much more conducive to extensive peat formation and ultimately economic exploitable coal seams than in the Triassic (Cadle *et al.*, 1990). Coals of Permian age therefore have a greater significance regarding mining. The Permian coals and the Vryheid Formation strata in which they occur are mostly confined to the northern and northeastern regions of the Karoo basin (Cadle *et al.*, 1990). The Volksrust Formation is mostly present along the western and southern escarpment and isolated occurrences of the Beaufort Group are encountered on the high ground towards the southern part of the coalfield. In the central part the Dwyka Formation and the Pietermaritzburg Formation are thin or absent. The

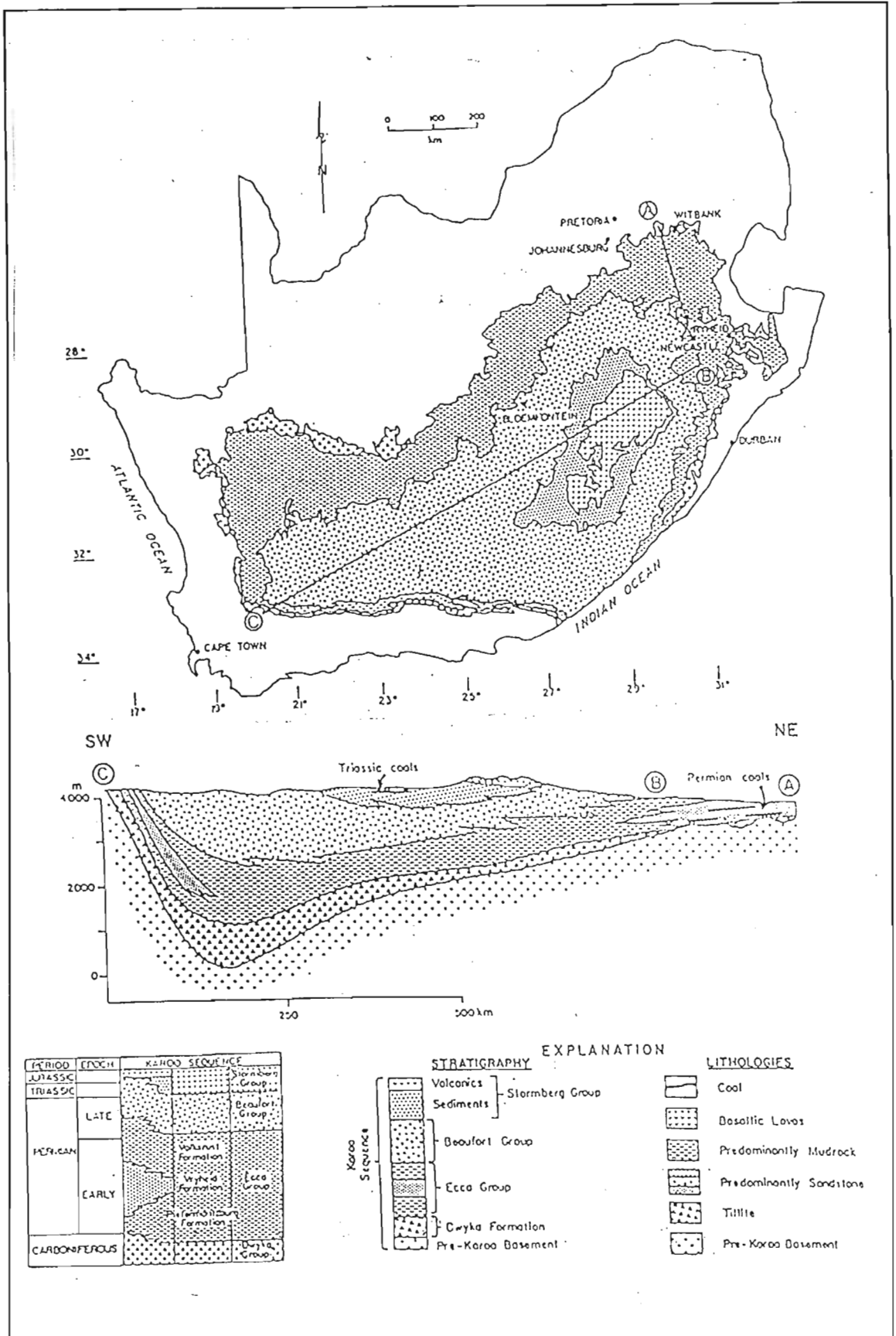


Figure 2.1 The Karoo Basin: Distribution, stratigraphy and geographic positions of the associated coal-bearing strata (after Cadle *et al.*, 1990).

distribution of the different groups and formations over the coalfield are mainly the result of basin topography and modern day erosional surfaces, according to Greenshields (1990). The thickness of the Karoo sediments varies over the whole area of the coalfield but thickens towards the south.

2.2.1. Ecca Group

During the Early Permian deep marine shales, submarine-fan sediments and shelf shales were deposited along the southern margin of the Karoo basin. At this time the sediments from the northern, more passive margin, were more shallow water, deltaic and fluvial sediments with associated coal seams (Cadle *et al.*, 1990). All these sediments together make up the Ecca Group. Sediments of the Ecca Group attain a maximum thickness of over 400 m (SACS, 1980).

The Ecca Group sediments can be subdivided into three distinct formations (from old to young): the Pietermaritzburg, the Vryheid, and the Volksrust formations (SACS, 1980). The Pietermaritzburg and Volksrust Formations merge southwards to form the central Ecca shale facies and represent shales deposited on the marine shelf. The Vryheid Formation on the other hand comprises a series of alternating conglomerates, sandstones and shales within which the coal seams are found. The sandstones are predominantly developed only at the margin of the basin (SACS, 1980). The marine shales of the Volksrust Formation grade up into the terrestrial sediments of the Beaufort Group, reflecting the climatic change (Cadle *et al.*, 1990). The Ecca shales are characteristically dark grey and carbonaceous. In the north-eastern part of the basin, i.e. the area covered by the Eastern Transvaal Coalfield, the sandstones are cross-bedded and consists of upwards fining cycles (SACS, 1980).

Greenshields (1986) states that at least four major cyclothems, each with an associated coal seam, occur in the Ecca Group. They are commonly called the "coal measures of South Africa" and crop out in the mountains near the town Vryheid, and so were named the Vryheid Formation (SACS, 1980).

2.2.2. Vryheid Formation

The tectonic style changes from east to west and from north to south in the Karoo Basin. These factors are the main control on the distribution and stratigraphic thickness of the formation. The Vryheid Formation pinches out northward as a result of the asymmetry of the basin (figure 2.1).

The Vryheid Formation consists mainly of sandstone and shale with some subordinate coal seams associated with it (SACS, 1980). The sediments of the Vryheid Formation probably represent alluvial plain, upper and lower delta plain deposits with associated shallow lagoon and coastal swamps (Jermy and Bell, 1990). The change from stable margin to subsiding foreland basin confined the Vryheid

Formation and the shales of the succession to "pinch-out" to the north. This "pinching-out" results in a gradation of a fluvial valley-fill sequence into sediments of deltaic origin (Van Vuuren, 1981). According to Cadle *et al.* (1990) the sandstones become interfingered with the deeper water shales, a so-called "shale-out", approximately 500 km from the present northern basin margin. They state that this is due to rapid basinward facies migration down the southerly dipping paleoslope.

The Formation attains a maximum thickness of 500 m in the deeper part of the basin (SACS, 1980), but in the area of the Eastern Transvaal Coalfield only attains a maximum thickness of 170 m (Greenshields, 1986) and thins to about 80 m in thickness in the proximal basin settings (Cadle *et al.*, 1990).

The Vryheid Formation contains 5 major coal seams, with locally developed partings and splits in the coal seams increasing the number to 8, within an 85 m thick stratigraphic horizon (Greenshields, 1986) although this horizon can attain thicknesses up to 160 m in the deeper parts of the basin (Cadle *et al.*, 1990). According to Cadle *et al.* (1990) all five major seams are still present in the thinnest and most proximal parts of the formation. Greenshields (1986) states that all four cyclothems exhibit a regressive phase where sedimentation occurred in fluvio-deltaic environments, followed by a transgressive phase where sedimentation was typical of both marine and non marine transgressive shorelines. A seam is therefore associated with clastic successions comprising carbonaceous shale or siltstone, fine to coarse grained sandstone and minor conglomerate (Cadle *et al.*, 1990).

Although the five major coal seams, and their associated overlying and underlying sedimentary packages, can be correlated between coalfields (Cadle *et al.*, 1990), they have different names in different coalfields (Greenshields, 1986). Table 2.1 draws a correlation between the names used in the different coalfields.

Greenshields (1986) states that the mining potential of the seams varies throughout the area but that the C seam has the biggest potential, although the B and E, and occasionally the D, seams attain mineable thicknesses over limited areas. The general distribution of the upper seams is often restricted by present-day topography, while the development of the lower seams is controlled by the pre-Karoo topography. Structurally the seams are flat-lying with a gentle south-westerly dip (Greenshields, 1986). The Dundas, Gus and Alfred seams are present in the Majuba Colliery mining area, but only the Gus seam is exploited by the colliery (Lear and Hill, 1989).

2.3. THE GEOLOGY AT MAJUBA COLLIERY

The complex geological history of the area led to the deposition of a large number of different

Table 2.1 Correlation between coal seams in different coalfields (from Greenshields, 1986)

Highveld Coalfield	Eastern Transvaal Coalfield		Utrecht Coalfield
	Northern half	Southern half	
No. 5	A	Eland	Eland
No. 4A	B	Alfred	Alfred
No. 4 Upper	C	Gus	Gus
No.4 Lower	C Lower	Dundas	Dundas
No. 3	D	Coking	Coking
No. 2	E	Targas	Targas

lithologies. Correlation of the engineering properties of the different lithologies encountered in the borehole cores led to their subdivision into four facies groups (Ward and Jermy, 1985; Jermy and Bell, 1990). These are called the arenaceous, argillaceous, diamictitic, organo-chemical, and heterolithic groups. Twenty-four facies types have been identified from the sediments in the four facies groups. Table 2.2 presents a list of the eleven facies types, and their descriptions, sampled in this study. This ignores the presence of numerous dolerite sills and dykes present in the mining area. A sill of over 170 m in thickness overlies the whole sedimentary package into which the six boreholes were drilled (appendix A).

The Dundas, Gus and Alfred seams are all present in the Majuba Colliery mining area, but only the Gus is mined (Lear and Hill, 1989). The sediment directly overlying the Gus seam is very important to this study as it would indicate if methane can flow into the mine opening through it or if it would block the migration of methane into the mine. A variety of facies types overlie the Gus seam, notably: cross bedded coarse grained sandstone (ARF39), fine grained sandstone with some argillaceous partings (AH 55 to 59), cross bedded fine grained sandstone (AH 58), cross bedded fine grained sandstone (AH 60), medium grained sandstone (AH 53) and cross bedded medium grained sandstone which becomes more argillaceous toward the roof of the Gus seam.

The samples were obtained from nearly 170 m of borehole core and two bulk samples from the immediate roof of the Gus seam. The core was obtained from five 10 m long holes drilled vertically up from the roof of the Gus seam (boreholes AH 53, AH 55, AH 58, AH 60 and AH 61) and one, nearly 400 m long vertical hole drilled from the surface to 4 m below the Dundas seam (ARF 39). The logs of the latter is reproduced in Appendix A and the logs of the five short holes are reproduced in Appendices B through F (after Jermy and Venter, 1993).

Table 2.2 Description of tested facies (after Jermy and Bell, 1990)

Facies	Description
2	Lenticular bedded mudrock
3	Alternating layers of mudrock and sandstone.
4	Flaser bedded sandstone.
5	Ripple cross laminated sandstone with grit.
7	Massive fine grained feldspathic sandstone.
8	Cross laminated fine grained feldspathic sandstone.
9	Massive medium grained feldspathic sandstone.
10	Cross laminated medium grained feldspathic sandstone.
11	Massive coarse grained feldspathic sandstone.
12	Cross laminated coarse grained feldspathic sandstone.
14	Sandstone with carbonaceous drapes and slump structures.
22	Coal, mixed dull and bright.

The two bulk samples (plates 2.1 and 2.2) were of facies type 10. Plate 2.1 show the micaceous foresets of the trough cross beds. The darker band on the bottom of the sample is a small argillaceous band (facies type 3). The transition from facies type 3 to facies type 10 is delineated by a very sharp discontinuity. The sandstone of facies type 10 is most probably part of a river channel cutting into the peat/mud deposit constituted by facies type 3 in plate 2.1. Plate 2.2 shows the through cross beds from a different angle. Here it can be seen clearly that the grain size is very variable in the same facies type.

2.4. COAL CHARACTERISTICS

Not much information has been published on the coals occurring in the Eastern Transvaal Coalfield. The usual practice is to equate the properties of the coals in this area with the data available from the Transvaal and Witbank coalfields for which more information is available (eg. Greenshields, 1986; Cadle *et al.*, 1990). According to Cadle *et al.* (1990) the Permian age coal seams are richer in mineral matter and more variable in type, organic matter and rock than coals in the northern hemisphere. In particular the Vryheid Formation coals are characterized by much higher internite content than their northern hemisphere counterparts. The coals range in rank from sub-bituminous to mid-bituminous, progressing to meta-anthracite locally (Cadle *et al.*, 1990).

Extensive intrusion of the Vryheid Formation by dolerite dykes and sills in the Jurassic, coupled

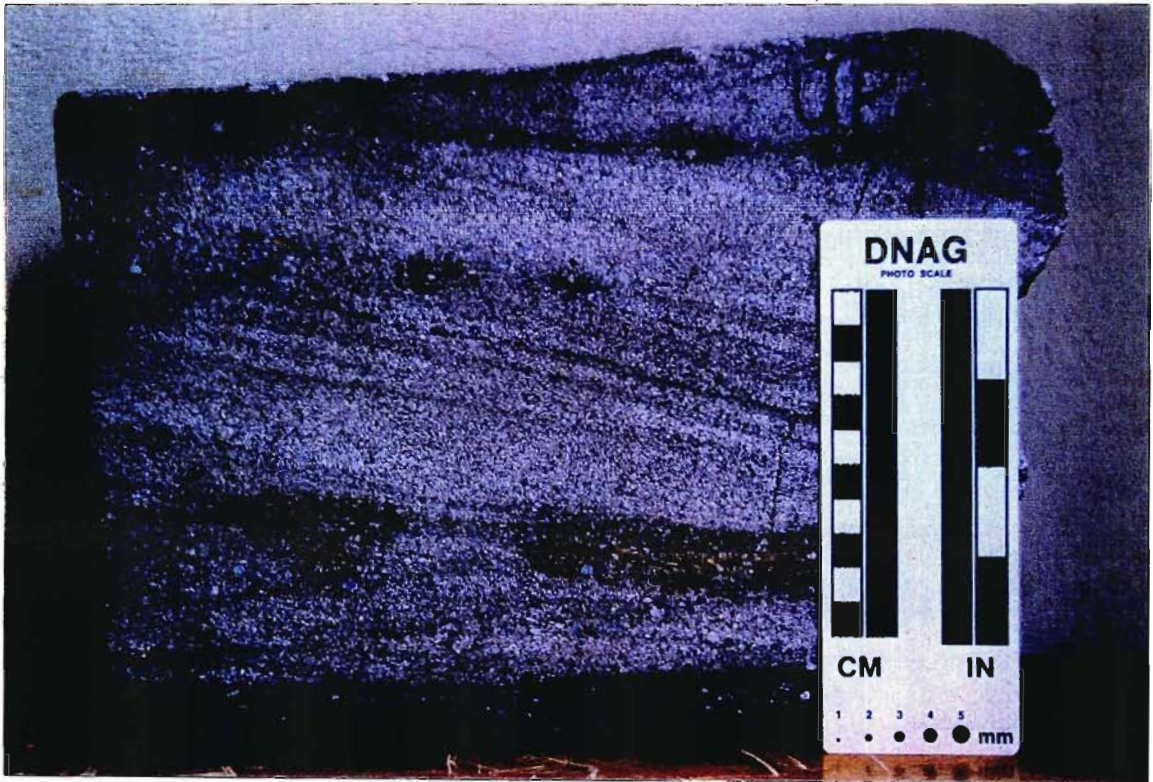


Plate 2.1 Bulk sample from roof of Gus coal seam showing trough cross bedding of facies type 10. Orientation of sample shown by arrow.

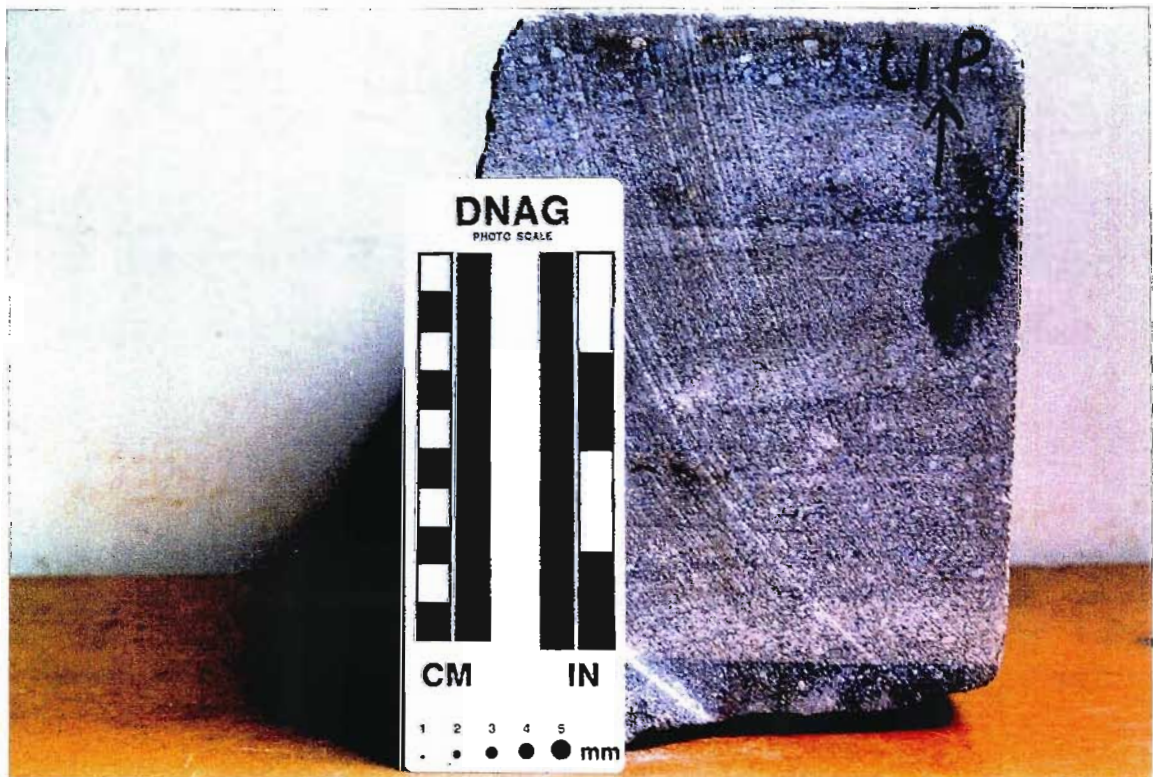


Plate 2.2 Bulk sample from roof of Gus coal seam showing variability in grain size for the same facies type. Arrow shows orientation of sample.

with changes in peat depositional settings, resulted in significant changes in grade, type and rank between and within the different coal seams of the area (Cadle *et al.*, 1991). This might be the reason why only two coal mines in the Eastern Transvaal Coalfield produce anthracite grade and most others produce bituminous coals (Anon, 1987). Average analyses of bituminous coal from the seams that were actively exploited in 1986 within the boundaries of the Eastern Transvaal Coalfield are presented in table 2.3. No information has been published for Majuba Colliery and their effect on the permeability could therefore not be investigated in this study.

Table 2.3 Average analysis for the coal seams mined in 1986 in the Eastern Transvaal Coalfield (from Anon, 1987).

Colliery	Calorific Value MJ/kg	Air-dry values				
		H ₂ O %	Ash %	Volatile Content %	Fixed Carbon %	Total Sulphur %
Ermelo	28.0	3.1	13.1	30.0	53.8	0.85
Goedehoop	29.7	2.4	10.3	30.5	56.9	0.79
Kobar	26.8	2.9	16.2	21.5	59.3	0.80
Savmore	28.0	3.6	12.6	29.0	54.9	0.77
Spitzkop	27.3	3.1	14.7	28.9	53.3	1.23

2.5. PETROGRAPHY

A number of thin sections were cut from samples for which the permeability had been determined toward nitrogen, methane and water. All the facies types used in the tests, except coal, were sampled. Most of the minerals could easily be identified by petrographical microscope, but some of the minor constituents could only be identified by scanning electron microscope.

Plate 2.3 shows a photomicrograph of a typical sample of facies type 10 (table 2.2). The basic mineral assemblage is as follows:

- A. Quartz.
- B. Plagioclase feldspar.
- C. Microcline feldspar.
- D. Detrital biotite.
- E. Detrital muscovite.

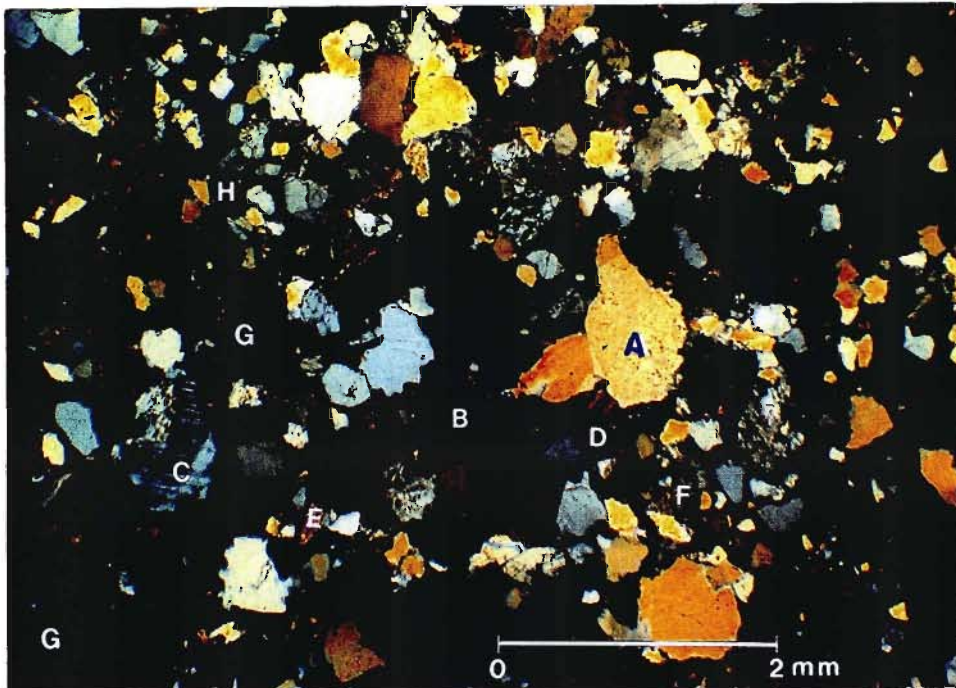


Plate 2.3 Photomicrograph of facies type 10. Magnification = 18.24x. A = Quartz, B = Plagioclase feldspar, C = Microcline feldspar, D = Detrital biotite, E = Detrital muscovite, F = Secondary biotite, G = Argillaceous minerals and H = Zircon.

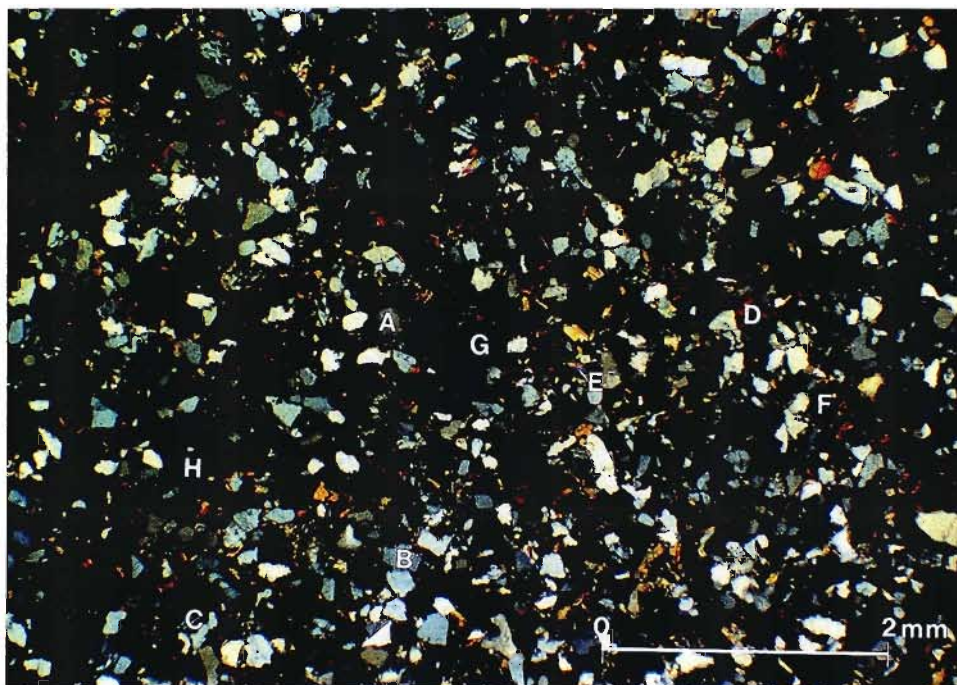


Plate 2.4 Photomicrograph of facies type 5. Magnification = 18.24x. A = Quartz, B = Plagioclase feldspar, C = Microcline feldspar, D = Detrital biotite, E = Detrital muscovite, F = Secondary biotite, G = Argillaceous minerals and H = Zircon.

Additional to this assemblage, minerals such as secondary biotite (F), some clay minerals (G), zircon (H), garnet and cordierite (neither visible in photomicrograph). The basic assemblage, however, were found to remain the same in all facies types, as can be seen in plates 2.3, 2.4, 2.5 and 2.6 (facies type 10, 5, 7 and 12 respectively), except that average grain size increases with increasing facies number. The sorting appears to decrease steadily from facies 5 (plate 2.4) to facies 12 (plate 2.6). This results in a better packing with increase in facies number. The facies types that are coarser grained than facies type number 9 have a more bi-modal grain size distribution. The ratio of primary to secondary biotite visible in the section is determined by the orientation relative to the trough cross bedding planes in which the section was cut. Each trough cross bed is delineated by a thin layer of micas. Due to diagenesis the clastic grains were punched through the biotite/muscovite layer and it appears that the clastic grains are cemented by primary biotite if the section is cut nearly parallel to the bedding planes. In the cases where the secondary biotite is more predominant, the section was cut perpendicular to the bedding planes. Secondary biotite could also be the result of alteration of argillaceous material due to the heat generated by > 170 m dolerite sill overlying all the sediments investigated.

Cracking of grains is common (eg. grain A, plate 2.3), but no cracks running through the whole sample were observed under the microscope. Cracks of any nature may play a role in increasing the permeability, so if the cracks pre-date the mining and sampling they are contributing to the real permeability of the sample, whereas if they were post extraction the measured permeability could be incorrect. The cracks in the grain are closed, but not infilled. This could be the result stress release due to mining or due to the extraction by drilling. If these cracks were formed during the deposition they most probably would have been infilled. If the stress difference between the *in situ* regime and atmospheric was large the cracks would have extended through the sample and not been confined to a few grains. This could also be because the sediments are poorly to moderately cemented meaning that any stress release would not produce visible cracks as the grains can move to a limited extent. The cracks in grain A (plate 2.3) could also be caused by the cutting and polishing of the sample and the thin section.

No measurement of the pore size and the amount of interconnection between the pore spaces were carried out, but increased sorting and decrease in packing with increase in grain size is thought to be responsible for the increase in permeability with increase in grain size. The mineralogy of the samples is very complex and the influence of the variable nature of the sediment on the permeability will become apparent in chapter 5.

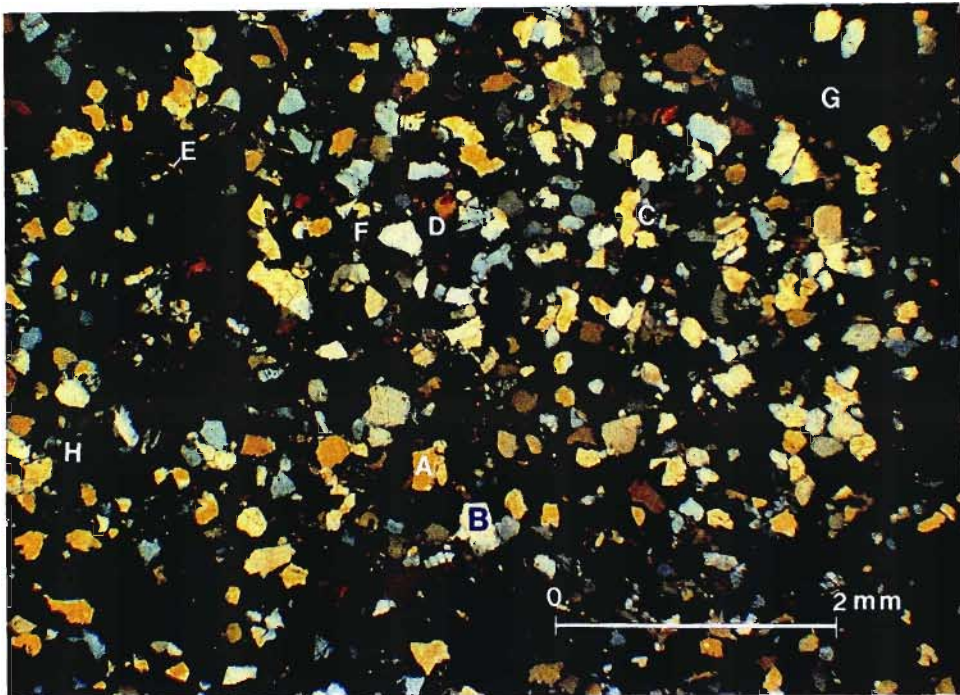


Plate 2.5 Photomicrograph of facies type 7. Magnification = 18.24x. A = Quartz, B = Plagioclase feldspar, C = Microcline feldspar, D = Detrital biotite, E = Detrital muscovite, F = Secondary biotite, G = Argillaceous minerals and H = Zircon.

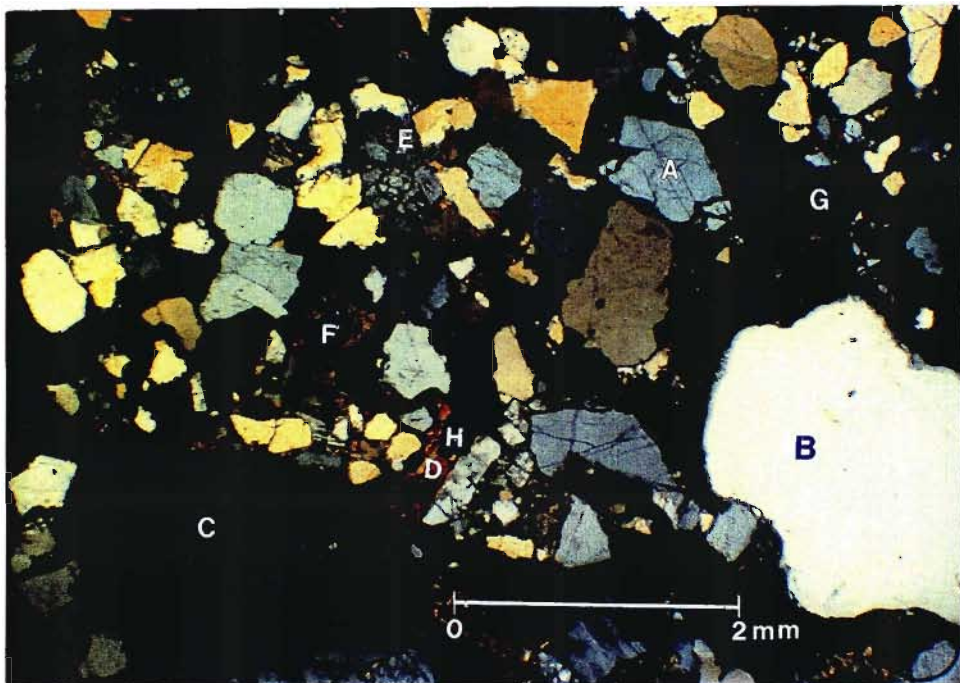


Plate 2.6 Photomicrograph of facies type 12. Magnification = 18.24x. A = Quartz, B = Plagioclase feldspar, C = Microcline feldspar, D = Detrital biotite, E = Detrital muscovite, F = Secondary biotite, G = Argillaceous minerals and H = Zircon.

CHAPTER 3

THEORETICAL CONSIDERATIONS

3.1. INTRODUCTION

For a fluid to flow through a porous medium, the pores must be interconnected to some degree. The measure of the resistance to flow of the fluid by the medium is called its permeability. The permeability of a porous medium can therefore be defined as the quantity of fluid that flows through a unit thickness of a porous medium in a unit time (eg. Bass, 1987). Many different types of permeability exist, but only three types are referred to in this study: "specific" permeability, "liquid equivalent" permeability and "relative" permeability. The permeability of a sample towards a specific fluid, at a specific fluid pressure, is called the specific permeability of that sample, k_s , (Bass, 1987). At infinite high gas pressure the permeability of a sample towards a specific gas approaches the permeability of that sample towards a liquid, i.e. it is the liquid equivalent permeability of that sample, k_{le} (Klinkenberg, 1941). The liquid equivalent permeability is obtained by plotting the specific permeability of a sample measured at a series of gas pressures against the reciprocal mean gas pressures and fitting a best fit line through the points. The best fit line is then extrapolated to infinite high gas pressure, i.e. the y-axis intercept (ASTM, 1990). The y-axis intercept is then taken as being equivalent to the liquid equivalent permeability (figure 3.1). If a fluid, such as water, partially fills the pores of a porous medium and a second fluid, such as methane, flows through the medium, no absolute specific permeability can be determined, so the permeabilities of the two fluids are expressed relative to each other. The permeability of the sample is then expressed as the relative permeability of the medium towards methane (gas), k_{rg} , and the medium's relative permeability to water, k_{rw} (Paterson and Meany, 1991).

A number of approaches can be used to characterize the flow of a fluid through a porous medium (Gawuga, 1979):

- a. Experimental (Based on Darcy's law).
- b. Theoretical (Based on Poisseuille's law).
- c. Semi-empirical (Based on the approaches of either Adzumi or Klinkenberg).

Experimental methods have the advantage that they give results directly, but the results may have to be scaled up from the laboratory scale to reality. Theoretical methods depend on the mathematical description of the internal structure of the porous medium and the type of flow at each point in the sample (Dullien, 1979). Such models can be very complex and direct results may be impossible to obtain. Semi-empirical methods are generally considered to give the best results. The methods usually involve measuring the flow induced by setting up a pressure gradient across the sample and then calculate the permeability with an empirical formula. Adzumi and Klinkenberg both reached the same conclusions but

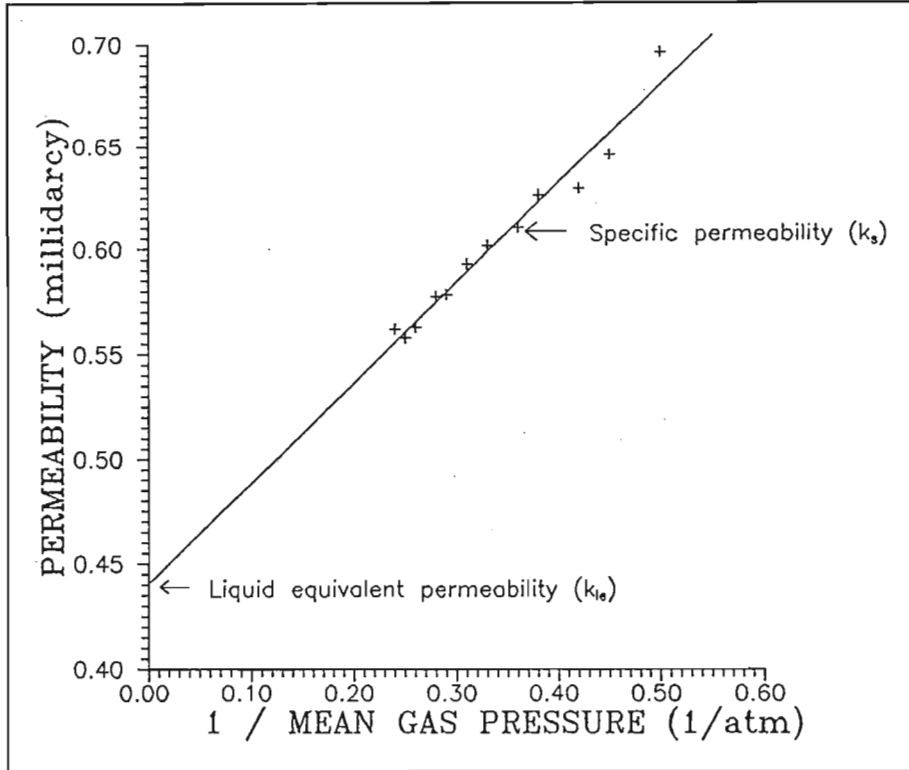


Figure 3.1 Plot of permeability versus $1/P_m$ illustrating the relationship between k_s and k_{le} . Facies 10, where methane was the permeating fluid.

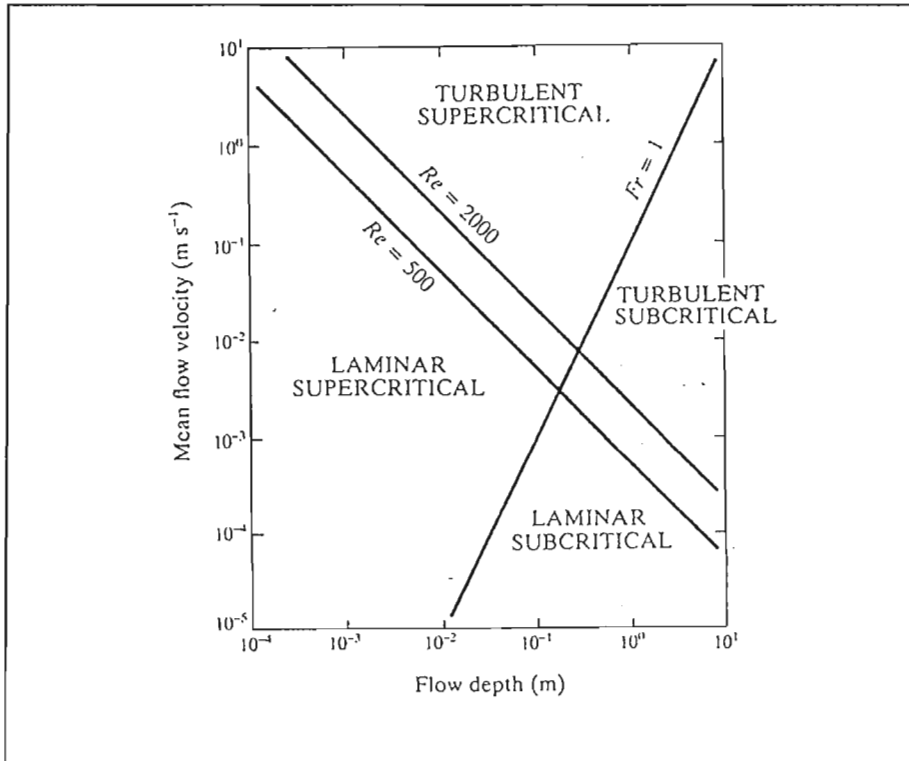


Figure 3.2 Regimes of free-surface flow in terms of critical Reynolds numbers (after Allen, 1985).

Klinkenberg's approach was more experimental, whereas Adzumi's approach was more theoretical. In this study experimental methods based on Darcy's law and Klinkenberg's approach have been used. The methods used are discussed in the next chapter. This chapter discusses some of the more important theoretical aspects of both the mathematical and experimental methods.

3.2. THEORETICAL MODELS FOR FLOW THROUGH POROUS MEDIA

To theoretically predict the permeability, a model of the internal structure of the medium must first be mathematically described (Dullien, 1979). The closer the model resembles the porous medium, the higher the degree of confidence that can be placed on the value obtained from that model. Most authors, however, agree that to model the pore structure of a natural porous medium, such as a sandstone, in three dimensions results in very complex mathematical formulations. Modelling the internal structure of a porous medium describes the path the fluid will follow when flowing through the medium, but the flow might be of different types at different points in the medium. This must also be taken into account when using mathematical models to predict the permeability of a porous medium. The flow could be one of the following types (Gawuga, 1979):

- Laminar flow (Poiseuille's law).
- Turbulent flow.
- Molecular streaming (Knudsen's law).

Knudsen's law describes the behaviour of a kinetic layer near the interface between a fluid and a solid (Bradey and Boss, 1988). Laminar and turbulent flow describes the flow conditions in the centre of the flow channel, in this case the pore space. At some point in any system flow will pass from laminar to turbulent (Scheidegger, 1974). In an open channel this point is considered to lie between a Reynolds number, Re , of between 500 and 1000 (Allen, 1985), as is illustrated in figure 3.2. The Reynolds number represents the kinematic viscosity in the fluid, i.e. the energy state (Waltz, 1976). The higher the internal energy of the fluid the more turbulent and unsteady the flow becomes.

Mathematical models are therefore developed for the movement of the fluid relative to the particles (or grains) of the medium; for the movements of the particles (or grains) of the medium relative to the fluid; and for the movement of the particles of the fluid in the fluid-solid boundary regions (Stevenson and Scott, 1991). A series of matrix equations, the Navier-Stokes equations, were developed to describe the motion of the fluid around a single grain, and the motion of the solid is expressed by Hooke's law.

Desai (1975), on the other hand, suggests that a number of assumptions must first be made in order to reduce the complexity of the calculations and to make the solid-fluid system more

understandable. These assumptions are:

- The medium is rigid and continuous.
- The fluid is homogeneous and incompressible.
- The flow is continuous and non-rotational.
- Capillary and inertia effects are negligible.

Such stringent conditions very seldom exist in nature. Most procedures and models are therefore based on the semi-empirical equation of Darcy (eg. Desai, 1975; Scheidegger, 1982).

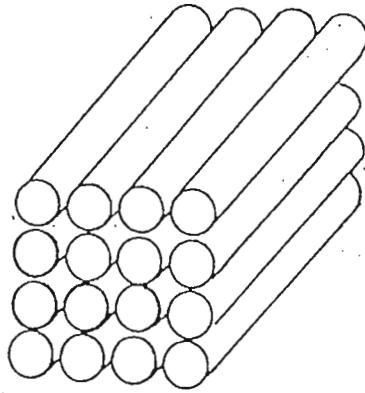
Flow in a geological environment occurs on two distinct scales: the macro- and the micro-scale (Stevenson and Scott, 1991). The macro-scale is concerned with flow through openings, cracks and fissures that can be observed by the naked eye, whereas the micro-scale flow is the flow in and around grains which can only be seen under magnification by hand lens or microscope. In most instances the macro-scale flow surpass the micro-scale flow by several orders of magnitude. Theoretical and laboratory investigations can very seldom include macro-scale flow, so some sort of conversion factor must always be used to scale the laboratory and theoretical finding up to *in situ* conditions (Stevenson and Scott, 1991).

The easiest way to visualize the internal structure of a porous medium for theoretical description, is a series of straight, circular tubes (capillaries on the scale of a laboratory sample) arranged on a square lattice (Scheidegger, 1974). Such a configuration is called an "idealized porous medium" and is illustrated in figure 3.3.A. If the fluid flowing through the configuration as shown in figure 3.3.A is considered to be incompressible, viscous and flowing steadily, an exact mathematical solution for the permeability can be obtained (Stevenson and Scott, 1991). The average of all the flows through all the capillaries is taken as representative of the macroscopic flow. This, according to Gray, Fatt and Bergammi (1963), means that the permeability depends on the number of pore channels per unit area, perpendicular to the direction of fluid movement. The number of pore channels per unit area is then inversely proportional to the square of the sphere radius. The permeability can therefore be theoretically predicted if the total cross-sectional area of the capillaries (i.e. pore spaces) is known.

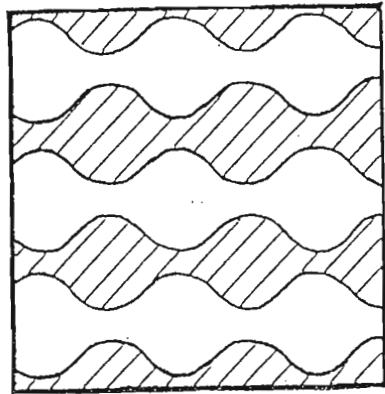
This treatment clearly results in an "idealized" permeability value. By varying the diameter of the capillaries and their orientation towards each other, a series of capillaric models can be described. Each different arrangement results in its own prediction of the permeability (Dullien, 1979). These models can be one-dimensional, in the case of the "bundle of capillary tubes" (figure 3.3.A). This model results in permeability predictions only in one flow direction (Scheidegger, 1974). Orientating a third of the capillaries in each of the three spatial directions, a two-dimensional model could be achieved. These are called parallel type models (figure 3.3.B). In order to make the models, in both cases, more realistic the diameter of the capillary tubes are varied along their lengths (figures 3.3.A and 3.3.B). The internal

A. STRAIGHT CAPILLARIC MODELS

UNIFORM DIAMETER

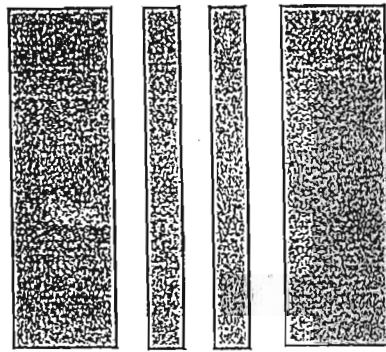


VARIABLE DIAMETER

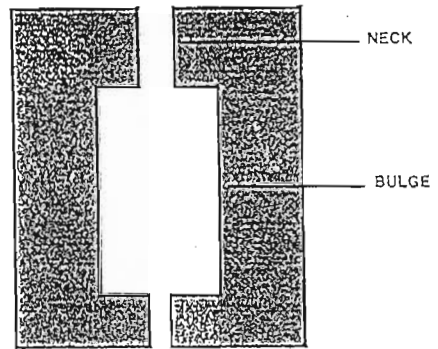


B. PARALLEL TYPE MODELS

UNIFORM DIAMETER

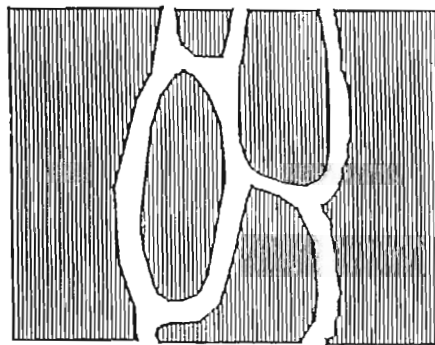


VARIABLE DIAMETER



C. NETWORK MODELS

REPRESENTATION OF THE INTERNAL STRUCTURE



"BRANCH-AND-NODE CHART"

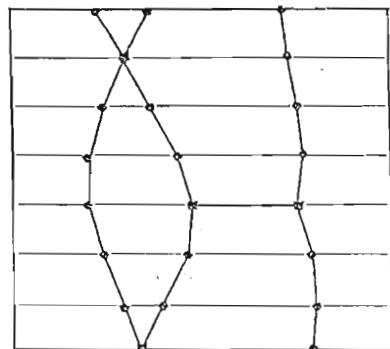


Figure 3.3 Various theoretical models for natural porous media used in the prediction of the permeability (after Dullien, 1979).

structure of the medium is then represented as a series of "necks" and "bulges". Large differences in the permeability predicted by such models are encountered when the diameter used in the calculation is that of a "neck" or that of a "bulge" (Dullien, 1979).

More realistic predictions of the permeability can be made by using three-dimensional interconnected capillary networks (figure 3.3.C). The representation of the three-dimensional internal structure of the medium, i.e. a sandstone made up of a series of irregular grains, can be transferred to a two-dimensional "branch-and-node" chart (figure 3.3.C). Each intersection of two or more capillary tubes as well as the diameter of any given capillary tube is given a specific mathematical value. By compiling the values as an imaginary fluid flows along a certain path, an approximation of the permeability can be made (Dullien, 1979). If the fluid is taken as flowing in such a way that it always selects the capillary tube with the largest diameter at each intersection, a permeability will be arrived at that is higher than if the fluid consistently chose the capillary tube with the smallest diameter. The permeabilities derived from these two cases are the extremes. Taking an average of such values calculated for each two-dimensional slice and then placing the values in a three-dimensional matrix, a very realistic value of permeability could be obtained. The largest failure of this model is it is nearly impossible to get an accurate representation of distribution and geometry of the grains and pore spaces within a natural substance such as a sandstone. By applying this approach, very good correlations between the theoretical and experimental permeability could be achieved (Dullien, 1979). This statement highlights the basic problem with any theoretical model: it has to be validated by experimental methods if it is to be of any use in practice.

3.3. THE THEORY OF LABORATORY PERMEABILITY MEASUREMENTS

Most laboratory techniques rely on Darcy's law or derivatives of that law for the calculation of the specific permeability of a porous medium (Scheidegger, 1974). Darcy's law assumes a linear relationship between quantity of flow and pressure gradient across the sample. It is now commonly realized that corrections have to be made to Darcy's equation if the fluid is incompressible, eg. a gas, and for physical effects such as pore geometry (Xue, 1991). For the most part, modifications to the law can be neglected, but when gas is used as the permeating fluid, Klinkenberg's effect should be taken into account and the equation modified accordingly. In its most basic form Darcy's law can be written as follows (Bass, 1987):

$$u_s = -\frac{k}{\mu} \left(\frac{\delta p}{\delta s} - g\rho \frac{\delta z}{\delta s} \right) \quad (3.1)$$

where: u_s = volume flux across unit area of the porous medium in unit time along flow path, s
(cm³/sec.)

- s = distance in direction of flow, always positive (cm).
 z = vertical coordinate, considered positive downwards (cm).
 ρ = density of the fluid.
 g = acceleration due to gravity (cm/s²).
 $\delta p/\delta s$ = pressure gradient along path s , at the point to which u_s refers.
 μ = viscosity of the fluid.
 k = permeability of the medium.
 $\delta z/\delta s = \sin \phi$, where ϕ is the angle between s and the horizontal.

Upon integration, equation 3.1 reduces to (Stormont and Daemen, 1991):

$$q = k \frac{\mu L}{A(P_1 - P_2)} \quad (3.2)$$

Equation 3.2 is valid for incompressible fluids, in the case of a compressible fluid, the second derivative of equation 3.1 is used to calculate the specific permeability (Stormont and Daemen, 1991):

$$q_e = -(k/\mu) \frac{(P_1^2 - P_2^2)A}{2P_0 L} \quad (3.3)$$

$$\therefore k = \frac{2q_e P_0 \mu L}{A(P_1^2 - P_2^2)} \quad (3.4)$$

- where: q_e = volumetric rate of flow at reference pressure P_0 (cm³/s).
 k = permeability in the direction of flow (Darcy).
 L = length over which the flow is measured (cm).
 μ = Viscosity of the fluid (cP).
 A = cross-sectional area across which q_e is determined (cm²).
 P_0 = reference pressure (atm).
 P_1 = upstream pressure (atm).
 P_2 = downstream pressure (atm).

Until 1941 the standard methods for the determination of the permeability of porous media were all based on the assumption that, as long as the rate of flow is proportional to the pressure gradient, the permeability constant of that medium is a property of that medium and is **not** dependent on the type of fluid used (Ohle, 1951). In 1941 Klinkenberg discovered that this was not the case for gases and that the permeability depended on the type of gas used.

Klinkenberg (1941) found that the only way to obtain a linear relationship from Darcy's law was to plot the permeability calculated by using equation 3.4 against the reciprocal mean gas pressure. This

method, according to Klinkenberg (1941), removes the effects of "gas slippage" and some of the effects of experimental error. Gas "slippage" occurs when the gas pressure increases to such an extent that a layer of gas molecules becomes compressed against the walls of the pores (i.e. grain boundaries). If the pressure on this gas layer becomes too high, the gas shears and the layer starts to move, or "slip". The effect is that abnormal permeability values are obtained, and is manifested in a non-linear permeability versus gas pressure graph, similar to the flow quantity versus pressure gradient graphs in figure 3.4.

Apart from influences such as the Klinkenberg effect (gas slippage), the physical measurement of permeability is a very straightforward process (Scheidegger, 1974). Many methods of determining the specific permeability, that is the ability of a formation to conduct or transport a specific fluid (Bass, 1987), are described in the literature. The methods fall into either one of two main categories; steady-state or transient pulse-decay, depending on the way the volume of fluid flowing through a sample is measured. If the measurement is made under a constant pressure differential across the sample it is labelled a steady-state method. If the change in pressure difference across the sample with time is measured, it is labelled a pulse-decay method (Jaeger, 1972).

3.3.1. Steady-state methods

Holder *et al.* (1988) state that steady-state methods involve the measurement of the flow rate of a sample under a constant pressure differential. Scheidegger (1974) asserts that the steady-state is characterized by the vanishing of the partial derivatives of physical quantities such as density and velocity from the first derivative of Darcy's equation (equation 3.1). The resulting equation for incompressible fluids is equation 3.2 and for compressible fluids it is equation 3.4. If the velocity vector is drawn at every point of a moving fluid, a vector field is obtained. If this vector field is independent of time, the flow is "steady" (Scheidegger, 1982). This is illustrated by figure 3.4.A.

3.3.2. Transient or pulse-decay methods

Pulse-decay methods, as opposed to steady-state methods, measure the time necessary for an applied fluid pressure to dissipate through a sample and equating the pore pressure dissipation rate to the permeability (Davit and Darot, 1989). The vector field changes with time as illustrated in figure 3.4.B.

3.3.3. Steady-state versus pulse-decay methods

Many authors consider steady-state methods to require an inappropriate lengthy equilibration process (eg. Somerton *et al.*, 1975; Gawuga, 1979; Jaeger, 1972). Holder *et al.* (1988) found that

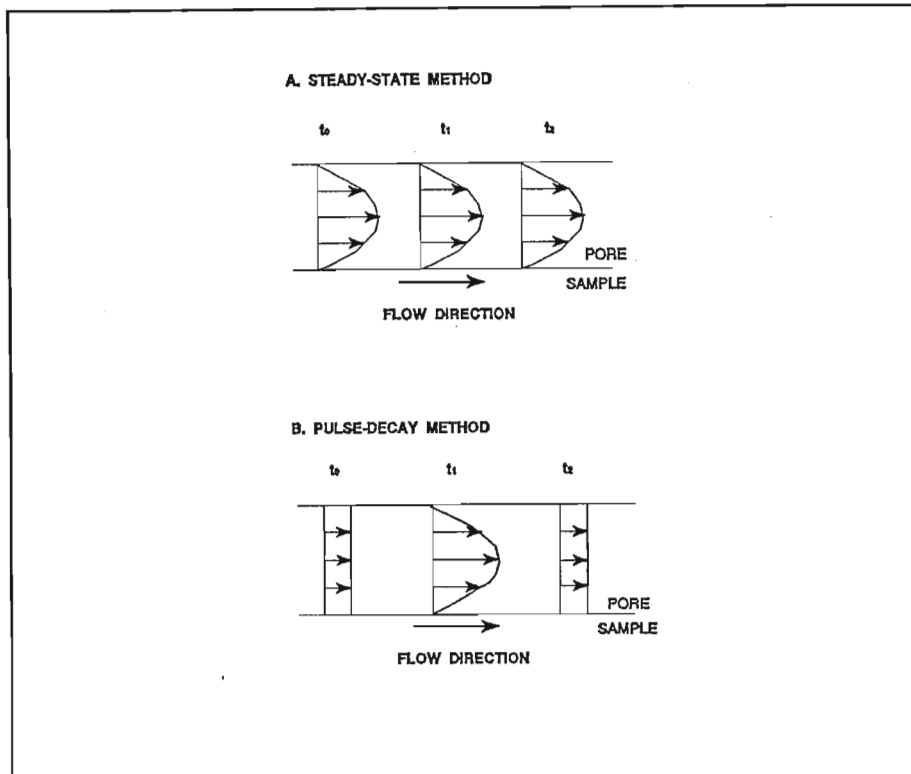


Figure 3.4 Schematic illustration of the change in the flow velocity at the same point at three different times under different applied pressure regimes (after Bober and Kenyon, 1980).

approximately one hour was needed for a sample with a permeability of one millidarcy to reach equilibrium.

Brace (1977) states that it is difficult to accurately measure permeabilities below one millidarcy using steady-state methods, but David and Darot (1989) suggest that pulse-decay methods are most appropriate for crystalline rocks.

Harpalani, Zhou and Farmer (1991) regard pulse-decay methods as having a distinct advantage over steady-state methods when it comes to the measurement of permeability under stressed conditions. Chakrabarti and Taylor (1968) on the other hand states that the Ohle-cell, which will be discussed in more detail in chapter 4, can measure permeabilities under steady-state conditions with reasonable accuracy to as low as 0.01 mD.

3.4. LIMITATIONS TO DARCY'S LAW

Darcy's law represents a linear relationship between the filtration velocity and the pressure gradient. The straight line representing this relationship passes through the origin of an x-y plot. Any deviation from this type of relationship represents 'Non-Darcian' flows. Deviations may be expected due

to: high flow rates, molecular effects, ionic effects, and non-Newtonian behaviour of the percolating fluid (Scheidegger, 1974). Figure 3.5 shows twelve different ways in which these effects manifest themselves

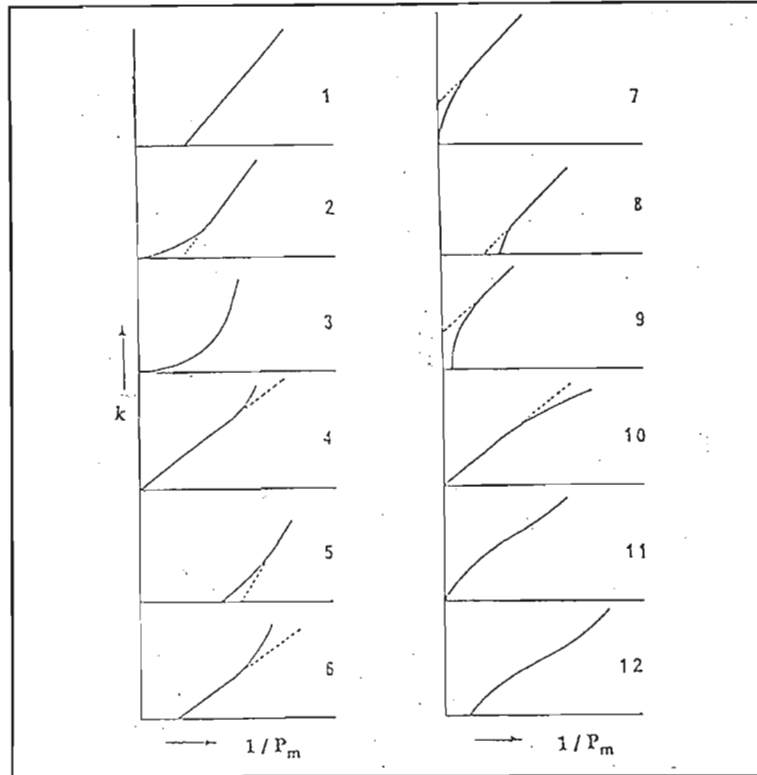


Figure 3.5 Twelve schematic flow curves for non-Darcian flow conditions (from Scheidegger, 1974).

when the permeability is plotted against the reciprocal mean gas pressure. The plots show that the relationship between pressure and permeability is no longer linear (dashed lines) and Darcy's law is no longer applies.

The velocity component of a flow is described by its Reynolds number. For a low Reynolds number, nearly equal to zero (figure 3.2), the flow is laminar and Darcy's law is valid (Desai, 1975). Furthermore the law in its original state, as was mentioned earlier, is only valid for incompressible fluids (Debschutz *et al.*, 1987). If the gas is a compressible medium and the pressure at the exit is equal to atmospheric pressure, as it is in the experiments described in the next chapter, the measured volume that passed through the sample is not equal to the volume in the specimen which is at a higher mean pore-pressure, requiring the introduction of a correction factor (Debschutz *et al.*, 1987). Measuring the specific permeabilities at a series of applied gas pressures, and then plotting them against the mean gas pressure at each point, these effects are largely negated (Klinkenberg, 1941).

Adsorption of gas molecules of the permeating fluid onto the carbonate molecules of the sample occur due to a lack of thermo-dynamic equilibrium between the sample and the gas where they are in

contact with each other (Dullien, 1979). The adsorbed molecules of gas forms a layer between the solid (sample) and the fluid (gas). The thickness of this layer is measured in molecules. The number of the layers of molecule layers are determined by the type of bond between the adsorbed molecules (gas molecules) and the molecules of the adsorbent (sample). If the bond is physical (i.e. a positively charged molecule of the gas attracted to a negatively charged molecule of the sample), the layer can only be one molecule thick. If the adsorption bond is chemical (i.e. one or more electrons of a atom of the gas are attracted by the proton of the atom of the sample, and they form a chemical bond between them), the layer may be several molecules in thickness (Dullien, 1979). This means that if a chemical reaction (bond) can occur between the molecules of the gas and the molecules of the sample through which it is permeating, a multi-molecule layer of gas can exist in contact with the solid in the pore spaces of the sample. This layer can be set in motion by the frictional forces between the permeating gas and the stationary adsorbed layer of gas molecules. The flowing layer is then referred to as Knudsen's flow because he was the first person to describe it mathematically (Scheidegger, 1974). The measured permeability is then higher than expected from Darcy's law, similar to the "gas slippage" of Klinkenberg (1941). In most cases, the flow in an adsorbed layer can be satisfactorily expressed as diffusion along a concentration gradient (Knudsen's law), but if capillary condensation plays a major role, this is not true, and a different mechanism, i.e. capillary condensation, must therefore dominate. Capillary condensation can also induce additional flow gradients, thus increasing the volume of flow (Scheidegger, 1974). Flow due to adsorption and flow due to capillary condensation constitute the extreme but opposite ends of the micro flow spectrum. In practice it is found that the flow is made up of a situation somewhere in between the two (Scheidegger, 1974).

Changes in permeability with changes in pH of the percolating solution are not linearly related (Scheidegger, 1974). It is generally thought that the permeability changes are caused by an electrochemical reaction between the permeating gas or liquid and the sample, such as ion exchange reactions in swelling clays (Scheidegger, 1974). The secondary biotite in the samples studied are thought to be the alteration products of argillaceous minerals. If the alteration process was not complete, some of the clay minerals might still be able to participate in ion exchange reactions and so influence the results of the experiments.

If the flow does not have a homogeneous temperature distribution a straight line plot of volumetric rate of flow versus the specific permeability cannot be obtained (Rose, 1987). In none of the experiments done in this study was any control enforced on the temperature of the permeating fluid. It is conceivable that the friction between the permeating fluid (especially in the case of gas) could cause temperature differences that could affect the values obtained. The distances involved as well as the rates of flow (typically $0.01 \text{ cm}^3/\text{s}$) argues against this having a significant influence on the values obtained.

It is commonly accepted that deviations from Darcy's law are encountered in the flow of gases, presumably due to molecular effects (eg. Klinkenberg, 1941; Ohle, 1951; Gawuga, 1979; Scheidegger, 1974). Air permeabilities are higher than liquid permeabilities in the same porous medium, as calculated from Darcy's law (Klinkenberg, 1941). When the pore diameter becomes comparable with, or smaller than, the molecular mean free path of the flowing gas, anomalous permeability values are obtained from Darcy's law (eg. Gawuga, 1979; Scheidegger, 1974).

An important difference between flow of liquids and gases in porous media is that in the latter case the velocity at the solid walls cannot, in general, be considered zero, but a so-called "slip" or "drift" velocity at the wall must be taken into account (Dullien, 1979). This fact has been recognized as early as 1875, by Kundt and Warburg, who had shown that when a gas is flowing next to the wall of the pore space, the layer of gas next to the surface is in motion with respect to that surface. This phenomenon is commonly called gas slippage (Ohle, 1951). This effect has been mathematically modelled by Knudsen and can be described, physically, through particulate diffusion movements between the layers in the laminar flow (Debschutz *et al*, 1989).

The phenomenon of gas slippage, or molecular streaming, occur mostly at high gas pressures. At elevated pressures there is a crowding of molecules at the interface, thus reducing the mobility of the gas and reducing the permeability of the porous medium (Harpalani and Schraufnagel, 1989). This "crowding" starts to happen when the diameter of the capillary openings approaches the mean free path of the gas (Klinkenberg, 1941).

The amount of slippage is proportional to the frequency of the collisions between the molecules of the gas. This means that the amount of slippage is also proportional to the mean free path of the gas. The term "mean free path" for the gas refers to the diameter of the opening through which the fluid is flowing, in natural systems such as rocks, this is the pore diameter. Therefore, the larger the gas molecules, the greater the slippage (Ohle, 1951). The opposite is also true, that is, if the mean free path is much smaller than the pore diameter the slip velocity becomes negligibly small (Dullien, 1979).

In liquids the mean free path of molecules is in the order of the molecular diameter, so the 'no-slip' condition always applies in liquid flow. In gas flow through a capillary, the molecules at a distance equal to the mean-free path from the wall have, on the average, a non-zero velocity in the direction of flow. As the mean free path becomes an increasingly greater fraction of the capillary diameter, the "wall velocity" increases in significance relative to average velocity. The limiting situation in which the mean-free path of the gas molecules is much greater than either the diameter of the capillary or its length is called "molecular streaming" or Knudsen flow (Dullien, 1979).

The effect of the slippage is that, if it occurs, the experimentally measured flow rate, and therefore the calculated permeability, is much larger than it should be. Klinkenberg (1941) recognized this and adopted the method of extrapolating the pressure to infinitely high values which is the same as reducing the molecular mean free path to infinitely small diameters to "correct" the permeability obtained from the semi-empirical Darcy law. This method has been adopted as standard practice (ASTM, 1990) and when anomalous values that can be attributed to the slippage of gas are encountered in permeability experiments, it is commonly referred to as the "Klinkenberg effect" (eg. Gawuga, 1979).

CHAPTER 4 METHODOLOGY

4.1. INTRODUCTION

As mentioned in the previous chapter, permeability can be tested under steady-state or pulse-decay pressure conditions. In the steady-state a constant pressure differential is maintained across the sample, requiring less complicated apparatus than the pulse-decay methods. The steady-state methods discussed in this chapter allowed the testing of the permeabilities of the sediments towards a range fluids.

This study concentrated on measuring the permeability of the roof strata sediments of the Gus seam, and to a lesser extent the coal itself, under various externally applied stress conditions. Similar studies, done on the Coal Measure strata in Britain and on the coal-bearing strata of the U.S.A., were mostly concerned with the influences of stress on the permeability of the coal itself and not on the sediments associated with it (eg. Gawuga, 1979; Mordecai and Morris, 1971; Somerton *et al.*, 1975).

Previous studies of sediments (not related to the northern hemisphere Coal Measure strata) were done under atmospheric conditions (eg. Ohle, 1951; Crook, Daw and Morgan, 1971; Crook *et al.*, 1973). Few authors describe the testing of coal under atmospheric conditions, mainly due to the difficulty in obtaining useable intact samples (eg. Gawuga, 1979; Ohle, 1951; Walker and Mahajan, 1987).

This study used a modified Ohle cell to measure the permeability of the sediments towards nitrogen, methane and water under atmospheric conditions and a modified Hoek cell for tests involving methane under triaxial conditions. To the author's knowledge no previous work of this nature has been carried out, or the results from such studies published, for laboratory tests on the coal-bearing strata the eastern Transvaal or anywhere else in South Africa.

4.2. SAMPLE PREPARATION

Core obtained from six boreholes drilled by Majuba Colliery for explorational purposes and from borehole core drilled by the author from two bulk samples from the immediate roof of the Gus seam were sampled for the project. Five of the holes were drilled vertically into the roof of the Gus seam and yielded core of NX (54 mm) diameter. The sixth borehole was drilled vertically from surface to intersect the coal seams present in the area and provided core of TNW (60.3 mm) diameter.

A post drill, fitted with an adjustable stage and an NX (54 mm diameter core) sized diamond drill bit and core barrel with a water swivel (figure 4.1), was used by the author to obtain core samples

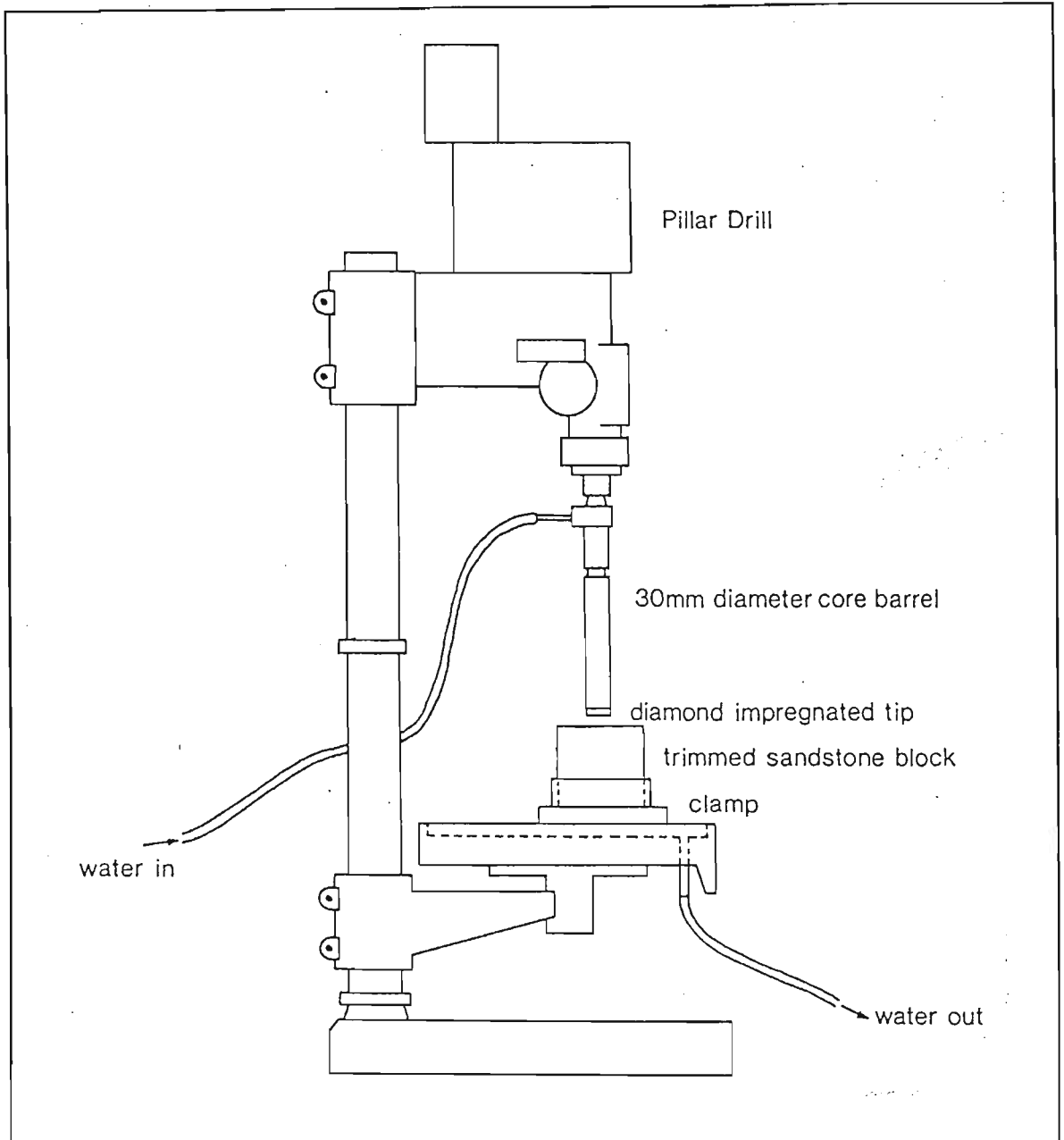


Figure 4.1 Post- or pillar drill setup used for core sample extraction (from Richards, 1992).

from the bulk samples. The bulk samples were first trimmed by circular diamond saw to ensure that core samples could be drilled parallel to, and perpendicular to, the bedding planes in the samples. The samples were clamped in place on the stage to minimise the lateral movement of the drill bit.

The drilled core samples were cut to their correct lengths by means of a circular diamond saw. For the Ohle cell the samples were cut into discs of roughly 15 mm in length, irrespective of their diameter. Triaxial tests, on the other hand, are influenced by the length to diameter ratio. A ratio of 2:1 is considered to reduce the end effects to acceptable levels (Obert and Duvall, 1967). As a result the samples were cut into 100 mm or 120 mm lengths, depending on the diameter of the core. Carborandum

paste was used to grind the ends of the samples until they were parallel and smooth. This was done so that an even load could be applied perpendicular to the long axis of the sample in the triaxial case, and to assure a better seal between the o-rings and the sample when tested in the Ohle cell.

Useable coal samples are notoriously difficult to obtain (eg. Gawuga, 1979) and this study was no exception. Although the samples were already cored and needed only to be cut to the correct length, only a small number of samples did not disintegrate completely when cut with the circular diamond saw. By encasing the whole length of the piece of coal that was intended to be cut with masking tape it was found that useable samples could be cut for use in the triaxial cell, but not for the Ohle cell. Coal samples had to be kept in a desiccator with the masking tape in place, otherwise it was found that they would fall apart within a few days, thereby making them unsuitable for the intended tests.

After the samples were sawn into their appropriate lengths and their ends ground to the required smoothness, the samples were washed to remove all the grit and carborundum paste. This was done with care to avoid impregnating the pores of the sample with the grit and paste, which could affect the permeability of the sample. The samples were then oven-dried at 110°C to remove all the excess moisture and placed in desiccators containing silica gel to keep them moisture-free. Drying over a period of twelve hours was found to be sufficient in most cases for the samples to attain a constant weight, i.e. assumed to be moisture-free. The coal samples could not be washed or oven dried, because washing dissolved the coal and speeded up the breaking up process and at a temperature of 110°C there is a danger of driving off all the volatiles from the coal. The excess moisture in the coal samples was removed by first drying them under 60 Watt lamps for a short period (3 to 4 hours), and then placing the samples in a desiccator with water absorbent silica gel.

In the cases where water was the permeating fluid the sandstone samples were first vacuum-saturated with de-aired water for 48 to 72 hours.

4.3. OHLE CELL

4.3.1. Apparatus

The original design of the Ohle cell as described by Ohle (1951) and Chakrabarti and Taylor (1978) was modified (figure 4.2), mainly concerning the material used for its construction and the sample holder. Brass was used instead of the original stainless steel because it allowed for the more flexible new design. Brass was chosen because it does not react with any of the fluids used (eg. does not rust when testing with water) and is strong enough to withstand the pressures used. Modification of the sample

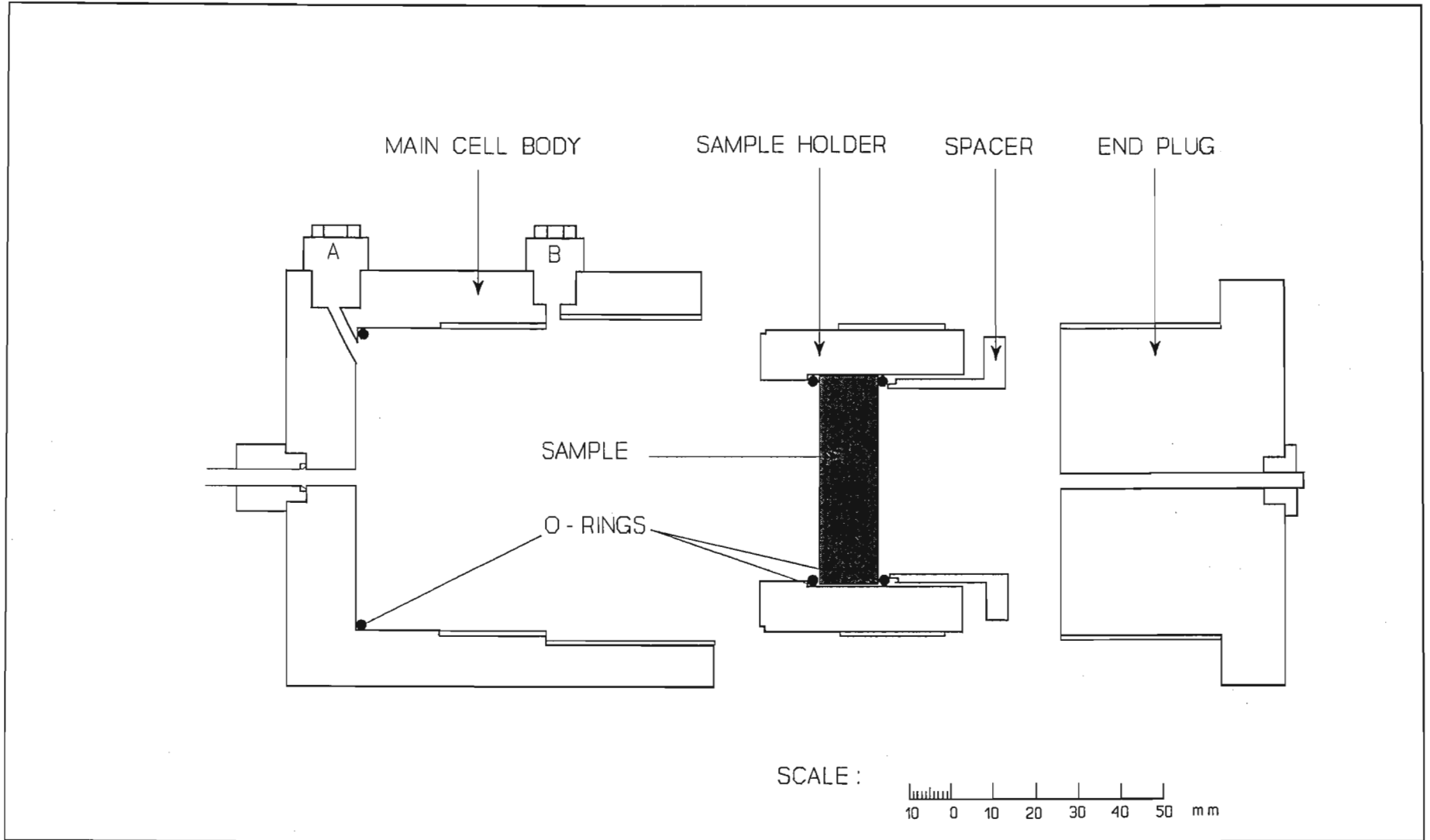


Figure 4.2 Cross-section of the Ohle cell dismantled.

holder allows it to hold a broader spectrum of samples with respect to diameter and length. Sealing between the sample and the sample holder is achieved by two rubber O-rings pressed against the sample by means of a spacer (figure 4.2). Plates 4.1 and 4.2 show the cell in its assembled and dismantled state.

This apparatus was chosen because of its proven ability to give accurate results in the 10^{-2} to 10^{-7} millidarcy range (Chakrabarti and Taylor, 1967). The cell also allows the testing of the permeability towards various fluids (gases and liquids) without the need to remove the sample from the cell. The present modifications also allow for speedier sample changing.

4.3.1.1. Gas

Figure 4.3 shows the various components of the apparatus used to test the permeability of the samples towards gas. The gas (either nitrogen or methane) was supplied by means of a commercial gas cylinder that is capable of delivering 20 MPa pressure. The supplied pressure was kept constant by means of a regulator and measured with a transducer and a digital readout. Flow rates were measured with a stopwatch and a series of bubble flow meters of 25, 100 and 250 cm³ capacity (figure 4.3).

4.3.1.2. Water

In the cases where water was used as permeating fluid, the setup of the apparatus differed slightly. The water pressure was supplied by either a constant pressure apparatus able to deliver 1600 kPa pressure (figure 4.4) or a hydraulic ram connected to a hydraulic pump that can deliver pressures up to 17 MPa. The water was de-aired by means of an ELE de-airing apparatus. Flow rates were measured with a stopwatch and a graduated burette (figure 4.4).

4.3.2. Test method

4.3.2.1. Gas

After a sample was installed in the chamber the apparatus (figure 4.2) was assembled. Sealing was achieved by compressing an o-ring against the sample. The effectiveness of the seal was tested by inserting a steel disc of the same dimensions as the sample in the cell, applying a pressure and noting if any fluid reached the bubble flowmeter. With a porous sample installed plug A was removed and a small pressure, 50 kPa, applied. This was done to expel any air in the space between the fluid inlet and the sample (figure 4.2). Plug A was then replaced after plumbers tape had been wound around its thread to guard against leakage, and plug B removed. The pressure was increased to 150 kPa which caused the sample to be "flushed" with the testing fluid and to expel any air that might have been trapped

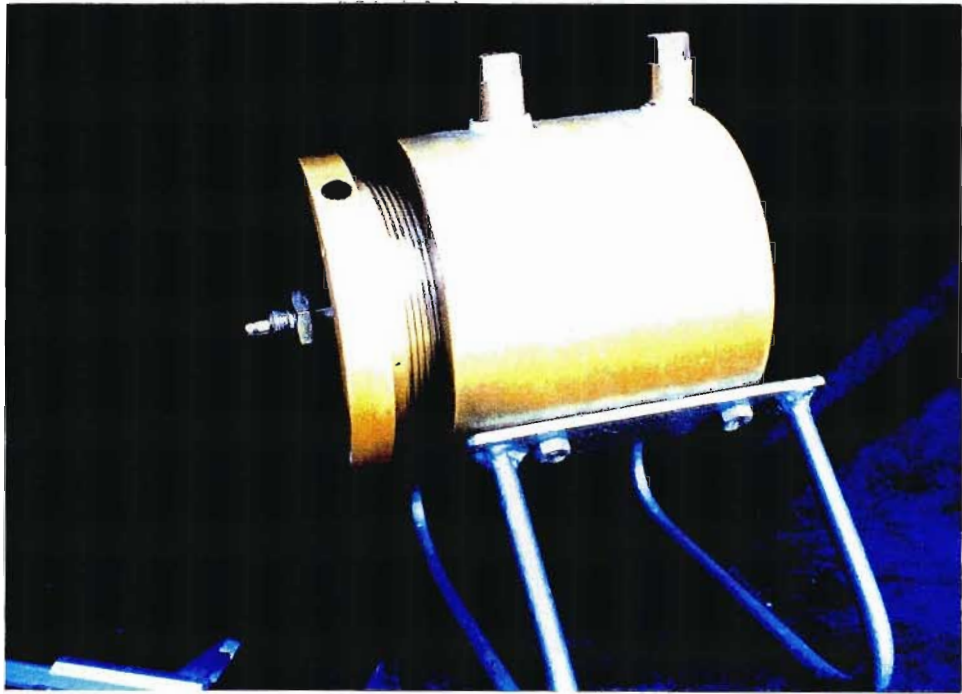


Plate 4.1 Photograph showing the assembled Ohle cell.
(Vernier calliper open at 50 mm)



Plate 4.2 Photograph showing the different parts of the Ohle cell.
(Vernier calliper open at 50 mm).

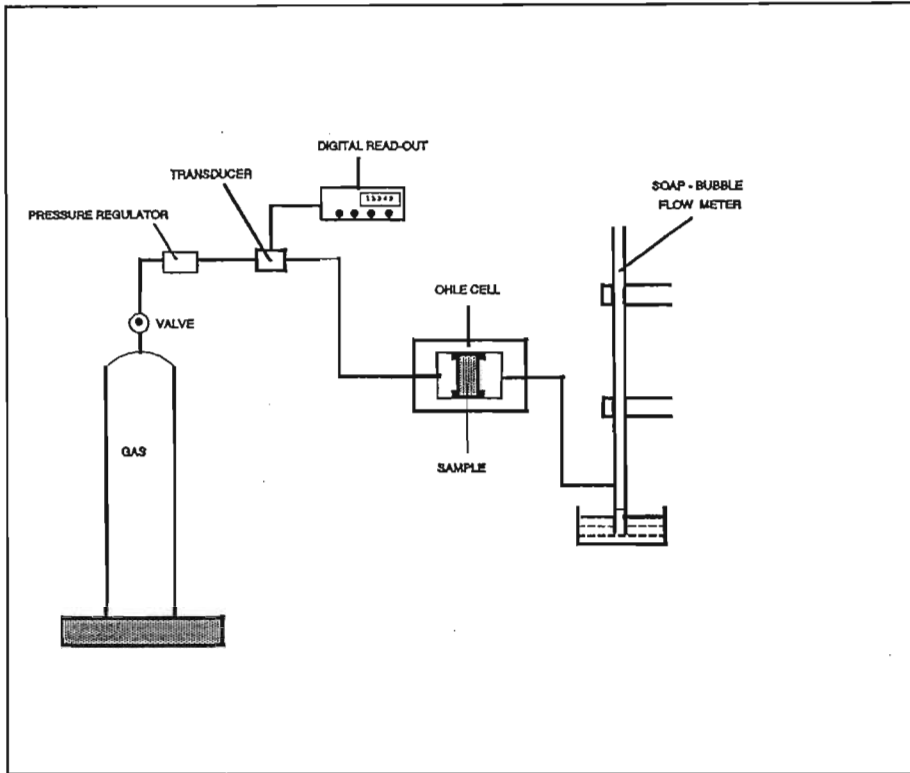


Figure 4.3 Diagram showing the different components of the Ohle cell for tests involving gas as the permeating fluid.

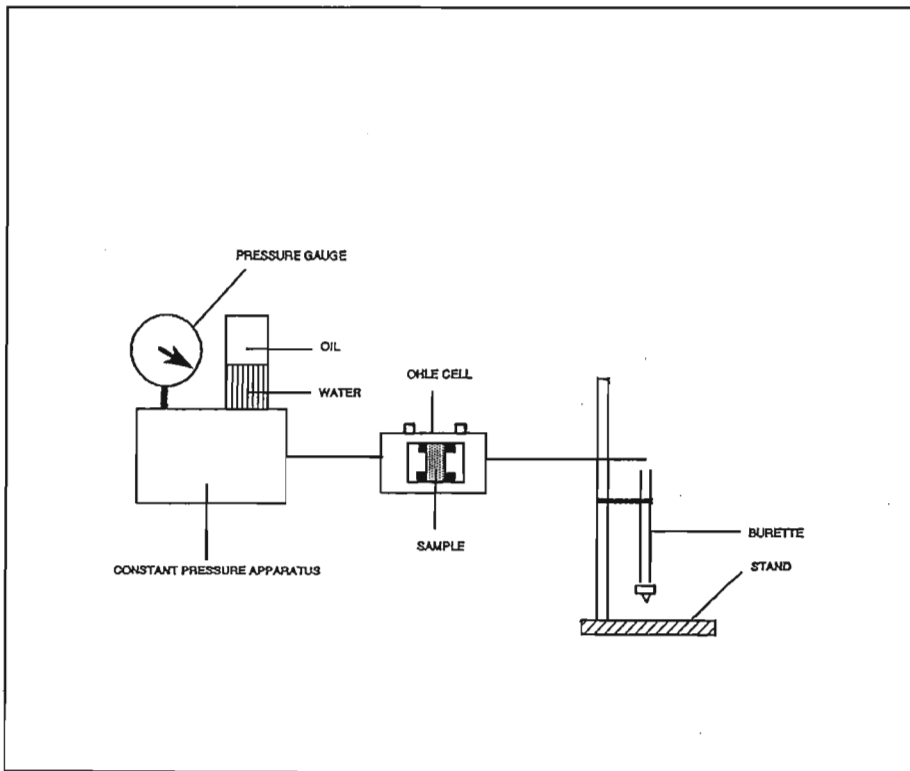


Figure 4.4 Diagram showing the different components of the Ohle cell tests involving water as the permeating fluid.

in the pores of the sample or the test apparatus. Coupled with the oven-drying of the sample this was assumed to produce a single-phase environment with respect to the testing fluid. When all the air at the low pressure side of the sample was replaced by the permeating fluid, plug B was replaced (normally after 15 minutes).

The rate of flow was then periodically measured, and at the point when the flow rate became constant, the sample was assumed to be fully saturated with the fluid pressure and the system was assumed to be in equilibrium. The gas pressure was now increased by 50 kPa. The system was left to equilibrate again and the flow rate was recorded. This incremental increase in gas pressure was continued until the pressure reached 700 kPa. A gas pressure of 700 kPa was chosen as termination point because the initial tests resulted in erratic specific permeability versus reciprocal mean gas pressure plots after a inlet gas pressure of 400 kPa was reached (figure 4.5). This behaviour was thought to be caused

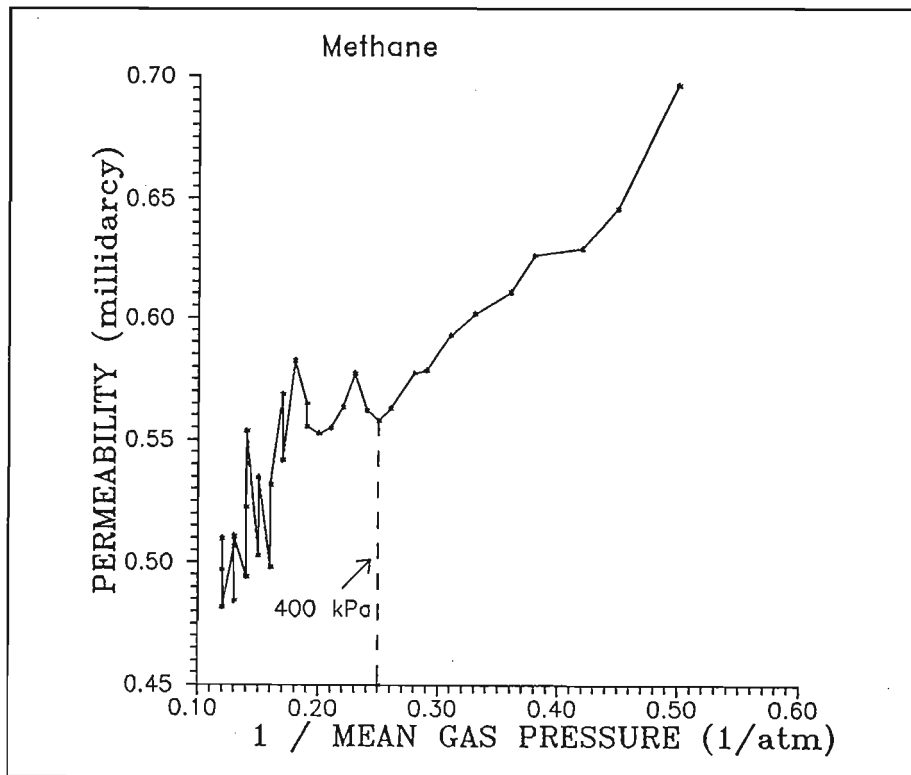


Figure 4.5 Plot of k_s versus $1 / P_m$ for methane showing erratic behaviour above 400 kPa inlet gas pressure.

by either the Klinkenberg effect (Klinkenberg, 1941) or by the flow becoming turbulent so that Darcy's law was no longer valid (Desai, 1975). Subsequent experiments were continued up to 700 kPa inlet gas pressure to make sure that the cause could be identified as well as to provide enough data points for the later statistical manipulations required by ASTM D4525-85 (1990). The data was then recorded on a data sheet like the one shown in appendix G. Appendix G is the data sheet for sample A in figure 5.9 (p. 51).

Usually the sample was first tested with nitrogen as the permeating fluid and directly afterwards with methane as the flowing fluid. Nitrogen was used first mainly for reasons of safety. If the geometry

of the sample did not allow a seal to be affected and a large quantity of gas escaped into the atmosphere, it does not pose a danger as does methane. To change over from one gas to another the gas pressure was reduced to zero and the pressure released from the system by removing plug A, without removing the sample from the cell. The same procedure as outlined above was then followed with the new gas.

The samples obtained by coring the bulk samples across bedding were orientated so that the flow into and out of the mine opening could be simulated. Some of the other samples, notably the samples from the lower parts of borehole ARF 39 (Appendix A), i.e. those nearest to the coal seam being mined, were also tested with in two directions to test for any permeability anisotropy. Approximately 10% of all samples tested were retested by the same method to test the reproducibility of the test method.

4.3.2.2. Water

After the sample was saturated with de-aired water it was installed in the cell. Plugs A and B were removed and a pressure of 200 kPa or 1000 kPa, depending if the constant pressure apparatus or the hydraulic ram was used, applied. When all the air was displaced in the space between the sample and the water inlet (figure 4.2) plug A was replaced. Plug A's thread was first covered with plumbers tape to ensure that no leakage of the testing fluid occurred. The system was then left until water started to emerge at the low pressure side of the sample. The space between the sample and the outlet (figure 4.2) was then filled with de-aired water through the hole of plug B, and the plug replaced. This was done to fill the outlet side of the cell as well as the whole length of the tube from the outlet to the burette and to ensure that the whole face of the sample on the low pressure side was covered with water. The tube connecting the outlet from the cell with the burette was transparent so that any air bubbles trapped in the water could be detected. If air bubbles were detected, plug B was removed again and more water added until the air bubbles were expelled from the tube. When a constant flow rate was achieved, the pressure was increased in 200 kPa steps (constant pressure apparatus) or 2000 kPa steps (hydraulic ram). After each pressure increase the system was left to equilibrate and the flow rate noted. The experiment was terminated when a pressure of 1600 kPa was reached with the constant pressure apparatus (its limit) and at 10000 kPa with the hydraulic ram. By removing the pressure and undoing plug A the sample could be extracted once the apparatus had been disassembled. The measurements were recorded on data sheets like the one shown in appendix G.

4.4. HOEK CELL

4.4.1. Apparatus

For the tests simulating *in situ* stress conditions a modified Hoek-Franklin triaxial cell was used (after Daw, 1971). Figure 4.6 shows a cross-sectional cut through the cell and plate 4.3 shows the cell in a partially assembled state. The modifications involve a series of interconnected circular grooves cut

into the end platens (plate 4.4). The grooves are designed to distribute the fluid over the whole cross-sectional area of the sample, at the high pressure end, and to collect the fluid that passed through the sample over the whole cross-sectional area of the sample, at the low pressure end. In the case of coal it was found that these grooves pressed into the ends of the coal thereby effectively blocking any gas penetrating the samples. Cinkered discs of the same diameter as the platens were used to counteract this.

Axial load was supplied by a RELSMA testing machine capable of delivering a load of 1000 kN. Confining stress was applied by means of an ENERPAC hydraulic pump that can supply an oil pressure of up to 50 MPa. Figure 4.7 shows, diagrammatically, how the different components fit in relation to each other. The gas supply system was the same as for the tests under atmospheric conditions and the flow rates are also measured with the use of a bubble flowmeter and a stopwatch.

4.4.2. Test method

Before the samples were placed in the assembled Hoek cell the annular space between the rubber sleeve and the cell was first filled with hydraulic oil. This was done by inserting two steel platens of the correct diameter into the sleeve and fitting one of the oil inlet valves (figure 4.6) with a apparatus that opens valve to the outside. Hydraulic fluid was then pumped gently into the cell from the hydraulic pump until all the air between the cell and the sleeve have been expelled. This is managed by observing when no more air bubbles flow out with the oil at the open valve. To ensure that the whole space between the cell wall and the sleeve is filled by oil, the two opposing valves must be kept as close to vertical as possible. If the whole space is not filled properly, the sample gets pushed into the sleeve and the oil, which is under pressure, sprays out. Apart from ruining the sample by saturating it with hydraulic oil, it can also be very dangerous.

The samples were then placed in the cell and a hydrostatic stress of 4 MPa applied (it was found to be the general stress at which no gas flowed between the sample and the sealing rubber sleeve of any of the samples). At the outset it was hoped to start the testing at the measured *in situ* stress conditions in the mine, but since this is estimated to be below 4 MPa this could not be carried out. Only tests using methane were carried out, first because of the importance of the methane tests to this study and secondly because of the time aspect involved in reaching equilibrium. A full range of tests on one sample could take up to four days to complete. First the gas pressure was increased in 50 kPa increments up to 700 kPa at a hydrostatic pressure of 4 MPa, similar to the Ohle tests. From this point a series of three tests were carried out:

- a. The axial stress was increased in 2 MPa intervals (usually to 20 MPa) while the confining stress was kept at 4 MPa and the gas pressure at 200 kPa. The flow rate was measured after each load interval. Axial load was then decreased in 2 MPa steps, until hydrostatic conditions at 4 MPa were reached again.
- b. The confining stress was increased in 2 MPa intervals while the gas pressure was kept

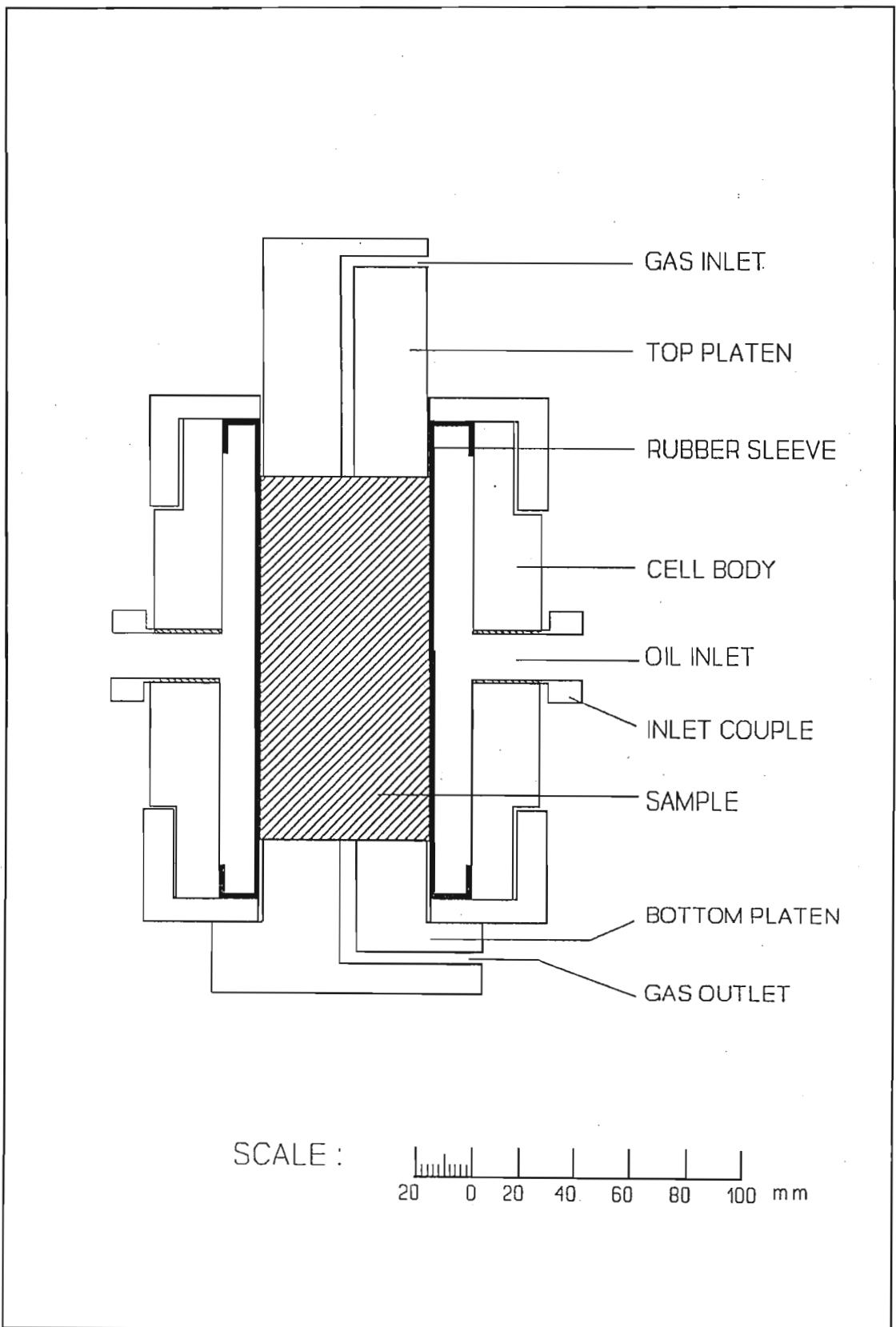


Figure 4.6 Cross-section of the Hoek cell.

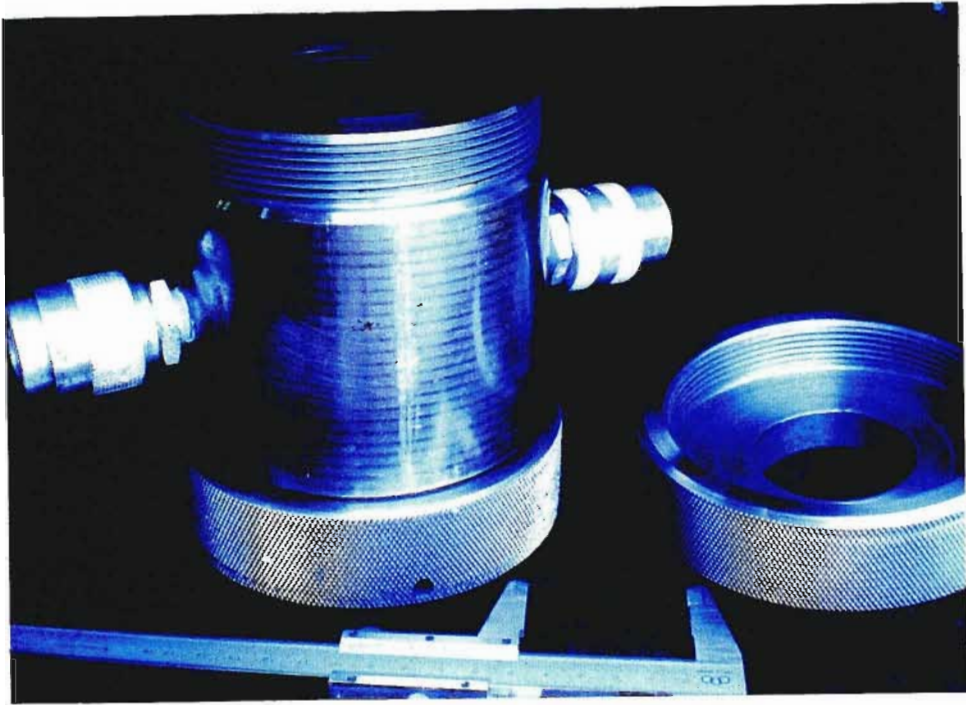


Plate 4.3 Photograph showing the Hoek cell with the rubber sleeve inserted.
(Vernier calliper opened at 50 mm).

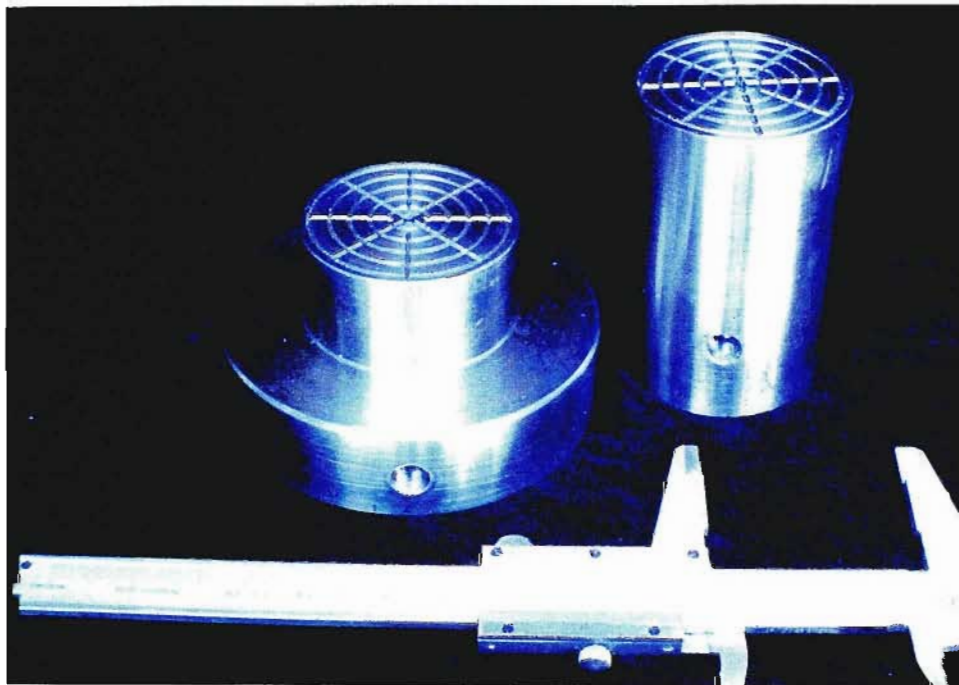


Plate 4.4 Photograph showing the modified platens for the Hoek cell.
(Vernier calliper opened at 50 mm).

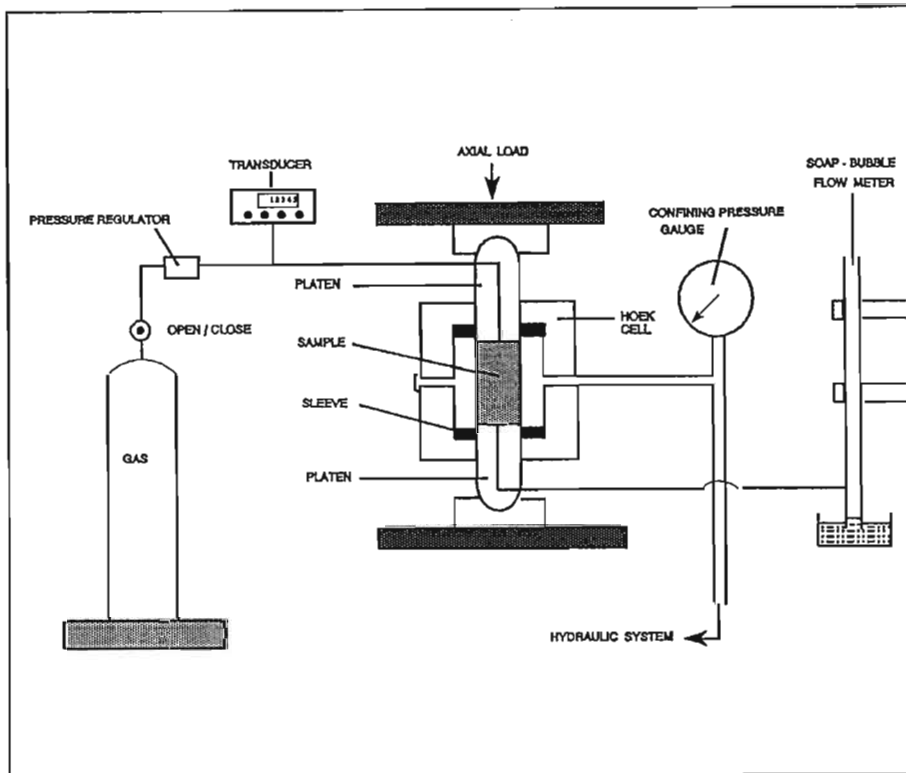


Figure 4.7 Diagram showing the different components of the Hoek cell tests involving methane as the permeating fluid.

constant at 200 kPa. This loading was also done until 20 MPa was reached at which time the hydrostatic load was decreased in steps of 4 MPa until the base 4 MPa hydrostatic conditions were reached again.

- c. The hydrostatic stress was increased in 2 MPa intervals while the gas pressure was kept constant at 200 kPa. Similar to the previous method the stress was increased until 20 MPa was reached. The confining stress was then relieved until the starting 4 MPa hydrostatic conditions were reached.

In each of the three cases the procedure was repeated two to three times. The effect of each cycle was determined by measuring the specific permeability at a series of gas pressures and determining the liquid equivalent permeability in each instance. The data were then captured on a sheet such as shown in appendix H. Appendix H contains only part of the data used to compile figure 5.14 (p. 57).

gas penetrating the samples. Cintered discs of the same diameter as the platens were used to counteract this.

Axial load was supplied by a RELSMA testing machine capable of delivering a load of 1000 kN. Confining stress was applied by means of an ENERPAC hydraulic pump that can supply an oil pressure of up to 50 MPa. Figure 4.7 shows, diagrammatically, how the different components fit in relation to each other. The gas supply system was the same as for the tests under atmospheric conditions and the flow rates are also measured with the use of a bubble flowmeter and a stopwatch.

CHAPTER 5

RESULTS AND DISCUSSION

5.1. INTRODUCTION

The measurement of the quantity of fluid at a single steady flow rate permits the calculation of the permeability from Darcy's law (Dullien, 1979). To overcome any experimental error, the measurements are performed at a series of flow rates (Klinkenberg, 1941). The specific permeabilities were calculated using derivations of Darcy's law. Equation 3.2 was used in the cases where water was used as the permeating fluid and equation 3.4 was used in the cases where gas was the permeating fluid (Somerton *et al.*, 1975). The calculated permeabilities were then plotted against the pressure gradient across the sample and a straight line fitted to the data points. According to Darcy's law, this line passes through the origin (Dullien, 1979). The results were plotted in accordance with the method described in ASTM D4525-85 (1990). Only the liquid equivalent permeabilities are reported in order to compare the results from the test involving different permeating fluids (i.e. methane, nitrogen and water).

The results are reported such that the main emphasis are on the relationship between facies type and liquid permeability (where water was used as permeating fluid) or equivalent permeability (where gas was used as permeating fluid).

5.2. OHLE CELL

5.2.1. Gas

Plotting the specific permeability against the reciprocal mean gas pressure (P_m) it was found that the permeability (k_s) generally decreased with increasing gas pressure. In the majority of cases the nitrogen and methane plots for the same sample followed the same pattern (figure 5.1). The specific permeabilities for tests involving nitrogen were found to plot higher than the specific permeabilities for the tests involving methane as one would expect for a gas of smaller molecular size (figure 5.1). The same does not apply to the liquid equivalent permeabilities. Nearly half of the resulting liquid equivalent permeabilities for methane were found to plot higher than the liquid equivalent permeabilities for nitrogen, and the rest were found to plot lower. The difference between the k_{le} for methane and the k_{le} for nitrogen, however, was found to average less than 10%. This result is the same as the findings of Ohle (1951), who ascribed the difference to experimental error.

Table 5.1 lists the permeability (k_{le}) ranges obtained from the tests using nitrogen as the permeating fluid for the eleven facies types listed in table 2.2. The liquid equivalent permeability was

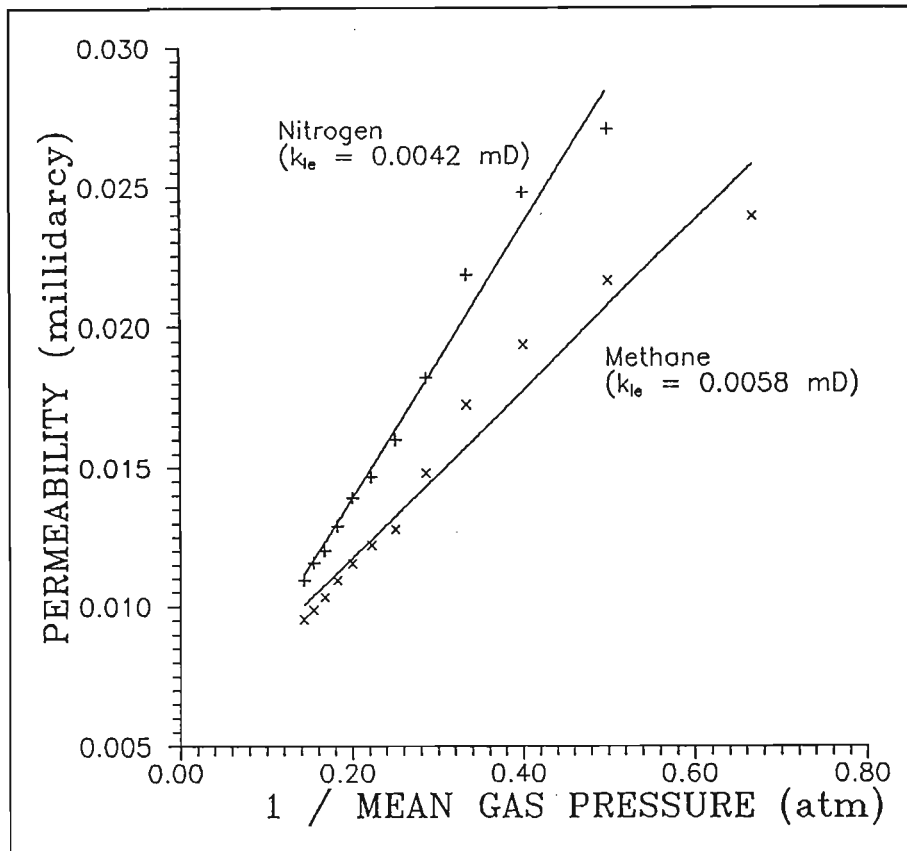


Figure 5.1 Plot of k versus $1 / P_m$ for nitrogen and methane. (Facies 9).

used so that a better comparison between the permeabilities of different fluids (nitrogen, methane and water) could be made. The reasons for a permeability range rather than for a single permeability for each facies type is due to the fact that the sediments represent different depositional environments. Each facies type also contain sediments of variable grain size which will naturally result in a range of permeabilities rather than in a unique permeability for each facies type. The definition of the upper and lower limit of the permeability range for each facies type is also very much dependent on the number of tests carried out on the samples of a specific facies type. Variations due to experimental error might also be a contributing factor. Table 5.1 represents the results of 90 tests carried out on 67 samples using nitrogen. By retesting 26% of the samples, it was found that the average reproducibility was 71%. Table 5.2 gives the permeability (k_{ie}) ranges obtained from the tests involving methane as the flowing fluid.

Table 5.2 is the summary of 267 tests carried out on 208 samples using methane. The average reproducibility of the results were found to be more than 75% (22% of the samples were retested to determine the reproducibility). Ohle (1951) found the reproducibility of his experiments to be as high as 90 %. The precision of the experiments should be 95 % according to ASTM D4525 (1990), meaning that the value obtained for the liquid equivalent permeability should not vary by more than 5 % in consecutive tests. This suggests that the reproducibility of the experiment in this study is low; however, the reproducibility values of 75 and 71 % quoted for this study is the average over all the facies

Table 5.1 Liquid equivalent permeability ranges for facies types tested with nitrogen as permeating fluid.

Facies Type	Permeability Range (mD)			Number Tested	Average r^2
	Minimum	Maximum	Average		
2	0.0042	0.3785	0.1389	4	0.91
3	0.0005	0.6083	0.2364	2	0.85
4	0.0013	0.0682	0.0315	4	0.94
5	0.0059	0.0059	0.0059	1	0.99
7	0.0110	0.0238	0.0167	3	0.90
8	0.0682	0.1106	0.0894	2	0.96
9	0.1237	1.0117	0.3708	5	0.86
10	0.0035	1.9470	0.3960	44	0.88
11	0.3239	0.3239	0.3239	1	0.96
12	0.3835	0.3835	0.3835	1	0.99

Table 5.2 Liquid equivalent permeability ranges for different facies types tested with methane as permeating fluid.

Facies Type	Permeability Range (mD)			Number Tested	Average r^2
	Minimum	Maximum	Average		
2	0.0057	0.2590	0.1197	4	0.94
3	0.0025	0.6146	0.0808	6	0.77
4	0.0018	0.0040	0.0029	5	0.81
5	0.0024	0.0070	0.0026	8	0.78
7	0.0020	0.0247	0.0108	7	0.81
8	0.0001	0.1161	0.0282	8	0.92
9	0.0213	1.5318	0.2788	22	0.80
10	0.0128	2.7132	0.4412	103	0.69
11	0.0681	2.1597	0.3902	34	0.80
12	0.1567	3.1960	1.0546	11	0.69

types, whereas the ones mentioned by Ohle (1951) and ASTM D4525 (1990) are for the same facies types. There is no guarantee that the flow of the fluid through the sample did not change the internal structure of the sample, thereby affecting the reproducibility.

The objective of this study was to determine if any correlation could be found between facies type and permeability. Tables 5.1 and 5.2 show that the tests involving nitrogen and the tests involving methane result in a similar relationship between liquid equivalent permeabilities obtained and facies type. This relationship is also illustrated in figure 5.2, with the left hand range at each facies type being the methane range and the right hand side range the range for nitrogen. Nonetheless a relationship of increasing permeability with increasing grain size was found in the coarser grained facies (facies type 8 and higher). For the finer grained facies types the permeability was found to decrease with increase in grain size. This could be the effect of many factors, but in the author's opinion the most likely cause is the number of tests done on that facies type. The more tests that are done on a specific facies type the more representative, statistically speaking, the definition of the permeability range for that facies type will be. The largest range in liquid equivalent permeabilities were obtained for the coarsest grained facies type, facies type 12 (figure 5.2). Another factor that could have a significant role in the actual liquid equivalent permeability quoted is the data points chosen for the best fit straight line. ASTM D4525-85 (1990) states that at least 3 data points should be located, at the highest gas pressure (lower values of reciprocal mean gas pressure), and a straight line drawn through them. The intersection of this line with the y-axis is the liquid equivalent permeability (figure 3.1). In this study 12 data points, between 150 kPa and 700 kPa gas pressure, was used to fit a straight line.

When plotting the flow rate against the inlet gas pressure it was found that both the plot for the nitrogen and the plot for the methane tests resulted in positive slopes. The plot of flow rate versus inlet gas pressure for the same sample as in figure 5.1 is shown in figure 5.3. In this case the k_s for the methane test plotted higher than the k_s of the nitrogen tests, with the methane plot having a steeper slope. In some cases the plots of specific permeability versus reciprocal mean gas pressure for the tests involving methane resulted in graphs with negative slopes, whilst the tests involving nitrogen resulted in plots with positive slopes (figures 5.4 and 5.5). Such results were unexpected as the plot of flow rate versus gas pressure for the same sample yielded positive, albeit non-linear, plots (figure 5.6). In other cases both the nitrogen and methane tests resulted in plots of specific permeability versus reciprocal mean gas pressure with negative, and very non-linear, slopes (figure 5.7). In these cases the plots of flow rate versus gas pressure was still positive, but non-linear for both the methane and the nitrogen tests (figure 5.8). This meant that Darcy's law no longer applied. Possible reasons for such behaviour were outlined in chapter 3.

The two main phenomena that could be causing such anomalous specific permeability versus

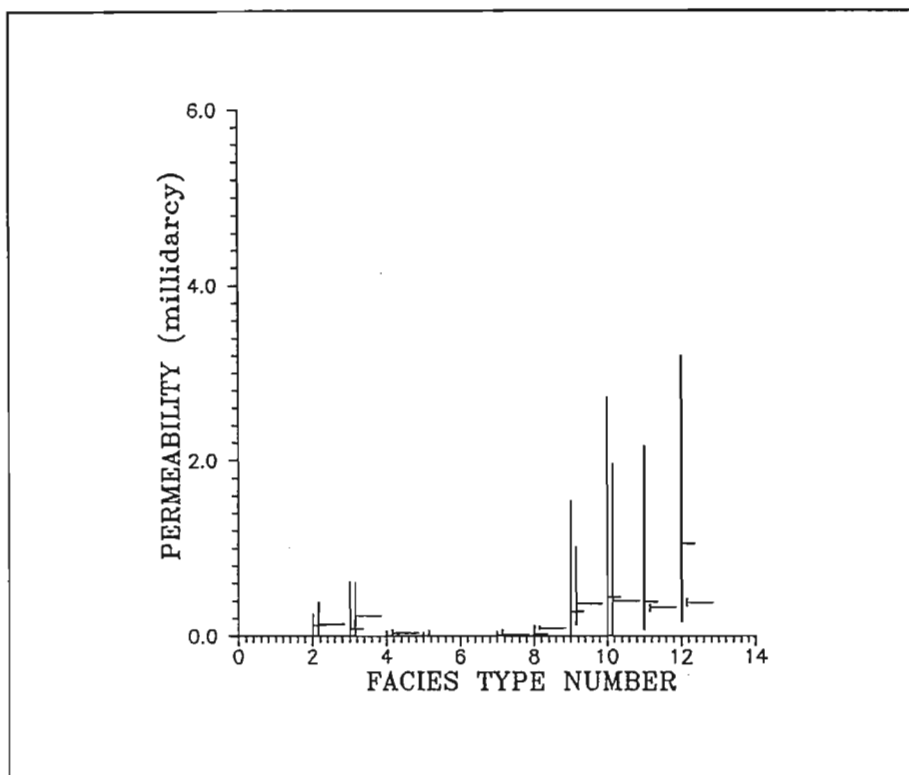


Figure 5.2 Plot showing the relationship between facies type and k_{θ} range for both methane (left) and nitrogen (right).

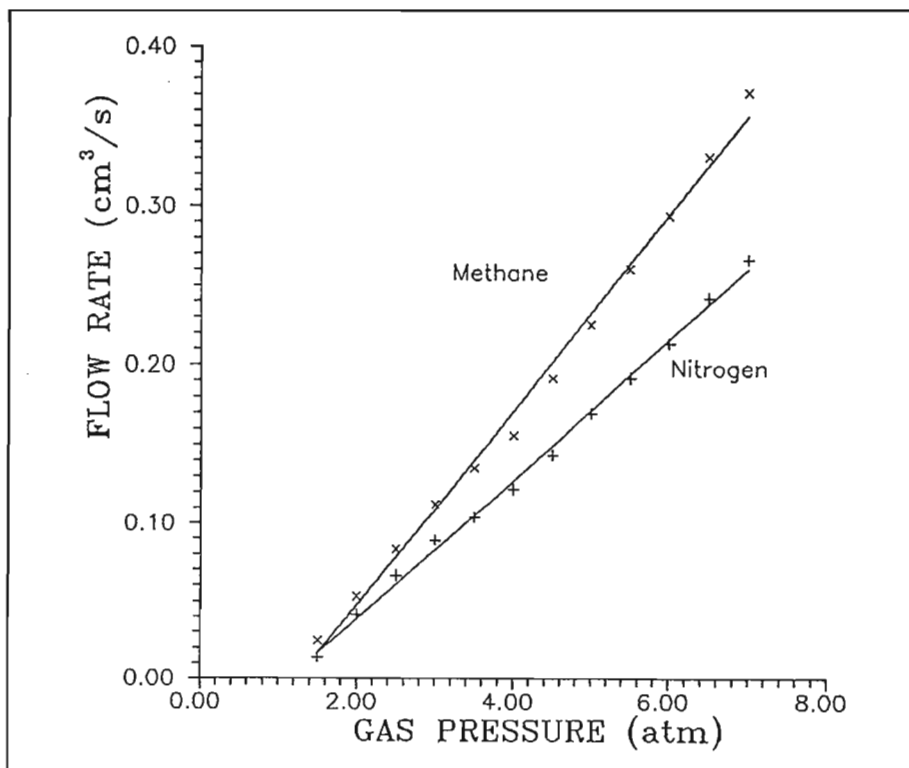


Figure 5.3 Plot of flow rate versus $1/P_m$ for nitrogen and methane. Same sample as for figure 5.1. (Facies 9).

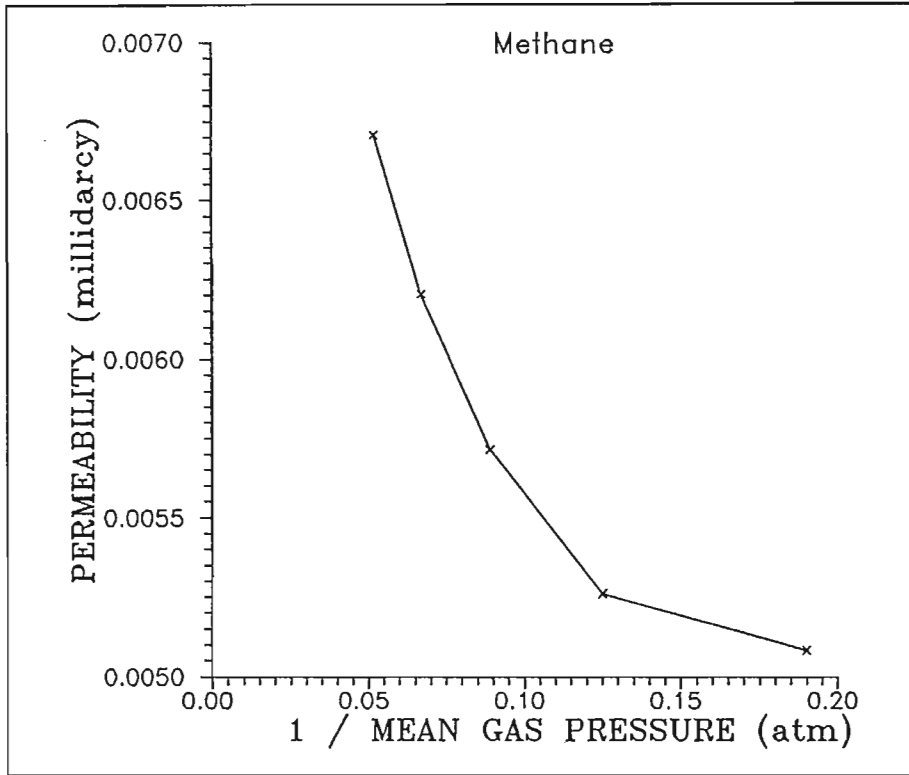


Figure 5.4 Plot of k_s versus $1 / P_m$ for methane, showing a negative slope. (Facies 5).

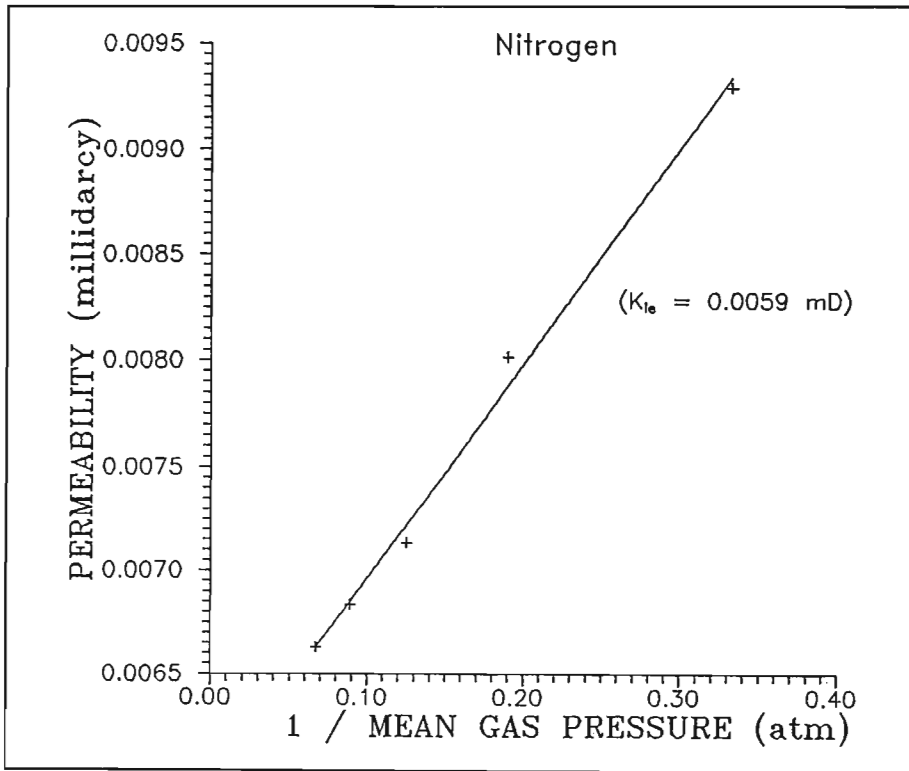


Figure 5.5 Plot of k_s versus $1 / P_m$ for nitrogen showing a positive slope. (Facies 5).

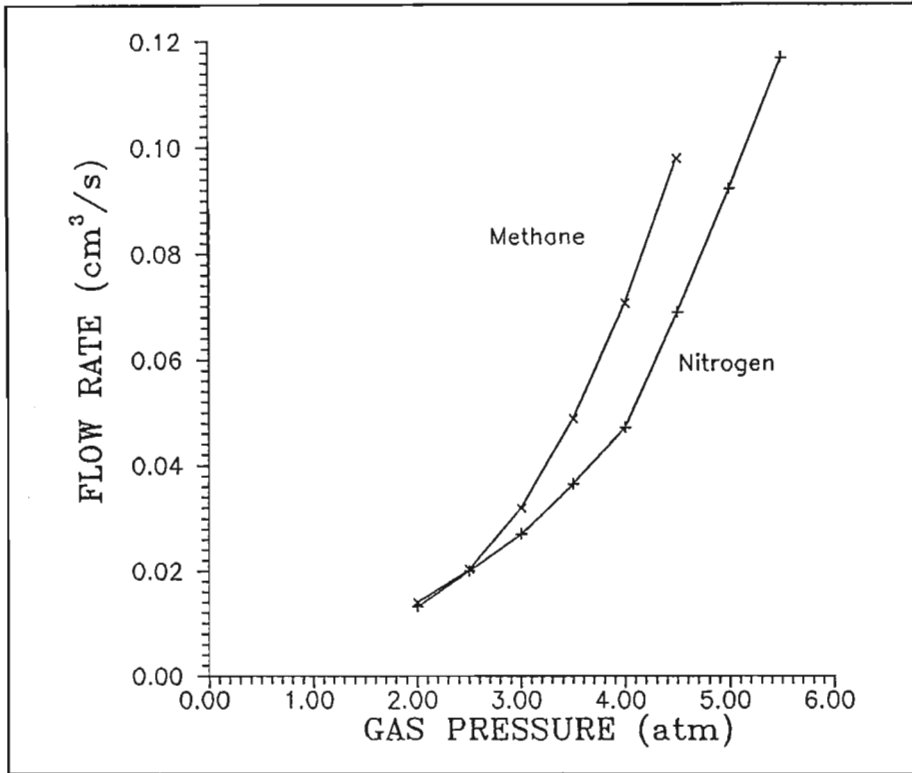


Figure 5.6 Plot of flow rate versus P_1 for both methane and nitrogen for the same sample as in figures 5.4 and 5.5. (Facies 5).

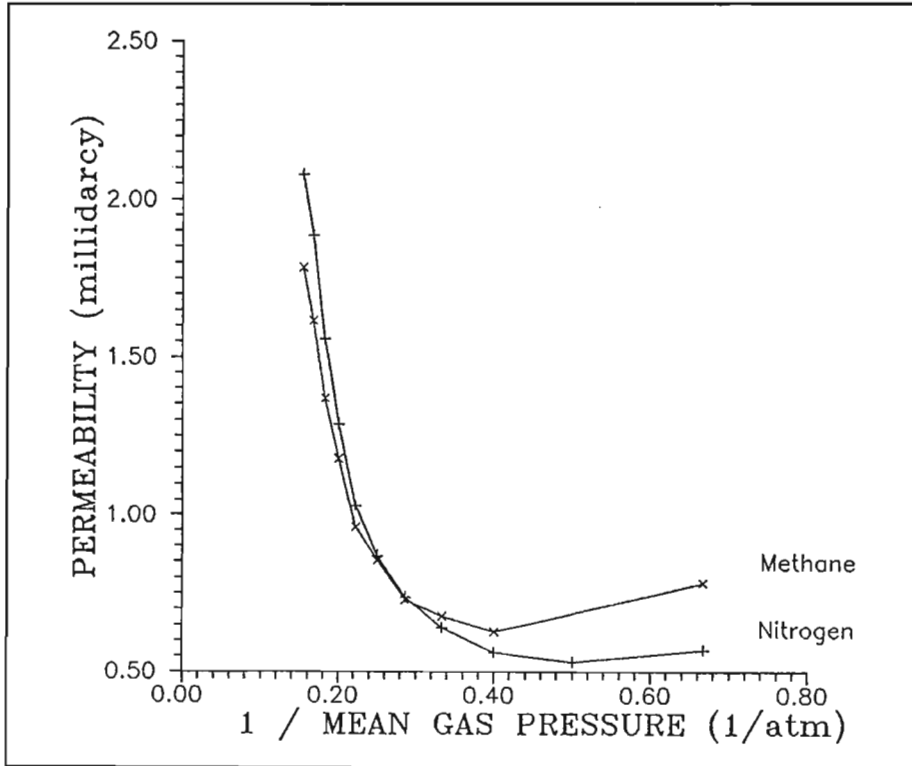


Figure 5.7 Plot of k_s versus $1/P_m$ with both nitrogen and methane showing a negative relationship. (Facies 10).

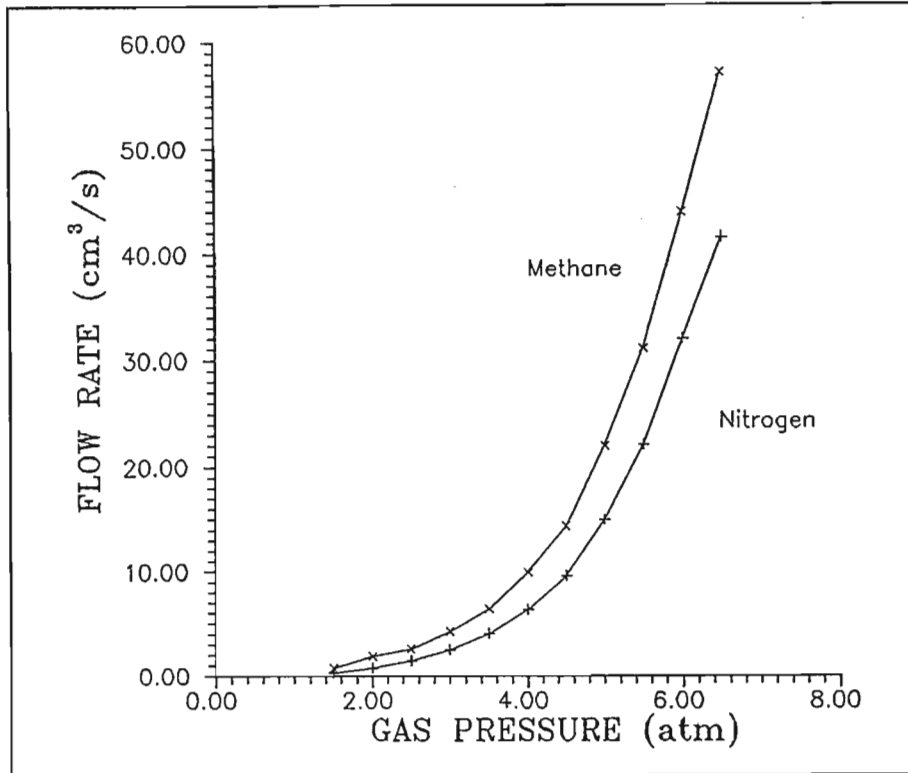


Figure 5.8 Plot of flow rate versus P_1 for nitrogen and methane. Same sample as figure 5.7. (Facies 10).

reciprocal mean gas pressure plots are the Klinkenberg effect and adsorption (eg. Gawuga, 1979). Using Klinkenberg's method of analysis (or ASTM D4525, 1990) the effects of experimental error is negated (eg. Klinkenberg, 1941; Ohle, 1951). If the methane plot has a negative slope but the nitrogen plot for same sample has a positive slope (figures 5.4 and 5.5) it can be assumed, in the author's opinion, that adsorption is the main mechanism responsible. All the facies types exhibiting this behaviour contained some percentage of carbon (determined with total percentage carbon analysis, table 5.3) which adsorb methane and not nitrogen. If both the permeability versus reciprocal mean gas pressure plots had negative slopes (figure 5.7), gas slippage or Klinkenberg's effect, must be the dominant mechanism present. Anomalous plots were obtained from 16% of the tests involving nitrogen and 23% of the tests involving methane. In a small number of cases the extrapolated liquid equivalent permeabilities were found to be negative, which is physically impossible. Scheidegger (1974) states that Darcy's law represents a straight line through the origin, small deviations due to experimental error could therefore result in such negative permeabilities. If the method prescribed by ASTM D4525-85 (1990) is followed, and only three data points on the high gas pressure side is used, the liquid equivalent permeability obtained can in some instances be changed from negative to positive. As negative liquid equivalent permeability values are a physically impossible and the plots with negative slopes indicates that Darcy's law is no longer applicable, those values were not quoted in tables 5.1 and 5.2, although they were recorded as having been tested.

All the specific permeabilities were calculated using a derivation of Darcy's law, equation 3.4,

Table 5.3 Total carbon analysis for different facies types.

Facies	% Carbon ($\pm 0.1\%$)	Number Tested
4	6.3	1
5	5.4	2
7	5.0	4
8	4.0	2
9	1.8	4
10	1.9	9
11	4.8	2
12	1.3	1
22	17.1	2

as mentioned earlier. This equation, according to a number of authors (eg. Scheidegger, 1974; Bass, 1987; Somerton *et al.*, 1975), represents a linear relationship between specific permeability and gas pressure. A straight line (of the form $y = a + bx$) was therefore fitted to all the plots by means of a computer program. For 86% of the nitrogen plots the confidence of fitting a straight line was more than 0.8, with 27% having confidence levels of more than 0.95. In the case of the methane plots 71% had a confidence of more than 0.8, and 40% had a confidence of more than 0.95 toward the fitting of a straight line. Only 5% of the methane and 7% of the methane plots were best fitted by a straight line. Fitting 25 different lines to the plots it was found that in both the cases of methane and nitrogen the most common best fit curve was a parabola ($y = a + bx + cx^2$), 15% of the methane plots and 22% of the nitrogen plots. The second most common best fit curve was found to be a second order hyperbola ($y = a + b/x + c/x^2$) in the case of the methane tests and a beta curve ($y = a \cdot x^b \cdot (1-x)^c$) in the case of the nitrogen plots. It must be realised that in the case of the gas as permeating fluid equation 3.4 was used, which is the second derivation of Darcy's original law (Bass, 1987). The relationship will therefore be exponential rather than linear. In this study none of the correction factors suggested by other authors (eg. Klinkenberg, 1941; Mordecai and Morris, 1971) were added to the basic Darcy equation (equations 3.2 and 3.4), as it is extremely difficult to obtain values for them and most authors agree that their influence is negligible on the final permeability value obtained (eg. Bass, 1987; Scheidegger, 1974). If these factors were included in the equation the overall effect would have been to make it in the form of a straight line, i.e. $y = mx + c$, where m and c are the correction factors.

The permeability (k_s and $k_{i,s}$) was found to vary over very short distances. In figure 5.9 the plots of k_s versus $1/P_m$ for 4 samples taken over a 10 cm distance, belonging to facies type 10 (table 2.2), were

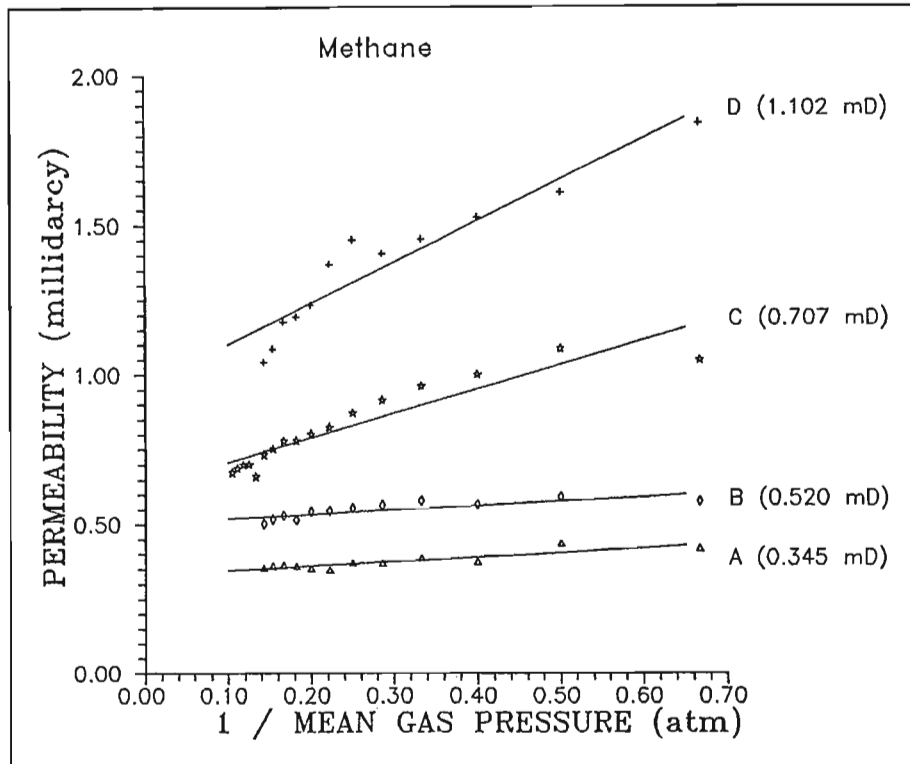


Figure 5.9 Plot of k_s versus $1 / P_m$ for methane, showing variation of k_s and k_{le} (in brackets) with grain size. (Facies 10).

combined to illustrate the variability in permeability (k_s and k_{le}). The grain size increases from the medium grained sample A, to more coarse grained sample D. As can be seen the permeability, both specific and liquid equivalent (quoted in brackets), increases with increasing grain size. The slopes of the graphs become less as the grain size decreases. The distribution of the data points also becomes less linear as the grain size increases. In other words the confidence factor for the fitting of a straight line increases as the grain size decreases. This might be the influence of better sorting, meaning that the flow paths available to the fluid became more or less of uniform geometry so that with an increase in gas pressure the path the fluid takes does not differ significantly from the path the fluid took at the previous gas pressure. Figure 5.9 could also be used as an argument for the fact that a range of permeabilities will be obtained for a specific facies type, and not just a single value.

Two oriented bulk samples from the immediate roof of the Gus seam were used to determine the permeability, and therefore the flow, characteristics in three directions. These samples were identified as belonging to facies 10, i.e. medium to coarse grained sandstone with trough cross beds. Samples used for tests in the Ohle cell were obtained parallel to, and perpendicular to, the bedding. Each sample was reversed so that they were subjected to flow in two directions. The results of the methane tests are given in table 5.4. The results for the tests involving nitrogen are not listed because they closely follow those in table 5.4. No obvious differences between the average liquid equivalent permeabilities could be found between the flow across and the flow parallel to the bedding planes, but this could be a function of the

Table 5.4 Liquid equivalent permeabilities for tests in three directions using methane as permeating fluid.

Orientation:	Direction of flow	Permeability Range (mD)			Number Tested
		Minimum	Maximum	Average	
Parallel to Bedding:	Left to Right	0.2822	0.8171	0.4740	12
	Right to Left	0.0605	1.4218	0.3701	27
Across the Bedding:	Top to Bottom	0.0918	1.8077	0.6225	8
	Bottom to Top	0.1206	0.5970	0.2376	5

difference in the number of tests carried out in each orientation. The average permeability (k_{ie}) was found to be different, in both cases, if the direction of flow was changed. The average permeability (k_{ie}) was found to be slightly less if the fluid flowed from bottom to top than from top to bottom. A flow from top to bottom is comparable with the flow into the mine opening and a flow from bottom to top is comparable to the flow out of the mine opening. Figure 5.10 shows that this is not necessarily the case

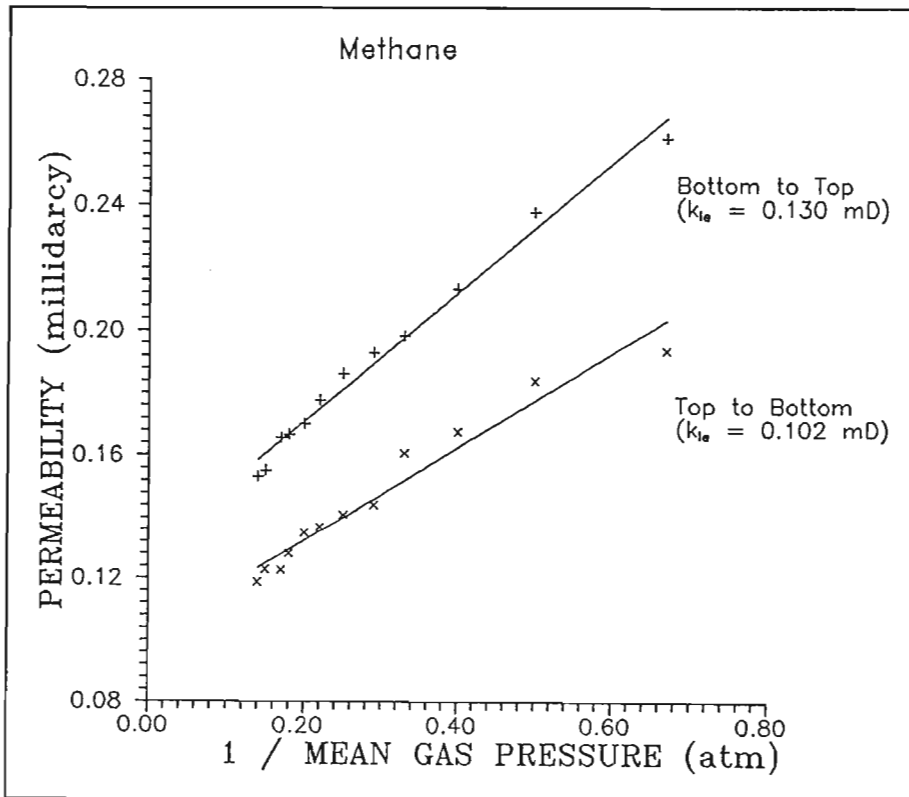


Figure 5.10 Plot of k_s versus $1 / P_m$ for methane, showing variations in k_s and k_{ie} with change in flow direction. (Facies 10).

in individual samples, although the geometry of the plot is the same in both cases. That is if a difference

of 0.03 mD could be shown as being significant. The results listed in table 5.4 also indicate that the permeability of a fluid flowing along a bedding plane will be affected by the direction in which it is flowing. In this instance there is a very slight difference in the average liquid equivalent permeability. Again the number of samples tested might have an influence on the accuracy of such differences.

5.2.2. Water

Tests involving water as the permeating fluid were found to require a substantially longer amount of time to equilibrate than the tests using gas as the flowing fluid. Where a test using methane or nitrogen would take approximately 1 hour to reach equilibrium (constant flow rate at constant pressure differential) it would take the same sample approximately 3 to 4 hours to equilibrate to the applied pressure differential if the permeating fluid was water. In the early stages of the project a hydraulic pump connected to a hydraulic ram was used to supply the water pressure to the sample. This apparatus was only capable of supplying pressures from 1 MPa upwards. In the case of the majority of samples with facies type numbers higher than 9, and a diameter of 60.3 mm, 1 MPa of water pressure at the inlet was enough to fracture them. In one case the water, at a pressure of 1 MPa, punched a hole of about 10 mm in diameter through the centre of the sample. From the geometry of the fractures (usually three radiating outward from the centre of the sample) it was inferred that this setup delivered the pressure in high intensity pulses. These problems were solved by using a constant pressure apparatus that was capable of delivering pressures from about 200 kPa.

Some of the samples broke apart while being vacuum saturated. A large number of samples were found to have increased in both diameter and length, by up to 1 mm, after the vacuum saturation was completed. If a sample broke up, even slightly, a seal between the sample and the O-rings (figure 4.2) may or may not have been achieved successfully, casting doubt on the accuracy of the resulting permeability. No doubt was cast on the results if the sample started to fracture during the test. The flow rate increased suddenly and dramatically, indicating that the flow regime had shifted from being intergranular to fracture flow. The samples that increased in size after being vacuum saturated, most probably due to clay minerals absorbing water and swelling, could not be tested as they could not be made to fit into the Ohle cell. They could be fitted into the cell again if they were allowed to dry out slightly, but then there was no way of knowing if the sample was still fully saturated or not making it unusable.

Table 5.5 gives a summary of the average permeabilities (k_s) obtained from the tests involving water as the permeating fluid for 38 samples. Figure 5.11 shows a plot of specific permeability versus a water pressure range of 200 to 1800 kPa. The specific permeability of the sample towards water increased with increasing water pressure, exactly opposite as the relationship found if gas was used as the

Table 5.5 Average permeability at 1 MPa water pressure for the facies types tested.

Facies Type	Average Permeability in millidarcy at 1 MPa water pressure	Average r^2	Number Tested
3	0.0004	0.48	1
4	0.0001	NA	1
7	0.0042	0.35	3
8	0.0084	0.51	6
10	0.0480	0.42	26
11	0.0660	0.91	1

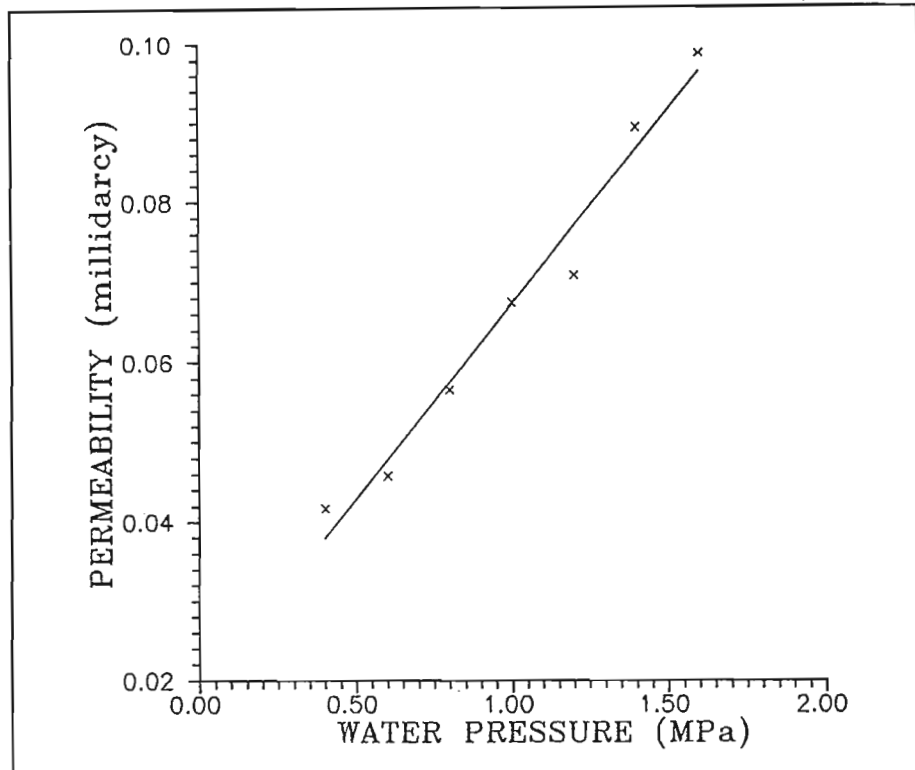


Figure 5.11 Plot of k_s versus water pressure. (Facies 10).

permeating fluid. Such behaviour can be ascribed to the incompressibility of water and the fact that the water molecules have a larger size relative to the mean free flow path (eg. Bass, 1987; Gawuga, 1979; Scheidegger, 1974). This means that the water molecules get pushed through the flow path one at a time whereas many gas molecules are pushed into the mouth of the pore space. The gas molecules then get "crowded" at the entrance with the result that less gas passes through the sample along flow path and thereby reducing the permeability the higher the pressure the gas is under. The values in

table 5.5 are those obtained at 1 MPa water pressure. Klinkenberg (1941) found that increasing the gas pressure to infinity the permeability approached that of the specific permeability of the medium to water (or any other liquid). He, however, does not mention the pressure at which the water must be to be comparable to the liquid equivalent permeabilities obtained when using gas as the permeating fluid. One megapascal inlet pressure were chosen in this study because at that pressure it was found that the specific water permeabilities for the different facies types showed the best correlation to the liquid equivalent permeabilities obtained from the tests involving gas as the permeating fluid. The average specific water permeabilities shows an exponential increase with increase in grain size, as would be expected (figure 5.12).

When plotting specific permeabilities for a range of water pressures, very few samples resulted in best fit straight lines with confidence levels higher than 0.5 (figure 5.11). The most common best fit curve was found to be a second order hyperbola ($y = a + b/x + c/x^2$) with 26% of the samples falling into

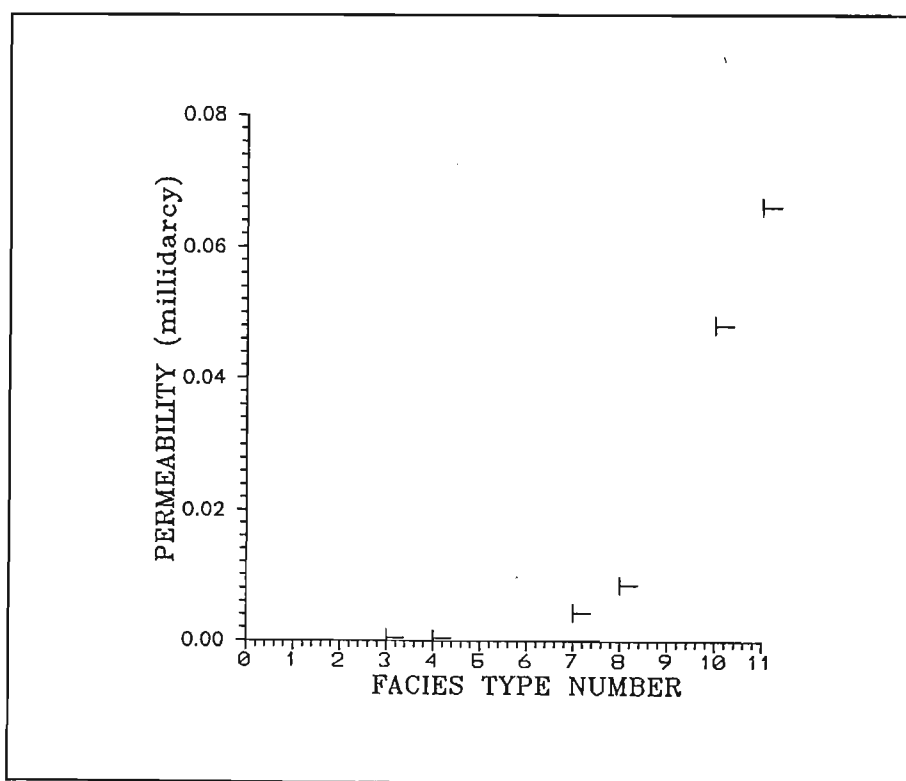


Figure 5.12 Plot showing the relationship between k_s for water (at 1000 kPa inlet pressure) and facies type.

this category. The second most common best fit curve was found to be a reciprocal relationship ($y = a + bx + c/x$) and this included 16% of the samples tested.

Permeabilities were also determined in three directions on the samples obtained from the two bulk samples. The majority of these samples swelled and were unusable. Results from the samples that

could be tested followed those set out in table 5.4 if the specific permeability at an inlet water pressure of 1000 kPa was taken as comparable to the liquid equivalent permeability of the sample obtained from the tests involving methane as the permeating fluid.

5.3. HOEK CELL

The time needed for tests involving methane as the permeating fluid to reach equilibration, was approximately 1 hour in the case of the Ohle cell tests. Applying a hydrostatic stress (i.e. $\sigma_1 = \sigma_2 = \sigma_3$) of 4 MPa, equilibration was only reached after about 5 hours in the Hoek cell. Figure 5.13 shows the typical time to reach equilibrium for a facies type 8 (table 2.2) sample, and it was found that higher numbered facies types, which are generally more permeable, required less time to equilibrate and facies types with lower numbers required more time to equilibrate.

In order to obtain a basis for comparison with the tests done under atmospheric conditions (Ohle cell), a series of permeability measurements were done at for a range of gas pressures at a hydrostatic load of 4 MPa in the Hoek cell. Table 5.6 shows the results obtained from 39 tests carried out on 21

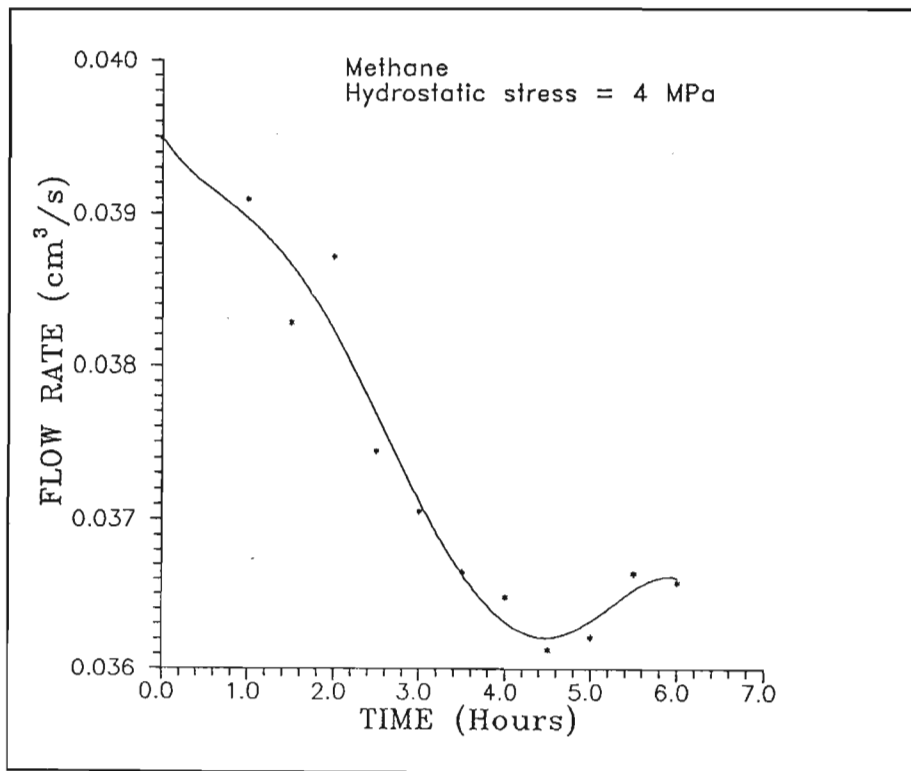


Figure 5.13 Plot showing the change in flow rate with time under a constant external hydrostatic stress of 4 MPa. (Facies 8).

samples. Sixteen percent (16%) of the tests produced plots showing deviations from Darcy's law. These

Table 5.6 Liquid equivalent permeability ranges obtained under a constant 4 MPa hydrostatic stress.

Facies Type	Permeability Range (mD)			Number Tested	Average r^2
	Minimum	Maximum	Average		
7	0.0061	0.0061	0.0061	1	0.92
8	0.0060	0.0666	0.0363	2	0.72
9	0.3492	3.3127	1.3837	3	0.87
10	0.0096	2.9999	0.5852	14	0.69
12	0.5280	0.5280	0.5280	1	0.99
14	0.0075	0.1316	0.0963	4	0.57
22	0.4182	0.4182	0.4182	4	0.67

included one of the coal samples and all of the facies type 2 and 6 samples. Their results are therefore absent from table 5.5. The most common, 30% of the tests, best fit curve to the data points was found to be a parabola ($y = a + bx + cx^2$). The second most common, 16% of the tests, best fit curve was found to be a second order hyperbola ($y = a + b/x + c/x^2$).

It was found that an increase in either axial stress (σ_1) or confining stress (σ_3) or both will lead to a significant reduction in both specific and liquid equivalent permeabilities. Figure 5.14 shows the

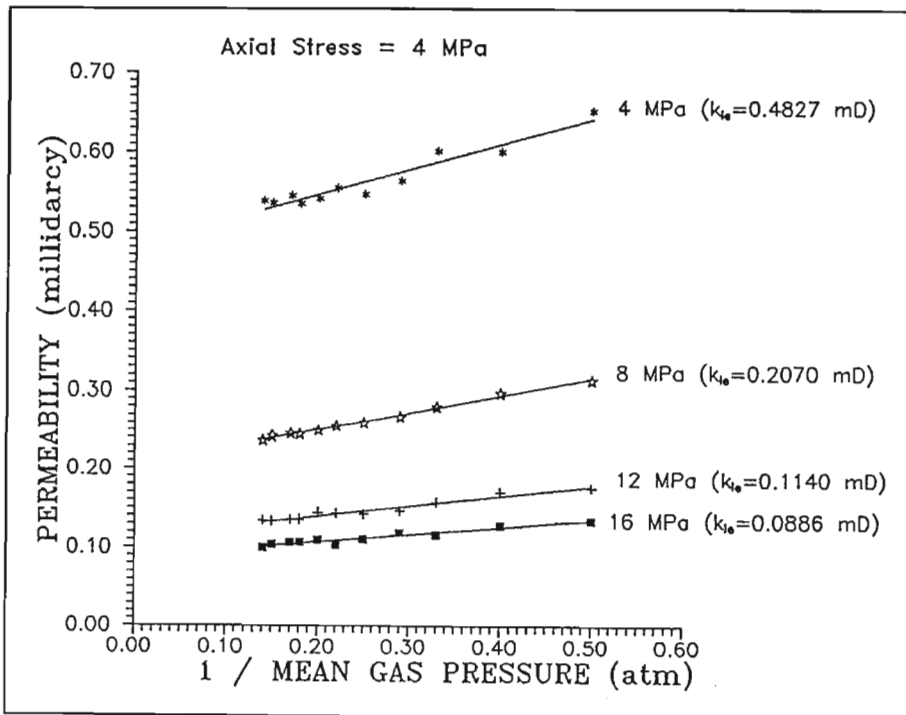


Figure 5.14 Plot of k_s versus $1/P_m$, for methane, showing the variation of k_{le} with an increase in σ_3 . (Facies 10).

consecutive decrease in both liquid equivalent and specific permeabilities with each increase in applied confining stress (σ_3). Gawuga (1979) found that at a certain point, the sample will no longer deform, and the permeability obtained will remain constant no matter by how much the applied load is still increased. The same effect is obtained if the axial stress (σ_1) or the hydrostatic stress ($\sigma_1 = \sigma_2 = \sigma_3$) were increased in steps of 4 MPa. In all the cases (axial stress, confining stress and hydrostatic stress increase) the reduction in specific and liquid equivalent permeability due to the first 4 MPa increase in stress (i.e. from 4 MPa to 8 MPa) was found to be the largest, up to 50%.

Loading the sample and then unloading it produced plots similar to figure 5.15. The specific

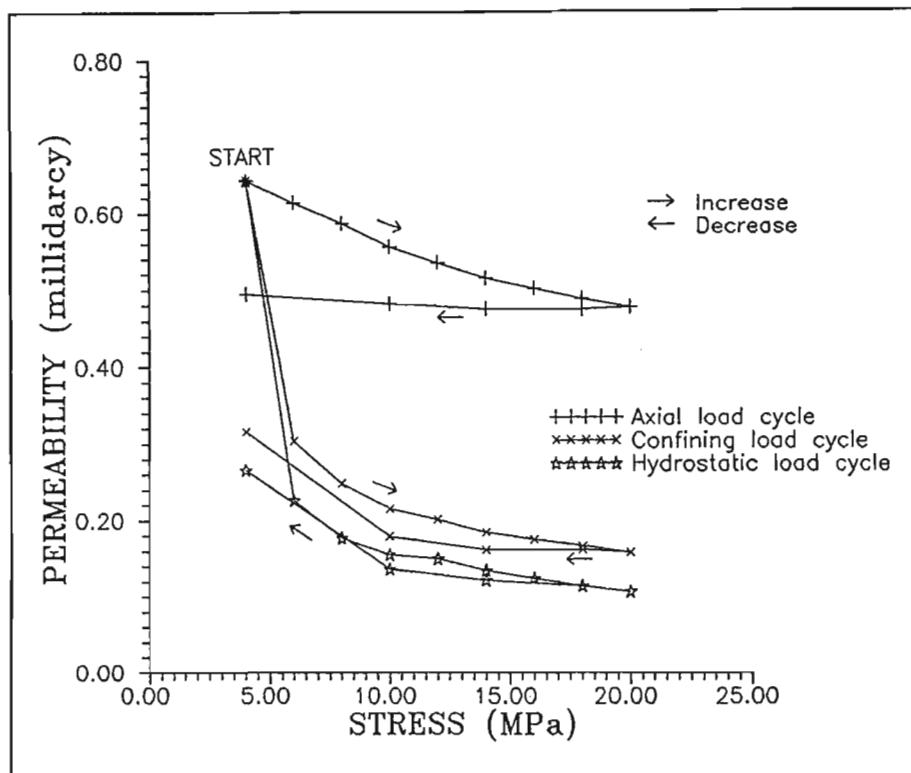


Figure 5.15 Plot of k_s versus $1 / P_m$ for methane showing the difference in reduction in k_{ie} produced by applying different stress loading cycles. (Facies 12).

permeability decreased with increase in applied stress and then increased with decrease in applied stress. In the case of the sample in figure 5.15 the stress had to be removed totally for 2 to 3 days before the same initial permeability could be obtained. This might seem to be a surprising large amount of time, but as figure 5.16 shows, the difference in permeability (k_{ie} and k_s) is still marked after the sample was relieved from its applied stress for more than 30 minutes. This kind of behaviour, where there is only a slight elastic recovery immediately after the stress is reduced, and a full recovery after a longer period of time, is referred to as time-dependent (or an-elastic) recovery (Dr. M.K. Watkeys, pers. comm., 1993). The permeability of the sediments is therefore influenced by the stress history, for a short while at least.

Figure 5.15 shows that the application of load cycles of different stress types affect the samples

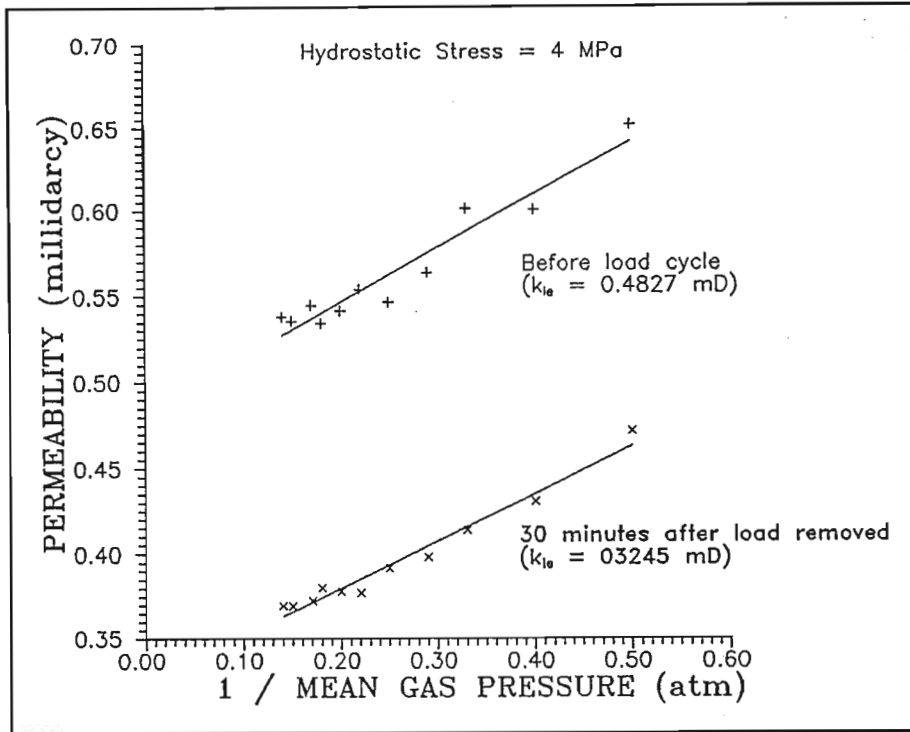


Figure 5.16 Plot of k_s versus $1 / P_m$ for methane, showing difference in k_{ie} before and after axial load cycle. (Facies 10).

similarly. The permeability reduction due to an axial load cycle is less than the permeability reduction due to a hydrostatic load cycle (figure 5.15). The permeability reduction due to a confining stress load cycle lies somewhere between the two, but more towards the amount of reduction experienced from a hydrostatic stress increase. If the stress is released in stages and the permeability measured after each stage, it is found that the permeability will increase with decrease in applied stress. The final permeability is, however, not the same as the starting permeability, meaning that some deformation of the internal structure of the sample have taken place.

Figure 5.17 shows that once a load cycle was applied, consecutive loading cycles have little influence on the permeability if the sample is not allowed to recover fully between the tests. The sample in figure 5.17 shows a 84 % reduction liquid equivalent permeability after the first load cycle and virtually no change, from 0.087 to 0.082 mD after the second load cycle. Gawuga (1979) and Mordecai and Morris (1971) found that, in the case of coal, the permeability no longer showed any reduction after the second load cycle. The permeability is then said to be stabilized. Due to the more elastic nature of the sediments, it can be assumed that they would require more than 2 load cycles to reach a stable permeability.

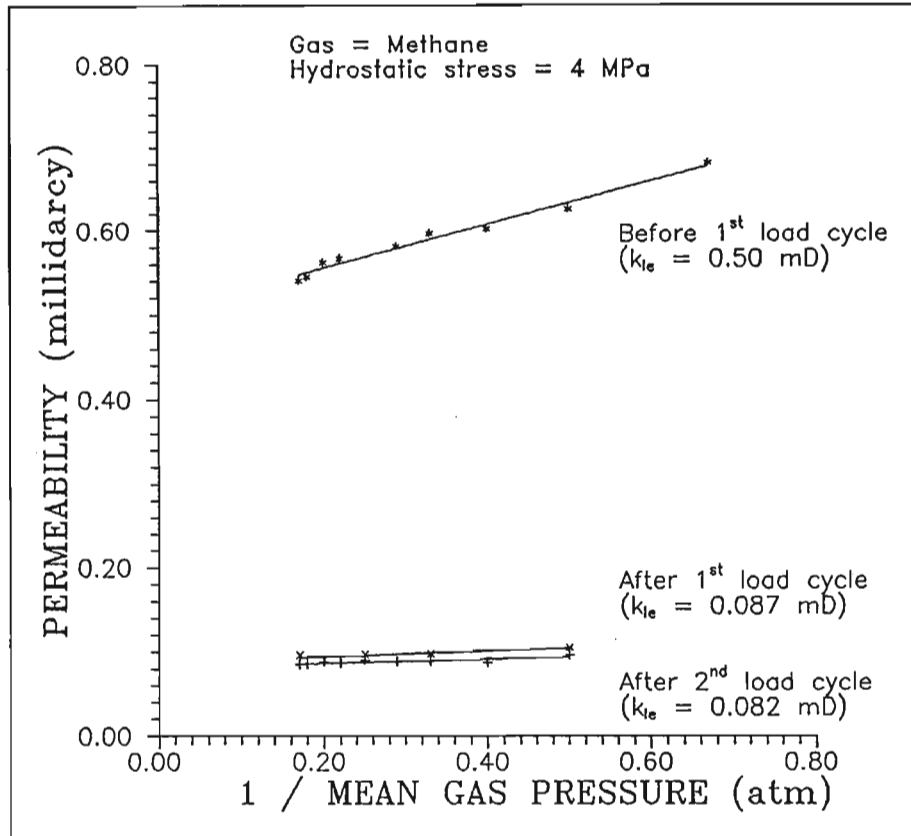


Figure 5.17 Plot of k_s versus $1 / P_m$, for methane, showing the change of k_e before and after a series of axial load cycles. (Facies 9).

By increasing and then decreasing the gas pressure while keeping the hydrostatic stress constant and determining the permeability after each increment, a plot like figure 5.18 is obtained. This figure shows that a permeability hysteresis exists, the flow does not follow the same path when the gas pressure is increased as when the gas pressure is decreased. The beginning and end values for the specific permeability, however, stays the same. Even hydrostatic stresses of 11 MPa are not able to change the internal structure of a natural porous medium to such an extent that the paths available to the fluid becomes isotropic. The permeability is therefore anisotropic under normal circumstances.

Some of the samples cored for the three dimensional analysis from the two bulk samples were also subjected to triaxial testing. Table 5.7 compares the liquid equivalent permeabilities measured parallel and across bedding for these samples at hydrostatic pressures of 4, 8, 12 and 16 MPa. Table 5.7 shows that at all stress levels, the liquid equivalent permeability across the bedding planes is significantly less than the liquid equivalent permeability parallel to the bedding planes. This results are the opposite of those listed in table 5.4, but the discrepancy might be due to the number of tests done, making the results in table 5.4 statistically more correct. As in table 5.4, table 5.7 shows that there are differences in the average liquid equivalent permeabilities when measured in two opposing flow directions. This is most probably due to the anisotropy of the flow path, i.e. the packing of the grains results in different

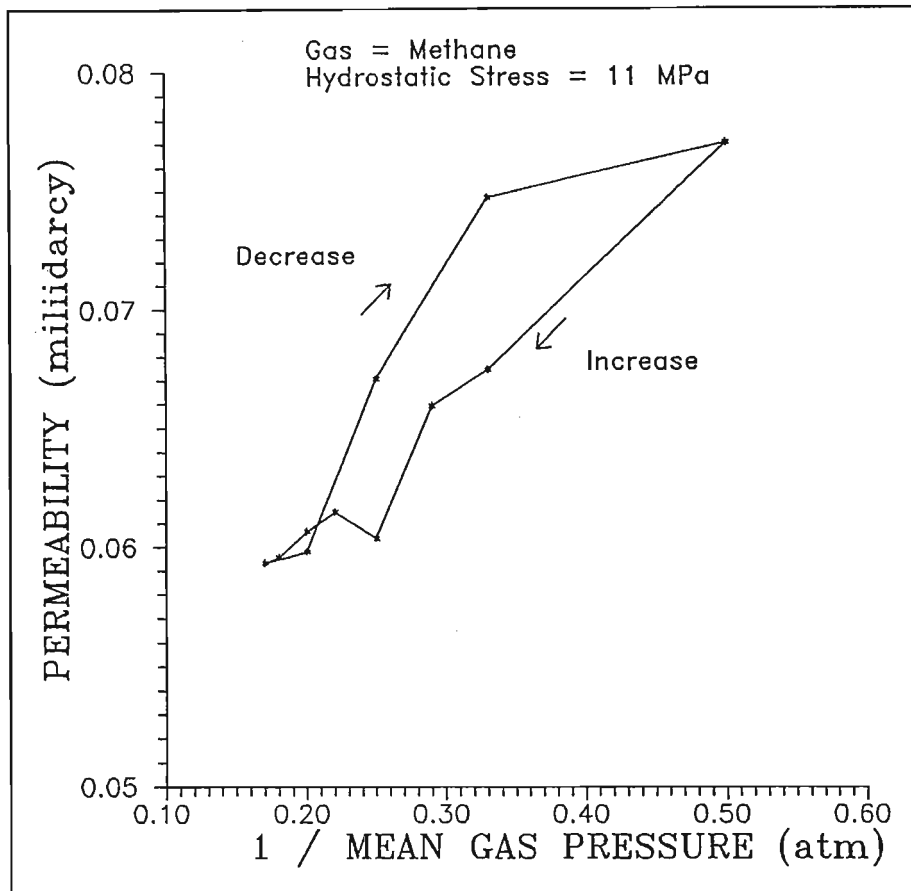


Figure 5.18 Plot of k_s versus $1 / P_m$, for methane, showing anisotropic behaviour, even at hydrostatic pressures of 11 MPa. (Facies 9).

flow path geometries in different directions.

5.4. POTENTIAL SOURCES OF EXPERIMENTAL ERROR

In any experiment dealing with natural substances there are always one or more factors that can give rise to unexpected results. Some of these factors can be controlled by the operator and others can not. Operator and apparatus errors that can occur are discussed separately for each experiment below.

5.4.1. Ohle cell

5.4.1.1. Gas

In his experiments Klinkenberg (1941) found the experimental error for the determination of k_s to be roughly 5 % on synthetic substances (Jena glass filters). This is also the allowable margin for error prescribed by ASTM D4525-85 (1990), but that value pertains to the difference obtained over three consecutive tests using air as the permeating fluid. Ohle (1951) found the difference between the liquid

Table 5.7 Liquid equivalent permeability ranges in three dimensions for methane as the permeating fluid at hydrostatic pressures of 4, 8, 12 and 16 MPa.

	Direction of Flow	Permeability Range (mD)			Number Tested	Average r^2
		Minimum	Maximum	Average		
Hydrostatic Pressure: 4 MPa						
Orientation: Parallel to Bedding	Left to Right	0.6308	2.9999	1.8153	2	0.79
	Right to Left	0.9200	1.4388	1.1794	2	0.89
Orientation: Across Bedding	Top to Bottom	0.2085	0.5152	0.3396	4	0.61
	Bottom to Top	0.1680	0.2983	0.2528	3	0.86
Hydrostatic Pressure: 8 MPa						
Orientation: Parallel to Bedding	Left to Right	0.2672	1.1388	0.7030	2	0.86
	Right to Left	0.5960	0.5960	0.5960	1	0.92
Orientation: Across Bedding	Top to Bottom	0.0819	0.1383	0.1101	2	0.56
	Bottom to Top	0.1071	0.3251	0.1808	3	0.84
Hydrostatic Pressure: 12 MPa						
Orientation: Parallel to Bedding	Left to Right	0.1564	0.8842	0.5203	2	0.91
	Right to Left	0.4391	0.4391	0.4391	1	0.89
Orientation: Across Bedding	Top to Bottom	0.0597	0.1100	0.0848	2	0.48
	Bottom to Top	0.0746	0.1644	0.1195	2	0.86
Hydrostatic Pressure: 16 MPa						
Orientation: Parallel to Bedding	Left to Right	0.1125	0.4514	0.2819	2	0.96
	Right to Left	0.3583	0.3583	0.3583	1	0.77
Orientation: Across Bedding	Top to Bottom	0.0461	0.0817	0.0639	2	0.75
	Bottom to Top	0.0508	0.1139	0.0749	3	0.80

equivalent permeabilities of different fluids to be around 10% with a reproducibility of 90 %. In this study the reproducibility was found to be between 71 and 75 % (section 5.2.1) and the variation between the liquid equivalent permeabilities for different fluids were on average still 10 %. The difference between Ohle's findings and the findings of this study might be explained by the inherent variability in the sedimentary strata used as samples for this study versus the synthetic regularity of the Jena glass filters used by Klinkenberg.

The specific permeability at each gas pressure differential is calculated by equation 3.4. The quantity of flow per unit time (Q), the length (L) and the diameter (d) of the sample is measured, while the inlet gas pressure (P_1) is read off the transducer's digital readout (figure 4.3) and the outlet gas pressure was assumed to be a constant at 1 atmosphere (100 kPa).

The largest source of potential error with this apparatus was gas leakage. The fluid might leak between the rubber o-ring and the sample (figure 4.2) resulting in a higher volume of flow than would be expected. The effectiveness of the seal could be tested by placing a steel disc in the cell, but it was found that the edges of the sample need only have a slight imperfection for a significant amount of fluid to leak by. The steel disc, however, allows the operator to determine if gas is leaking from plugs A or B when the gas pressure is increased. If fluid leaks out of the connection between the outlet of the cell and the tube leading to the bubble flow meter, the measured flow rate might be underestimated. The quantity of flow measured depends on the time a soap bubble travels between two set calibrations on the graduated burette. Apart for the obvious error of parallax, errors can also occur from the lapse in time between the point at which the bubble crosses the graduation and the point when the stopwatch is stopped. A hundredth of a second translates into an error of 0.22 % in the k_{le} permeability obtained. If the volume recorded between the two graduations on the burette for which the time was obtained was in error of 0.1 cm³ an error of up to 0.99% can be made in the calculation of the liquid equivalent permeability. Misreading the volume by 1 cm³ an error of up to 9 % can be introduced in the calculation of the liquid equivalent permeability.

The lengths of the samples were measured by means of a Vernier calliper calibrated to within 0.01 mm. Such small variation introduces a negligible error (less than 0.00001 %) into the calculated liquid equivalent permeability. A variation of 0.1 mm, on the other hand can introduce an average error of 0.6 % in the k_{le} obtained. Varying the diameter by 1 mm can introduce an average error of 5.9 % in the k_{le} obtained.

As a large part of equation 3.4 is involved with the pressure differential across the sample, and because the equation uses the square of these values, the values used for both the inlet and the outlet pressure are very important. The applied gas pressure was obtained by reading a number from the digital

readout of the transducer (figure 4.2). A difference could exist between the gas pressure displayed on the transducer's readout and the actual pressure applied to the sample. This difference, however, could be assumed to be constant in all cases. Any leak in the joints and taps from the cylinder to the inlet of the cell could cause the applied pressure to be less. If the whole of the annular space between the gas inlet and the sample is not filled by the same gas (eg. air and methane) pressure differences could occur. Nitrogen and methane are compressible gases and some compression of the gas molecules in the annular space between the gas inlet and the sample have to be assumed, although it is hard to quantify the amount of pressure loss this represents. Lastly the transducer's accuracy (± 0.01 kPa) could result in the use of an inappropriate value in the calculation of the k_s , and therefore in the k_{ie} obtained. The gas pressure used in the equation is therefore designated the mean inlet pressure and not the exact inlet pressure. Table 5.8 shows the percentage change in k_{ie} for the sample used in the construction of figure

Table 5.8 Table showing the percentage error introduced by varying the inlet gas pressure for a specific sample.

Change in inlet gas pressure (kPa)	Percent change in liquid equivalent permeability (k_{ie})	
	Nitrogen	Methane
0.1	0.28	0.26
1	2.21	1.78
2	4.24	3.74
3	5.33	5.27
4	6.61	6.53
5	8.26	7.92
10	14.08	13.35

5.1 for a series variations in the inlet gas pressure. As the table indicates the amount of the error is virtually the same for nitrogen as for methane. A change in outlet pressure is much more dramatic as an error of 0.1 kPa can produce an error of up to 3 % in the k_{ie} . The increase in the percentage error is also not linear, but exponential in the k_s . An error of 1 kPa can produce an error of up to 135 % in the obtained k_{ie} .

Errors due to dirt and dust clogging up the pores because the sample was not washed properly could be significant, as the pore volume and pore interconnectedness is the vital factors controlling the permeability of the sample. As the pore volume or porosity of the samples was not determined, the effect of this could not be judged.

If all the different errors were active during one particular test, the total experimental error would be around 10 % as indicated by the difference in k_s for tests involving different gases.

5.4.1.2. Water

The basic assumption of equation 3.2 is that water is an incompressible liquid. Air is not. If the de-airing was not complete, or all the air was not displaced out of the pores of the sample, some degree of compression might result. The quantitative effect of this was not calculatable as the amount of air present cannot be determined. That it has an effect on the results is obvious in view of figure 3.5 and the discussion of the limitations of Darcy's law in section 3.4 to which it refers.

Table 5.9 shows the influence on the specific permeability at different fluid pressures. The

Table 5.9 Table showing the variation in k_s due to errors in the factors used to calculate it.

Factor	Error in factor	% Change in k_s	Inlet fluid pressure (kPa)
Inlet fluid pressure	1 kPa	0.11	
Viscosity	0.001 cP	1.0	1000
Volume measured in burette	0.01 cm ³	0.1	1000
	1 cm ³	40	200
	1 cm ³	9	1600
Time	1 s	0.11	1000
Length	0.1 mm	0.61	1000
Diameter	0.1 mm	0.33	1000
Outlet fluid pressure	1 kPa (0.01 atm)	0.1	1000
	10 kPa (0.1 atm)	1.0	1000

cumulative effect of all the errors can be more than 10 % in the specific permeability at 1000 kPa inlet water pressure. In all cases the effect of an error decreases with increase in inlet water pressure so that if the k_s at 200 kPa was used as the reference permeability, the cumulative error would have been in the order of 50 %.

5.4.2. Hoek cell

All the tests were done using methane which precluded the determination of the experimental error by comparing the variation in k_{ie} obtained for different gases (Ohle, 1951). Equation 3.4 was also used to calculate the specific permeabilities in this experiments, thus the same errors as discussed in the Ohle cell section could be introduced here. The external stress regime obviously has an effect on the size of the error introduced. Table 5.10 illustrates the difference in influence that the same error had under different applied stress conditions. The effect of the error on the liquid equivalent permeability was less the higher the applied hydrostatic stress. The influence of the errors on the specific permeability decrease with increase in inlet gas pressure. On average the cumulative effect of the errors can be up to 10 %.

Table 5.10 The influence on the k_{ie} at different hydrostatic stresses due to variations in the factors used to obtain it.

Factor	Change in factor	% Change in k_{ie}	Hydrostatic stress (MPa)
Inlet gas pressure	1 kPa	0.7	4
	1 kPa	0.4	11
	5 kPa	3.0	4
	5 kPa	1.6	11
Time	0.01 s	2.6	4
	0.01 s	1.2	11
	1 s	13.5	4
	1 s	4.3	11
Volume	0.01 cm ³	0.1	Same at both 4 and 11 MPa applied hydrostatic stress
	0.1 cm ³	0.5	
	1.0 cm ³	5.5	
Length	0.01 mm	0.1	4
	0.01 mm	0.8	11

CHAPTER 6

CONCLUSIONS

It can be concluded that permeability (k_s and k_{lg}) is a physical property of a rock, which varies even over very short distances, and depends on many internal and external factors. The permeability is also anisotropic and depends on the path the fluid will take as it flows through the medium. A change in direction of flow can result in up to an order of magnitude difference in the specific permeability. Resultingly, liquid equivalent permeability ranges rather than singular liquid equivalent permeabilities are quoted for any facies type. The definition of the minima and maxima for the ranges depends on the number of samples tested for each facies type and on the exact data points used to extrapolate from.

It can be seen that the specific permeability of a sediment towards a gas, such as nitrogen and methane, will decrease with an increase in gas pressure. On the other hand the specific permeability of a sediment towards a liquid, such as water, will increase with an increase in water pressure. For comparison between the tests using methane and nitrogen and the tests involving water as the permeating fluid, it was found that the liquid equivalent permeability for the test involving gas and the specific permeability at 1 MPa gives the best results.

The allowable experimental error, according to previous researchers, is between 5 and 10%. This value depends on how the error is calculated. If the error is calculated as the difference between the liquid equivalent permeabilities obtained from different gases or by the difference in permeability obtained from consecutive tests on the same sample. The experimental error in this study was found to be 10% in if the percentage error is determined by comparing the k_{lg} obtained from two different gases and if all the variables in the equations used are varied together. The influence of a variation in any one of the variables in the equation diminishes with increase in applied fluid pressure.

If carbon in one form or another is present in the sample, it may adsorb methane and result in anomalous plots. It can be shown that this effect can be distinguished from the Klinkenberg effect by the simple expedient of testing the same sample consecutively with nitrogen and methane and then plotting the specific permeabilities obtained against the reciprocal mean gas pressure.

Plotting the specific permeability at a series of gas pressures against the reciprocal mean gas pressure does not result in a linear plot, but rather in a parabola in the case of gas being the permeating fluid, and a second order hyperbola in the case of water being the permeating fluid. This indicates that the equations used do not represent a linear relationship between volume of flow and pressure differential across the sample such as their parent equation, Darcy's law, does.

Application of an external stress result in a decrease in specific and liquid equivalent permeability. The amount by which the permeability decreases is controlled by the type of external stress applied. The biggest decrease occurs when the applied stress is hydrostatic and the smallest decrease is obtained when the applied stress is axial. An increase in confining stress results in a larger decrease than an increase in axial stress alone, but results in a smaller decrease than an increase in hydrostatic stress. Permeability (k_s and k_{le}) is dependent on the stress history of the sample. The influence of the stress history decreases with each application of a load cycle and will disappear after two to three load cycles. Internal deformation due to the application of the load was not recovered immediately after the load was removed, the samples therefore could be said to show an-elastic behaviour.

Under the influence of a load the permeability will decrease with time. This decrease will continue until equilibrium is reached. Equilibrium is assumed when the flow rate stabilizes. The permeability decreases with time, and at a certain stage will reach equilibrium.

Tests involving gas as the permeating fluid requires substantially less time to complete than tests involving water as the permeating fluid. The liquid equivalent permeability obtained from the tests involving nitrogen and methane can be compared to the specific permeability obtained using water as the permeating fluid. Correlation between liquid equivalent permeability and specific water permeability, however, depends on the pressure of the water when permeating through the sample. In practice it is therefore not necessary that the lengthy tests involving water as the permeating fluid need to be carried out to obtain a significant correlation between permeability and facies type. It is only advisable to use water as the permeating fluid if it can be shown that the water might be reactive to the samples tested.

The definition of the lower and upper limits for each range were found to be dependant on the number of tests done on samples for that facies type. Nonetheless a relationship of increasing permeability with increasing grain size was found in the coarser grained facies (facies type 8 and higher). For the finer grained facies types the permeability was found to decrease with increase in grain size. This is not detrimental if the results were to be used as roof fall hazard indicator or to characterize the flow character for the extraction of coalbed methane. A permeability versus facies type graph can be constructed, such as shown in figure 5.2. If a well was sunk for the extraction of coalbed methane or holes were drilled in advance of the mining face, an idea of the permeability and therefore the flow character could be formed just by identifying the facies type and looking up the permeability from the graph.

In general it can be concluded that the methods discussed can be useful in characterizing the flow in one specific location, but more work is needed to define the relationship between facies type and permeability more fully, especially with reference to the influence of macro structures such as joints,

fractures and discontinuities. A more detailed microscopic study might delineate the borders between the different facies types more conclusively and so enable a better relationship of facies type to permeability to be produced.

REFERENCES

- Allen, J.R.C. (1985). *Principals of physical sedimentology*. George Allen and Urwin, London. pp. 14 - 15.
- Anon (1987). R.S.A. Coal 1987: Operating and developing coal mines in the Republic of South Africa. *Minerals Bureau, Directory 2/87*. Department of mineral and energy affairs. 61 p.
- ASTM D4525-85. (1990). *Standard test Method for Permeability of rocks by flowing air*, Vol. 04.08. pp. 730 - 733.
- Bass, D.M. (1987). Properties of reservoir rocks. *Petroleum engineering handbook*. Bradley, H.B. (Ed). Society of Petroleum Engineers, Richardson, TX, U.S.A. Chapter 26.
- Bober, W. and Kenyon, R.A. (1980). *Fluid mechanics*. John Wiley and Sons. pp. 285 - 335.
- Brace , W.F. (1977). A note on permeability changes in geologic material due to stress. *Proc. of Conference II: Experimental Studies of Rock Friction with Application to Earthquake prediction., U.S.G.S. Menlo Park, CA - Best concise summary of literature results*.
- Bradey, J.F. and Boss, G. (1988). Stokesian dynamics. *Ann. Rev. Fluid Mech.* Vol. 20. Annual Reviews Inc., Paolo Alto. pp. 111 - 157
- Cadle, A.B., Cairncross, B., Christie, A.D.M. and Roberts, D.L. (1990). The permo-triassic coal-bearing deposits of the Karoo basin, Southern Africa. *Economic geology research unit (WITS), Information circular*. No. 218, March 1990. 37 p.
- Chakrabarti, A.K. and Taylor, R.K. (1968). The porosity and permeability of the Zawar dolomites. *Int. J. Rock Mech. Min. Sci.* Vol.5. Pergammon Press, Great Britain. pp. 261 - 273.
- Crook, J.M., Daw, G.P. Howell, F.T. and Morgan, F.R. (1971). Permeation properties of unfissured Bunter sandstones of Lancashire and Yorkshire. *Geotechnique*, Vol 21. pp. 256 - 259.
- Crook, J.M., Howell, F.T., Woodhead, F.A. and Worthington, P.F. (1973). Permeation properties of Bunter sandstones from the Chesire and Fylde basins. *Geotechnique*, vol 23. pp. 262 - 265.
- Cyru, T. (1989). Structural analysis of the methane content in the deposit. *Rock mechanics as a guide for Efficient utilization of Natural Resources*. Khair (ed). Balkema. Rotterdam. pp. 883 - 891.

David, C. and Darot, M. (1989). Permeability and conductivity of sandstones. *Rock at great depth*, Vol. 1. Maury and Fourmaintraux (eds). Balkema, Rotterdam. pp. 203 - 210.

Daw, G.P. (1971). A modified Hoek-Franklin triaxial cell for rock permeability measurements. *Geotechnique*, Vol. 21. pp. 89 - 91.

Debschütz, W., Krückel, U and Schopper, J.R. (1989). Effects of geostatic stress and pore pressure on the klinkenberg permeability factor and other fluid flow parameters. *Rock at great depth*, Vol 1. Maury & Fourmaintraux (Eds.). Balkema, Rotterdam. pp. 179 - 180.

Desai, C.S. (1975). Finite element methods for flow in porous media. *Finite elements in fluids - Volume I: Viscous flow and hydrodynamics*. Galagher, R.H., Oden, J.T., Taylor, C. and Zienkiewicz, O.C. (Eds). John Wiley and Sons. Chapter 8, p 157 - 182.

Dullien, F.A.L (1979). *Porous media: Fluid transport and pore structure*. Academic press, Inc. New York. Chapter 2. pp. 5 - 74.

Gawuga, J.K. (1979). *Flow of gas through stressed carboniferous strata, Parts 1 and 2*. Unpublished Ph.D. thesis, University of Nottingham. 152p. + 362p.

Gray, D.H., Fatt, I and Bergamini, G. (1963). The effect of stress on Permeability of sandstone cores. *Society of Petroleum Engineers Journal*. June 1963.

Greenshields, H.D. (1986). Eastern transvaal coalfield. *Mineral deposits of Southern Africa*. Anhaeusser, C.R. and Maske, S. (Eds) Vol. I and II., Geol Soc South Africa. pp. 1995 - 2010.

Harpalani, S and Schraufnagel, R.A. (1989). Flow of methane in deep coal seams. *Rock at great depth*, Vol. 1. Maury and Fourmaintraux (Eds.), Balkema, Rotterdam. pp. 195 - 201.

Harpalani, S. and McPherson, M.J. (1984). Technical note: The effect of gas evacuation on coal permeability test specimens. *Int. J. Rock Mech. Min. Sci. & Geomech. Abstr.* Vol. 21, No. 3. Printed in Great Britain. pp. 161 - 164.

Harpalani, S. and McPherson, M.J. (1985). Effect of stress on permeability of coal. *7th US Symposium on Rock Mechanics*. Rapid City, SD. 26-28 June 1985. pp. 831 - 839.

Harpalani, S., Zhao, X. and Farmer, I.W. (1991). The mechanics of gas flow in coal - A laboratory investigation. *7th Int. Congress. on Rock Mech.* Aachen.

Holder, J., Koelsch, T., Fruth, L. and Donath, F. (1988). Laboratory measurement of permeability in rock. *Key questions in rock mechanics.* Cudall et al (eds). Balkema, Rotterdam. pp. 207 - 215.

Jaeger, J.C (1972). *Elasticity, fracture and flow.* Third edition. Methuen & Co. (Ltd), London. pp. 70 - 72, 164 - 166

Jermy, C.A. and Bell, F.G. (1990). A survey of some engineering properties of coal bearing strata from South Africa in relation to the stability of roof rocks in coal mines. *6th Int. Congress LAEG.* Amsterdam. pp. 2601 - 2609.

Jermy, C.A. and Venter, B.J. (1993). *Report to Majuba Colliery on the geotechnical properties and permeability of borehole core obtained from the colliery.* Unpublished. 45 p.

Klinkenberg, L.J. (1941). The permeability of porous media to liquids and gases. *Drilling and Production Practice,* Dallas. pp. 200 - 213.

Lear, C.D. and Hill, R.W. (1989). Systematic sidewall support of coal pillars at depth. *Sangorn symposium: Advances in rock mechanics in underground coal mining* - September 1989.

Mordecai, M. and Morris, L.H. (1971). An investigation into the changes of permeability occurring in a sandstone when failed under triaxial stress conditions. *Proc. 12th Symp. Rock Mech. AIMMPE.* New York. Chapter 11. pp. 223 - 239.

Obert, L. and Duvall, W.I. (1967). *Rock mechanics and the design of structures in rock.* John Wiley & Sons, Inc., London. pp. 337.

Ohle, E.L. (1951). The influence of permeability on ore distribution in limestone and dolomite: Part I. *Economic geology, and the society of economic geologist.* Vol. 46, No. 7, November, 1951. pp. 667 - 705.

Paterson, L. and Meaney, K. Relative permeability in coal. *Gas in Australian coals. Geological society of Australia - Symposium Proceedings 2.* Bamberry, W.J. and Depers, A.M.(Eds). 4-5th February 1991. pp. 105.

Richards, N.P. (1992). *The engineering geology of the Lower Greensand of south-east England with particular*

reference to the microfabric, geotechnical index properties and shear strength characteristics. Ph.D. thesis, University of Southampton. Unpublished. pp. 34.

Rose, W. (1987). Relative permeability. *Petroleum engineering handbook*. Bradley, H.B. (Ed). Society of Petroleum Engineers, Richardson, TX, U.S.A. Chapter 20.

SACS (South African Committee for Stratigraphy), 1980. *Stratigraphy of South Africa. Part 1* (Comp. L.E.Kent). Lithostratigraphy of the Republic of South Africa, Namibia, and the Republics of Boputhaswana, Transkei and Venda: Handb. geol. Surv.S.Afr., 8. Printed by the Government Printer. pp.535-543.

Scheidegger, A.E. (1974). *The physics of flow in porous media*. Third edition. University of Toronto Press. 353 p.

Scheidegger, A.E. (1982). *Principals of geodynamics*. Third, completely revised, edition. Springer-Verlag. 395 p.

Somerton, W.H., Söylemezoglu, I.M. and Dudley, R.C. (1975). Effect of stress on permeability of coal. *Int. J. Rock Mech. Min. Sci. & Geomech. Abstr.* Vol. 12. Pergammon Press, Great Britain. pp. 129 - 145.

Stevenson, J.J. and Scott, T.R. (1991). Mechanics of fluid-rock systems. *Ann. Rev. Fluid Mech.*, Vol 23. Annual Reviews Inc., Paolo Alto. pp. 305 - 339

Stormont, J.C., and Daemen, J.J.K. (1992). Laboratory study of gas permeability changes in rocksalt during deformation. *J. Int. Rock Mech. Min. Sci. & Geomech. Abstr*, Vol 29, No.4. Pergammon Press, Great Britain. pp. 325 - 342.

Van Vuuren, C.J. (1981). Depositional models for the Vryheid Formation in the North-eastern part of the Karoo basin: A review. *Department of Mineral and Energy Affairs: Annals of the Geological Survey*, Vol. 15, No. 1.

Walker, P.L. and Mahajan, I (1978). Methane Diffusion in coals and chars. *Analytical methods for coal and coal products*, Vol. I. Karr, C. Jr (Ed). Chapter 5, pp. 163 - 188.

Waltz, J.P. (1976). *Introduction to physical hydrology*. Third edition, Chorley, R.J. (ed). Methuen and Co. pp. 132 - 133. Chapter 6.1.

Ward, J.R. and Jermy, C.A. (1985). Geotechnical properties of South African coal bearing strata. *SANGORM Symposium: Rock Mass Characterization*. Randburg. pp. 57 - 65.

Xue,S and Thomas, L.J. (1991). The permeability of coal under various confining stresses. *Gas in Australian coals: Geological society of Australia - Symposium Proceedings 2*. Bamberry, W.J. and Depers, A.M. (Eds). 4-5th February 1991.

BIBLIOGRAPHY

- Armstrong, M. and Hill, M. (1991). The implications of methane drainage operations for New South Wales. *Gas in Australian coals: Geological society of Australia - Symposium Proceedings 2*. Bamberry, W.J. and Depers, A.M. (Eds). 4-5th February 1991. p.1
- Archer, J.S. and Wall, C.G. 1986. *Petroleum Engineering - Principals and Practice*. Graham and Tratman, London. 362p.
- Arscott, R.L. and Hackett, P. (1969). The effect of geological features on the occurrence of gas outburst fractures in the East Midland Coalfield. *Quarterly Journal of Engineering geology*. Vol.2. Printed in Great Britain. pp. 89 - 101
- Battino, S. (1991). Determination of in situ permeability to gas for Australian coals. *Gas in Australian coals: Geological society of Australia - Symposium Proceedings 2*. Bamberry, W. J. and Depers, A.M. (Eds). 4-5th February 1991. p.3
- Bear, J. (1988). *Dynamics of fluids in porous media*. Dover Publications, Inc. New York. 764 p.
- Bocking, M.A. and Weber, C.R. The electricity commission's involvement in coal bed methane, with early results from the sydney basin. *Gas in Australian coals: Geological society of Australia - Symposium Proceedings 2*. Bamberry, W. J. and Depers, A.M. (Eds). 4-5th February 1991. p.13
- Brace, W.F., Walsh, J.B. and Frangos, W.T. (1968). Permeability of granite under high pressure. *J. Geophy. Res.* Vol. 73. No. 6. March 1968. pp. 2225 - 2236
- Brighenti, G. (1989). Effect of confining pressure on gas permeability of tight sandstones. *Rock at great depth, volume 1*. Balkema, Rotterdam. pp. 187 - 194.
- Chilangar, G.V and Adamson, L.G (1964). Does some migration of oil occur in a gaseous form? *International Geological Congress 22nd Session, India, 1964 - 1* (General Ed. R.K.Sundaram). New Delhi. pp. 64 to 70.
- Christie, A.D.M. (1988). *Sedimentary models for coal formation in the Klip River coalfield, northern Natal*. Unpublished Ph.D. thesis, Univ. Natal, Durban, 282p.

Craft, B.C. and Hawkins, M. (1991). *Applied petroleum reservoir engineering*. Second edition, revised by R.E. Terry. Prentice Hall. 431 p.

Daines, M.E. (1968). Apparatus for the determination of methane sorption on coal at high pressures by a weighing method. *Int. J. Rock Mech. Min. Sci.* Vol.5. Pergamon Press, Great Britain. pp.315-323

Daw, G.P, Howell, F.T and Woodhead, F.A. (1974). The effect of applied stress upon the permeability of some permian and triassic sandstones of northern England. *Proceedings, 3rd Congress ISRM*. VIIa, Denver. pp. 537 - 542.

Duderstadt, J.J. and Martin, W.R. (1979). *Transport theory*. John Wiley and Sons, Inc. 613p.

Faiz, M.M. and Cook, A.C. (1991). Influence of coal type, rank and depth on the gas retention capacity of coals in the southern coalfield N.S.W. *Gas in Australian coals. Geological society of Australia - Symposium Proceedings 2*. Edited by W.J. Bamberry, and A.M. Depers. 4-5th February 1991. pp.19

Foggm, P.G.T. and Gerrand, W. (1991). Solubilities of methane and other gaseous hydrocarbons. *Stability of gases in liquids*. John Wiley and Son. Chicheeys. pp. 332.

Gangi, A.F. (1978). Variation of whole and fractured porous rock permeability with confining pressure. *Int. J. Rock. Mech. Min. Sci. & Geomech. Abstr.* Vol. 15. Pergamon Press. Printed in Great Britain. pp. 249 - 257.

Garrity, P. (1982). Water percolation into fully caved longwall faces. *Strata mechanics: Developments in geotechnical engineering, Proc. Symp. Strata Mech., Newcastle upon Tyne, 5 - 7 April*. Farmer, I.W. (Editor). pp. 25.

Godden, S.J. 1982. Mechanism for outbursts of coal and gas in the South Wales Coalfield. *Strata mechanics: Developments in geotechnical engineering, vol 32*. Farmer, I.W. (Editor). *Proc Symp Strata Mech*, 4 - 7 April 1982, Newcastle upon Tyne, England. Elsevier. pp. 43 - 46

Guney, M. (1975). An investigation of methane in carboniferous rocks. *Journal of the mine ventilation society of SA*. Vol. 28, No.7 July 1975.

Harpalani, S. and McPherson, M.J. (1984). Technical note: The effect of gas evacuation onn coal permeability test specimens. *Int. J. Rock Mech. Min. Sci. & Geomech. Abstr.* Vol. 21, No. 3. Printed in Great Brittain. pp. 161 - 164.

- Harpalani, S. and McPherson, M.J. (1985). Effect of stress on permeability of coal. *7th US Symposium on Rock Mechanics*. Rapid City, SD. 26-28 June 1985. pp. 831 - 839.
- Harpalani, S. and Zhao, X. (1989). The unusual response of coal permeability to varying gas pressure and effective stress. *Rock Mechanics as a guide for Efficient Utilization of Natural resources*. Khair(ed). Balkema, Rotterdam. pp. 65 - 72.
- Joubert, J., Grein, C.T. and Beinstock, D. (1973). Sorption of methane in moist coal. *Fuel*, Vol.52, July 1973. pp. 181 - 185.
- Kranz, R.I, Frankel, A.D., Engelder, T and Scholz, C. (1979) The permeability of whole and jointed Barre Granite. *J. Int. Rock. Mech. Min. Sci. & Geomech. Abstr*, Vol 16. Pergammon Press Ltd, Great Britain. pp. 225 to 234.
- Lama, R.D and Vutukuri, V.S. (1978). *Handbook on mechanical properties of rock*. Volume 4. Trans Tech. Publications. 515 p.
- Lawrie, J.P. (1941). *Methane, its production and utilization*. Second Edition. Chapman & Hall. 66p.
- Lowe, L. (1988). *A palaeoenvironmental investigation into a coal deposit in the Southeastern Transvaal* (Goldfields, Luipaardsvlei Geol. Centre, Krugersdorp). Paper presented at Geocongress 1988.
- Lunarzewski, L., Mahoney, M.R. and Wood, J. (1991). *Practical implication of in situ gas content testing methodology for ventilation and gas drainage systems design*. p 87
- MacCormack, R.W. and Lomax, H. (1979). Numerical solution of compressible viscous flows. *Ann. Rev. Fluid Mech*, Vol. 11. Annual Reviews Inc., Paolo Alto. pp. 289 - 316
- Mackie, T.A. (1986). *The metamorphic effect of Karoo dolerite intrusions on coal seams of the Witbank coalfield with special reference to their coking properties*. M.Sc. thesis, University of Natal, Durban.
- Metcalf, R.S. (1987). Gas Production and correlations. (1987). *Petroleum engineering handbook*. Bradley, H.B. (Ed). Society of Petroleum Engineers, Richardson, TX, U.S.A. Chapter 20.
- Oda, M and Hatsuyama, Y. (1985). Permeability tensor for jointed rock masses. *Proc. Int. Symp on Fundamentals of Rock Joints*, Björkliden. 15-20 September 1985.

- Oda, M., Saito, T. and Kamemura, K. (1989). Permeability of rock masses at great depth. *Rock at great depth, volume 1*. Maury and Fourmaintraux (Eds.). Balkema, Rotterdam. pp. 449 - 456.
- Park, A., Dewers, T. and Ortoleva, P., 1990. Cellular and oscillary self-induced methane migration. *Earth-Sci. Rev.* Vol. 29. Elsevier, Amsterdam. pp. 249 - 265.
- Read, M.D., Meredith, P.G. and Murrell, S.A. (1989). *Rock at great depth, volume 1*. Maury and Fourmaintraux (eds). Balkema, Rotterdam. pp. 211 - 217.
- Ryan, T.M, Kimbrell, A.F. and Farmer, I.W. (1987). Laboratory determination of fracture permeability. *Rock mechanics: Proceedings of the 28th US Symposium*. Farmer, Daemen, Desai, Glass, and Neuman, (Eds.). University of Arizona, Tuscon. Balkema. pp. 593 - 600.
- Sato, K. Ito, Y., Sakaguchi, T. and Shimizu, T. (1991). Fundamental study of gas seepage in rocks. *7th Int. Congress on Rock Mechanics*. Aachen. 1991.
- Statham, I.C.F. (1951). *Coalmining*. English University Press Ltd., London. pp. 365 - 425.
- Stuffken, J. (1957). *De mijngasafgifte van kolenlagen: Een berekiningsmethode ten behoeve van die ontginning van mijnvelden*. Excelsior Publishers. 121p.
- Tanner, R.I. 1985. *Engineering rheology*. Oxford Science Series 14. Clarendon press, Oxford. pp. 1 - 11.
- Teufel, L.W. (1987) Permeability changes during shear deformation of fracured rock. *Rock mechanics: Proceedings of the 28th US Symposium*. Farmer, I.W., Daemen, J.J.K., Desai, C.S., Glass, C.E. and Neuman, S.P. (Eds.). University of Arizona, Tuscon. Balkema. pp. 473 - 480
- Thiel, K.(1989). Rock mechanics in hydro-engineering. *Developments in geotechnical engineering*, Vol. 51. Elsevier - PWN (Polish Scientific Publishers). 408 p.
- Truswell, J.F. (1977). *The geological evolution of SA*. Pussell and Sons, pp. 138-140.
- Walsh, J.B. and Brace, W.F. (1984) The effect of pressure on porosity and the transport properties of rock. *Journal of geophysical research*. Vol.89. No. b11. October 10. pp. 9425 - 9431.
- Whitworth, K.R. 1982. Induced changes in permeability of coal measure strata as an indicator of the mechanics of rock deformation above a longwall coal face. *Strata mechanics: Developments in geotechnical*

engineering, Vol. 32. Farmer, I.W. (Editor), Proc. Symp. Strata Mech., Newcastle upon Tyne, England. Elsevier. pp. 18 - 24.

Wübben, P., Seewald, J. and Klein, J. (1987). Effect of stress on the permeability of gas in coal. *Coal science and technology II. International conference on coal science*. pp. 139 - 142

Yoshida, H., Matsumoto, T., Aoki, Kenji and Ohnishi, Yuzo (1985). Permeability property effect on saturated-unsaturated seepage flow analysis in rock. *26th US symposium on Rock mechanics*. Radip City, SD. 26-28th June 1985.

Zhou, S. (1987). The design of gas pre-drainage for exposing outburst-prone coal seams at crosscuts. *China institute of mining and technology, Mining science and technology*, Trans Tech Pubs, Clanshathal.

APPENDIX A

Borehole log of borehole ARF 39.
Vertical hole from surface to a depth of 381.8 m.

DEPT. OF GEOLOGY AND APPLIED GEOLOGY
 UNIVERSITY OF NATAL
 DURBAN

MINE: Majuba

BOREHOLE REF. NO.: MF

BOREHOLE NO.: ARF 39

DATE LOGGED: Sept '92

DATE DRILLED: Jan. '91

SHEET: 1 OF: 13

Sample No.	Facies	K (md)	DEPTH (m)	Key	Description
			251		
			252		
			253		No core.
			254		
			255		
MF 1			256		
MF 6			257		
MF 8			258		Dolerite: light grey, speckled, unweathered.
			259		
MF 13	8 3		260		Fine grained sandstone: faintly bedded Argillaceous: decrease in sand componer
	8				Fine grained sandstone: faintly bedded

DEPT. OF GEOLOGY AND APPLIED GEOLOGY
UNIVERSITY OF NATAL
DURBAN

MINE: Mojuho

BOREHOLE REF. NO.: MF

BOREHOLE NO.: ARF 39

DATE LOGGED: Sept. '92

DATE DRILLED: Jan. '92

SHEET: 2 OF: 13

Sample No.	Facies	K (md)	Depth (E)	Key	Description
			261		Breccia: possible shear zone.
					Grit: quartz grains.
MF14			262		Cross bedded fine grained sandstone:
MF18	5		263		
MF19					
	10		264		Cross bedded medium grained sandstone: becoming contorted near the bottom.
					Dolerite:
MF20		0.006	265		
MF27	7	0.020	266		Very fine grained sandstone: uniform.
MF33		0.101	267		
MF34	8	0.067			Fine grained sandstone: faint bedding.
			268		
MF37			269		
MF39	10	0.052			Cross bedded medium grained sandstone:
MF47					
MF48	5		260		Medium grained sandstone: alternating with argillaceous lamina.

DEPT. OF GEOLOGY AND APPLIED GEOLOGY
UNIVERSITY OF NATAL
DURBAN

MINE: Majuba

BOREHOLE REF. NO.: MF

BOREHOLE NO.: ARF 39

DATE LOGGED: Sept. '92

DATE DRILLED: Jan. '92

SHEET: 3 OF: 13

Sample No.	Facies	K (md)	DEPTH (m)	Key	Description
MF54	7		271		Fine grained sandstone: friable.
	8				Cross bedded fine grained sandstone:
MF60			272		Grit:
MF63	8	0.006			Cross bedded fine grained sandstone:
MF64	7				Very fine grained sandstone: dirty.
MF68	11		273		Coarse grained sandstone: some grit.
	10				Medium grained sandstone:
MF69	7		274		Very fine grained sandstone: clean.
MF72	3				Argillaceous: interlayered with fine grained sandstone.
MF74	8		275		Cross bedded fine grained sandstone:
MF75	4		276		Very fine grained sandstone: foresets argillaceous.
MF78	8				Cross bedded fine grained sandstone:
	4		277		Very fine grained sandstone: flaser bedded.
MF79	10				Very fine grained sandstone: flaser bedded.
	4		278		Very fine grained sandstone: flaser bedded.
MF80					Grit:
	5		279		Very fine grained sandstone: with argillaceous lamina.
MF84	6				Fine grained sandstone:

DEPT. OF GEOLOGY AND APPLIED GEOLOGY
UNIVERSITY OF NATAL
DURBAN

MINE: Majuba

BOREHOLE REF. NO.: MF

BOREHOLE NO.: ARF 39

DATE LOGGED: Sept. '92

DATE DRILLED: Jan. '92

SHEET: 4 OF: 13

Sample No.	Facies	K (md)	DEPTH (E)	Key	Description
MF86	4				Fine grained sandstone: flaser bedded.
MF88	3		281		Argillaceous: lenses of very fine grained sandstone.
MF91	2				
MF92	2		282		Mudrock: lenticular bedded.
MF96	3				
			283		Argillaceous: lenses of very fine grained sandstone.
MF101	2				
			284		
MF104					
			285		
MF107					
			286		
MF111					
	4		287		Fine grained sandstone: flaser bedded, predominantly argillaceous.
	2				
			288		Mudrock: lenticular bedded.
MF115	4				
	2				
			289		Very fine grained sandstone: mixed with argillaceous laminations.
MF116					
	2				Mudrock: lenticular bedded, with drop stones in an argillaceous matrix.
MF119	4				
					Very fine grained sandstone: flaser beds.
MF122	7				
					Fine grained sandstone: uniform.

DEPT. OF GEOLOGY AND APPLIED GEOLOGY
UNIVERSITY OF NATAL
DURBAN

MINE: Mojuaba

BOREHOLE REF. NO.: MF

BOREHOLE NO.: ARF 39

DATE LOGGED: Sept. '92

DATE DRILLED: Jan. '92

SHEET: 6 OF: 13

Sample No.	Facies	K (md)	DEPTH (m)	Key	Description
MF 173	3				Argillaceous:
MF 174	10				Cross bedded medium grained sandstone:
MF 176	14		301		Medium grained sandstone: slumped beds.
	6				Cross bedded very fine grained sandstone
	3				Argillaceous:
MF 178			302		Cross bedded very fine grained sandstone some grit and argillaceous zones.
	6				
MF 181			303		
	10				Medium grained sandstone: faint bedding.
MF 184			304		
MF 187	2				Dolerite:
			305		Mudrock: lenticular bedded, more sandy toward bottom of layer.
MF 188	10	0.103			
MF 189	3				Argillaceous:
MF 190			306		
	9				Medium grained sandstone: dirty.
MF 195					
MF 196	14		307		Medium grained sandstone: slumped beds.
	8				Flat laminated: fine grained sandstone.
MF 199			308		
	3				Argillaceous: not true Facies 3.
MF 203		0.006			
			309		
MF 204	6				Cross bedded very fine grained sandstone 80% argillaceous, 20% arenaceous.
MF 205					
			310		

DEPT. OF GEOLOGY AND APPLIED GEOLOGY
UNIVERSITY OF NATAL
DURBAN

MINE: Mojuba

BOREHOLE REF. NO.: MF

BOREHOLE NO.: ARF 39

DATE LOGGED: Sept. '92

DATE DRILLED: Jan. '92

SHEET: 8 OF: 13

Sample No.	Facies	K (md)	Depth (m)	Key	Description	
MF236	4	0.704	321		Fine grained sandstone: flaser bedded.	
	10				Cross bedded medium grained sandstone:	
MF239	12				Cross bedded coarse grained sandstone:	
MF245					322	
MF250	10				323	Cross bedded medium grained sandstone:
					324	
MF254	4				325	Fine grained sandstone: flaser bedded.
MF261						
MF266	11				326	Coarse grained sandstone: uniform, gritty in places.
MF273					327	
MF280					328	
MF281	10					Cross bedded medium grained sandstone:
MF283		329				
	9		Medium grained sandstone: uniform.			
MF286	10					
MF290		330				
MF292			Cross bedded medium grained sandstone:			

DEPT. OF GEOLOGY AND APPLIED GEOLOGY
UNIVERSITY OF NATAL
DURBAN

MINE: Majuba

BOREHOLE REF. NO.: MF

BOREHOLE NO.: ARF 39

DATE LOGGED: Sept. '92

DATE DRILLED: Jan. '92

SHEET: 9 OF: 13

Sample No.	Facies	K (md)	Depth (m)	Key	Description
MF293	9		331		Medium grained sandstone: uniform.
MF296	11				Coarse grained sandstone: uniform.
MF297	7				Fine grained sandstone: dirty.
MF300	11	0.255	332		Coarse grained sandstone: uniform.
MF302	14	0.008			Cross bedded medium grained sandstone: carbonaceous drapes.
MF304			333		Fine grained sandstone: to medium grained, contorted and slumped beds.
MF308	8				Fine grained sandstone:
MF309	7		334		Argillaceous: with lenses of very fine grained sandstone.
MF311	3				Fine grained sandstone: flaser bedded.
MF313	4		335		Argillaceous: with lenses of very fine grained sandstone.
MF316	3				Fine grained sandstone: flaser bedded.
MF319	3		336		Argillaceous: with lenses of fine grained sandstone.
MF321	4				Fine grained sandstone: flaser bedded.
MF323	7		337		Fine grained sandstone: uniform, dirty matrix.
MF324	3				Argillaceous: interlayered with fine grained sandstone, flat laminated.
MF325	6		338		Cross bedded very fine grained sandstone.
MF326	4				Fine grained sandstone: flaser beds, argillaceous.
MF329	7		339		Siltstone: fine grained, dark matrix.

DEPT. OF GEOLOGY AND APPLIED GEOLOGY
UNIVERSITY OF NATAL
DURBAN

MINE: Mojubo

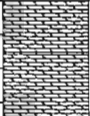
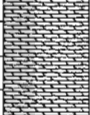











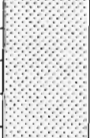
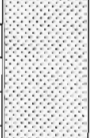
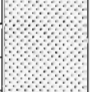

BOREHOLE REF. NO.: MF

BOREHOLE NO.: ARF 39

DATE LOGGED: Sept. '92

DATE DRILLED: Jan. '92

SHEET: 10 OF: 13

Sample No.	Facies	K (md)	Depth (m)	Key	Description
MF326A	2				Mudrock: weathered, water present?
MF327A	2		341		Mudrock: lenticular bedded, lenses of fine grained sandstone.
MF328A			342		Argillaceous: some grits, diamicite?
MF331	11				Coarse grained sandstone: interlayered with fine grained sandstone.
MF334	9		343		Medium grained sandstone: fining down.
MF336	8				Coarse grained sandstone: cross bedded.
MF337	12				Fine grained sandstone: cross bedded.
	8				Coarse grained sandstone:
	11		344		Fine grained sandstone: flaser bedded.
MF342	4				Medium grained sandstone: flat bedded, some carbonaceous drapes.
MF344	14		345		Fine grained sandstone: flaser bedded.
MF345	8				Medium grained sandstone: flat bedded, some carbonaceous drapes.
MF347	4		346		Fine grained sandstone: flaser bedded.
			347		Medium grained sandstone: uniform.
MF355	9		348		Medium grained sandstone: uniform.
MF358			349		Very fine grained sandstone: silty and carbonaceous, prominent marker horizon.
MF363	15		350		Very fine grained sandstone: silty and carbonaceous, prominent marker horizon.

DEPT. OF GEOLOGY AND APPLIED GEOLOGY
UNIVERSITY OF NATAL
DURBAN

MINE: Majuba

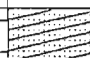



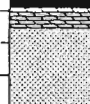
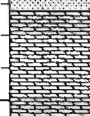
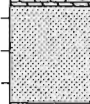
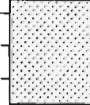

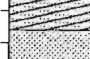
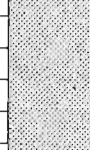
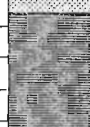
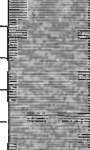
BOREHOLE REF. NO.: MF

BOREHOLE NO.: ARF 39

DATE LOGGED: 12/09/92

DATE DRILLED: 12/09/92

SHEET: 13 OF: 13

Sample No.	Facies	K (md)	DEPTH (m)	Key	Description
MF490	12		371		Cross bedded coarse grained sandstone:
MF494		0.418	372		Coal: Gus seam.
MF499	22		373		Coal: Dundas seam.
MF504 MF506	1		374		Mudrock: lenticular bedded, carbonaceous
MF508	5		375		Fine grained sandstone: ripple cross laminated.
MF510	3		376		Mudrock: interlayered siltstone, flat laminated.
MF513	5		377		Fine grained sandstone: ripple cross laminated.
MF519 MF520	14	0.132	378		Medium grained sandstone: carbonaceous drapes.
MF521	22		379		Coal: Dundas seam.
MF527 MF528	10		380		Cross bedded medium grained sandstone:
	5		381		Fine grained sandstone: ripple, cross laminated.
		0.309	382		Argillaceous: with siltstone lenses.
MF535	3		383		Argillaceous: with siltstone lenses.
					End OF Hole

APPENDIX B

Borehole log of borehole AH 55 - 59.

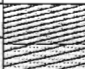


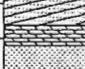

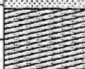




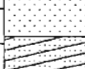
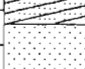


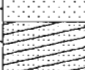


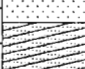



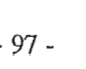

10 m long vertical hole drilled up from roof of Gus coal seam.

APPENDIX C

Borehole log of borehole AH 58.
10 m long vertical hole drilled up from roof of Gus coal seam.

DEPT. OF GEOLOGY AND APPLIED GEOLOGY
UNIVERSITY OF NATAL
DURBAN

MINE: *Mojuba*BOREHOLE REF. NO.: *MB*BOREHOLE NO.: *AH 58*DATE LOGGED: *May '92*DATE DRILLED: *Dec. '91*SHEET: *1* OF: *1*

Sample No.	Facies	K (md)	Depth (m)	Key	Description
	8				Cross bedded fine grained sandstone:
	10		1		Cross bedded medium grained sandstone: some argillaceous partings.
	3				Mudrock: some lenses of sandstone.
MB1	5		2		Fine grained sandstone: ripple cross laminated, dirty.
MB2	7				Cross bedded fine grained sandstone:
MB7	8		3		Cross bedded fine grained sandstone:
	9	0.279			Medium grained sandstone: feldspathic.
MB12			4		Medium grained sandstone: feldspathic.
	11				Coarse grained sandstone: gritty.
MB20	22				Coal: stringer.
	11		5		Coarse grained sandstone: gritty.
MB22	12	0.699			Cross bedded coarse grained sandstone:
MB27	11	0.869			Cross bedded coarse grained sandstone:
	11		6		Coarse grained sandstone: gritty.
MB30					Medium grained sandstone:
MB32	9				Medium grained sandstone:
MB34	11		7		Coarse grained sandstone: gritty.
	12				Cross bedded coarse grained sandstone:
MB37					Cross bedded coarse grained sandstone:
	9				Medium grained sandstone:
MB39		0.450	8		Medium grained sandstone:
	11				Coarse grained sandstone: gritty.
MB44		0.084			Cross bedded medium grained sandstone: broken up.
MB45	22		9		Coal: Alfred seam.
MB46	10				Medium grained sandstone: E.O.H.

APPENDIX D

Borehole log of borehole AH 60.
10 m long vertical hole drilled up from roof of Gus coal seam.

APPENDIX E

Borehole log of borehole AH 53.
10 m long vertical hole drilled up from roof of Gus coal seam.

DEPT. OF GEOLOGY AND APPLIED GEOLOGY
UNIVERSITY OF NATAL
DURBAN

MINE: Majuba

BOREHOLE REF. NO.: MD

BOREHOLE NO.: AH 53

DATE LOGGED: May '92

DATE DRILLED: Dec. '91

SHEET: 1 OF: 1

Sample No.	Facies	K (md)	Depth (m)	Key	Description
	9				Medium grained sandstone:
	10		1		Cross bedded medium grained sandstone: some argillaceous partings.
MD1	5				Ripple cross laminated: fine grained sandstone
MD3	7	0.008	2		Fine grained sandstone: dark matrix.
MB ⁴ ₆	22				Coal: stringer.
MD6	10	0.050			Cross bedded medium grained sandstone:
MD8	11		3		Coarse grained sandstone:
	10				Cross bedded medium grained sandstone:
MD12	10	0.774	4		
MD14	11	0.121			Coarse grained sandstone: gritty.
MD19	11		5		
MD20	9	2.343			Medium grained sandstone: massive.
MD22	11		6		Coarse grained sandstone:
MD25	10	0.460			Cross bedded medium grained sandstone: some grit bands.
MD31	11		7		
MD36	11		8		Coarse grained sandstone: dirty.
MD41	9	0.746	9		Mudrock: black, gritty.
MD42	9				Medium grained sandstone:
MD45	22				Coal: Alfred seam, calcite present.
MD47	9				Medium grained sandstone: E.O.H.

APPENDIX F

Borehole log of borehole AH 61.
10 m long vertical hole drilled up from roof of Gus coal seam.

APPENDIX G

Data capture sheet - Ohle cell.

APPENDIX G
Permeability - Ohle cell

Mine: MAJUBA COLLIERY

Sample No: MF241A

Facies: 10

Sample length (cm): 1.73

Sample diameter (cm): 6.03

Area (cm²): 28.56

Weight wet (g):

Weight dry (g): 118.67

Porosity (%):

Gas: Methane

Liquid:

Temperature (°C): 24

Tested by: B.J.VENTER

Date: 4/12/92

Pressure (kPa)	Viscosity (cP)	Quantity (cm ³)	Time (sec)	Flow rate (cm ³ s ⁻¹)	Permeability (mD)	1 / mean pressure
150	0.010938	20	50.81	0.394	0.02160	0.667
200	0.010938	20	20.38	0.981	0.4173	0.500
250	0.010938	20	13.53	1.478	0.4335	0.400
300	0.010948	20	17.22	2.323	0.3731	0.333
350	0.010948	40	19.16	3.132	0.385	0.286
400	0.010958	60	19.12	4.184	0.369	0.250
450	0.010958	80	15.94	5.019	0.370	0.222
500	0.010968	80	12.63	6.334	0.346	0.200
550	0.010968	100	12.65	7.905	0.351	0.182
600	0.010978	100	10.5	9.524	0.362	0.167
650	0.010978	100	8.94	11.186	0.361	0.154
700	0.010988	100	7.85	12.739	0.353	0.143

APPENDIX H

Data capture sheet - Hoek cell.

APPENDIX H
Triaxial Permeability Test
 (Hoek Cell)

Borehole Number: Bulk, Sample - Y4

Sample No.: CC4

Facies: 10 - Parallel to bedding
 (Towards Y4)

Sample Length (cm): 10.8

Sample diameter (cm): 5.22

Area (cm²): 21.4

Weight wet (gm):.....

Weight dry (g): 560.17

Porosity (%):.....

Gas: Methane

Liquid:.....

Temp (°C): 25.0

Tested by: B.J.Venter

Date: 25/5/93

σ_3 (MPa)	Axial Load (kN)	σ_1 (MPa)	Gas Pressure (kPa)	Time (s)	Volume (cm ³)	Quantity (cm ³ /s)	Permeability (mD)
4.0	8.5	4.0	200	25.75	5	0.194	0.720
4.0	8.5	4.0	250	14.65	5	0.341	0.723
4.0	8.5	4.0	300	19.38	10	0.516	0.718
4.0	8.5	4.0	350	14.50	10	0.690	0.683
4.0	8.5	4.0	400	11.06	10	0.904	0.672
4.0	8.5	4.0	450	13.28	10	1.130	0.654
4.0	8.5	4.0	500	10.97	15	1.367	0.636
4.0	8.5	4.0	550	8.90	15	1.685	0.643
4.0	8.5	4.0	600	7.56	15	1.984	0.633
4.0	8.5	4.0	650	6.50	15	2.308	0.625
4.0	8.5	4.0	700	5.53	15	2.712	0.632
8.0	17.5	8.0	200	69.85	5	0.0108	0.265
8.0	17.5	8.0	250	41.22	5	0.072	0.257
8.0	17.5	8.0	300	27.84	5	0.121	0.250
8.0	17.5	8.0	350	21.35	5	0.234	0.232
8.0	17.5	8.0	400	32.78	10	0.305	0.227
8.0	17.5	8.0	450	26.09	10	0.383	0.222
8.0	17.5	8.0	500	21.50	10	0.465	0.216
8.0	17.5	8.0	550	18.03	10	0.555	0.212
8.0	17.5	8.0	600	15.31	10	0.653	0.208
8.0	17.5	8.0	650	13.07	10	0.765	0.207
8.0	17.5	8.0	700	11.4	10	0.877	0.204